Retroviral Lineage Analysis of the Vagal Neural Crest Reveals Multipotency Towards the Cardiac and Enteric Fates

Thesis by
Weiyi Tang

In Partial Fulfillment of the Requirements for
the Degree of
Doctor of Philosophy

CALIFORNIA INSTITUTE OF TECHNOLOGY
Pasadena, California

2022
(Defended March 4, 2022)

Weiyi Tang
ORCID: 0000-0002-1279-1001

To mom and dad

ACKNOWLEDGEMENTS

First, I would like to thank my advisor Prof. Marianne E. Bronner for her endless support and input into every bit of my progress during my journey as a graduate student. Marianne impresses me with her sharp scientific mind, elegant writing style, and positive attitude towards all aspects of life. What I deeply appreciate is her unconditional support and genuine care, making sure that I am happy and productive, especially during those tough months in 2020 when new research results were scarce, and uncertainties prevailed. Marianne, I would have never reached this point without your encouragement. When I was new to the lab, you helped me with all the precise injections; you turned my first paper draft into a great shape; you spent hours to show me ways to make an effective scientific talk. Outside of the lab, you cured my allergies, showed me the best hiking route in Woods Hole, and filled the hike with funny jokes that still make me laugh. Thank you for being the best mentor and role model. Your email "welcome to my lab!" made that sunny June afternoon of 2017 shine. I wish I can be like you one day.

I would like to express my sincere appreciation to Prof. Angelike Stathopoulos, Prof. Ellen Rothenberg, and Prof. Matt Thomson who have been extremely supportive, providing invaluable insights into my graduate work as my thesis committee. Angela, Ellen, and Matt, thank you for those inspiring conversations. I love every moment with you during our meetings.

In the Bronner lab, I have received a great amount of support from my mentors and friends. I would like to thank Dr. Yuwei Li for the tremendous efforts from showing me every detail about the RIAs to helping me reach out for collaborations. Thank you for sharing your experiences in performing challenging experiments. I learned a lot from you and will always help others the way you helped me. I would like to give you a lot of credit because this thesis work would not have been possible without your help.

My appreciation also goes to Dr. Felipe Vieceli, Dr. Ezgi Kunttas and Dr. Max Ezin, who patiently showed me chick embryology techniques. I cannot imagine such a smooth transition into my graduate research if you were not there. I would like to thank Can Li for

kindly sharing protocols and going through the optimization steps with me. Can, thank you for helping me every early morning when I needed to sort the cells. I enjoyed our scientific and non-scientific conversations a lot.

I would also like to thank Drs. Megan Martik, Shashank Gandhi, and Ang Li for their help with RNA-seq techniques, quantitative analysis and great collaboration. Thank you, Drs. Meyer Barembaum, Michael Piacentino, and Erica Hutchins for providing great ideas for my projects. I would like to thank Johanna Tan-Cabugao, Constanza Gonzalez, David Mayorga, and Ryan Fraser for being so helpful and accommodating, making the lab like a home for me. It was a great enjoyment working with all Bronner lab members—you are a terrific group of people.

My appreciation extends beyond the Bronner lab community. Thank you so much, Prof. Bruce Blumberg for taking me into your lab in my sophomore year. When I did not have knowledge about the lab's research topic, you encouraged me to learn from hands-on experience. Thank you, Dr. Amanda Janesick for introducing the world of molecular and developmental biology to me. Bruce and Amanda, thank you so much for encouraging me to pursue my graduate career. I really appreciate that both of you have invited me to spend Thanksgiving with your families in 2015.

I would like to thank Dr. Ben Deverman and Dr. Wei-Li Wu for their dedicated support as my mentors during and beyond my rotations. Wei-Li, thank you for helping me out through tough times. Next, I would like to express my appreciation to Prof. Carlos Lois for sharing his lab equipment and patiently answering all my questions. I would have no RIA to use without the help from Carlos. I would like to thank Elizabeth Ayala and Raina Beaven for their administrative guidance throughout my graduate career. I also received a lot of support from Dr. Andres Collazo and Dr. Giada Spigolon at the Biological Imaging Facility, which makes an indispensable part of my research. Andres, thank you so much for your input during the lab meetings and for all your help. I would like to thank Drs. Igor Antoshechkin and Vijaya Kumar and the Millard and Muriel Jacobs Genetics and Genomics Laboratory at California Institute of Technology for their guidance and support in bulk RNA-sequencing,

Jamie Tijerina and Rochelle Diamond from the Caltech Flow Cytometry Facility for their help with the FACS. I would like to thank Dr. Sisi Chen, Jeff Park, and SPEC at Caltech for their dedicated support in optimization and guidance in single-cell RNA-sequencing, and Dr. Fan Gao and the Caltech Bioinformatics Resource Center for guiding us through each step of single-cell transcriptomic analysis.

I would also give all my friends from and outside of Caltech lots of credit for making this time unforgettable for me. Ge Chen, thank you for showing me ways to prepare a quick, healthy, and delicious dinner. You have amazing characteristics: never in a hurry, always enjoying the moment of life. I was just the opposite and have learned so much from you. Thank you, Ziqing Jessica Liu and Kexin Zhang for chatting with me on a daily basis and for being the best listener for decades.

Last but most importantly, I would like to express my deep appreciation to my mom Chunling Tang and dad Weihua Tang, who have been supportive toward all choices I made and had to give up a lot of time together when I decided to pursue higher education in the U.S.. I am here today and looking forward to many tomorrows, all because of your love and support.

ABSTRACT

The neural crest is a migratory stem cell population that gives rise to the craniofacial skeleton, heart septa, pigment cells, and peripheral nervous system. Defects in neural crest development can lead to a broad range of congenital diseases, e.g., persistent truncus arteriosus, characterized by a mixture of oxygenated and deoxygenated blood, is related to the absence of the neural crest-derived outflow tract septum. Thus, a thorough understanding about neural crest migration, differentiation, and cell fate can shine lights on diagnosis and treatment of many congenital defects. A long-standing question is whether neural crest cells are composed of multipotent cells capable of giving rise to a wide range of cell types, or a mixture of fate-determined cells migrating to their destinations. Avian embryos resemble humans during neural crest development, but are more accessible to experimental manipulations than mammalian models, making them an ideal model to study the neural crest. Despite the abundance of information obtained from elegant experiments through interspecies grafting, the avian model lacks a direct tool to determine whether these cells are multipotent *in vivo*.

Here, we present a new clonal analysis tool that takes advantage of Replication Incompetent Avian retroviruses (RIAs). We validate the method *in vitro* and present the potential application in the chick embryo to test the multipotency of the trunk neural crest. Next, we perform RIA-mediated lineage tracing at a population level and uncover cardiomyocytes as a previously unknown cardiac neural crest derivative in both chicken and mouse. Furthermore, we utilize RIA-mediated clonal analysis to identify individual premigratory vagal neural crest cells as a multipotent stem cell that forms cell types in both the heart and

the gut. We then confirm the results by single-cell photoconversion assay that further confirms that migrating neural crest cells are also multipotent. Time-lapse imaging shows that stochastic post-mitotic migration is a cellular mechanism underlying multipotency. Finally, molecular perturbation experiments show that CXCR4 and RET are essential guidance cues for migratory neural crest cells to enter the heart and the gut, respectively. Together, these results demonstrate the utility of using RIA viruses to tackle questions regarding the lineage, developmental potential, and migratory pathways followed by neural crest cells in avian embryos.

PUBLISHED CONTENT AND CONTRIBUTIONS

Tang, W. & Bronner, M. E. Neural crest lineage analysis: From past to future trajectory. *Development* 147, (2020). DOI: 10.1242/dev.193193

W.T participated in project conceptualization, literature collection, and manuscript writing.

Tang, W., Li, Y., Gandhi, S. & Bronner, M. E. Multiplex clonal analysis in the chick embryo using retrovirally-mediated combinatorial labeling. *Dev. Biol*. 450, (2019). DOI: 10.1016/j.ydbio.2019.03.007

W.T participated in project conceptualization, experimental design, experiments, data analysis, and manuscript writing.

Tang, W.*, Martik, M. L.*, Li, Y. & Bronner, M. E. Cardiac neural crest contributes to cardiomyocytes in amniotes and heart regeneration in zebrafish. *Elife* 8, (2019). DOI: 10.7554/eLife.47929

W.T participated in project conceptualization, experimental design, performed RIA and Wnt1-Cre lineage tracing experiments, data analysis, and manuscript writing.

Tang, W., Li, Y., Li, A. & Bronner, M. E. Clonal analysis and dynamic imaging identify multipotency of individual Gallus gallus caudal hindbrain neural crest cells toward cardiac and enteric fates. *Nat. Commun*. 12, (2021). DOI: 10.1038/s41467-021-22146-8

W.T participated in project conceptualization, experimental design, experiments, imaging data collection, and manuscript writing.

Gandhi, S., Li, Y., **Tang, W**., Christensen, J. B., Urrutia, H. A., Vieceli, F. M., Piacentino, M. L., Bronner, M. E. A single-plasmid approach for genome editing coupled with long-term lineage analysis in chick embryos. *Development* 148, (2021). DOI: 10.1242/dev.193565

W.T participated in RIA concentration, clonal analysis experiments, visualization, and original manuscript writing.

Li, Y, Gonzalez, W. G., Andreev, A., **Tang, W**., Gandhi, S., Cunha, A., Prober, D., Lois, C., Bronner, M. E. Macropinocytosis-mediated membrane recycling drives neural crest migration by delivering F-actin to the lamellipodium. *Proc. Natl. Acad. Sci. U. S. A.* 117, 27400–27411 (2020). DOI: 10.1073/pnas.2007229117

W.T participated in embryo slice culture experiments and visualization.

Li, Y., Vieceli, F. M., Gonzalez, W. G., Li, A., **Tang, W**., Lois, C., & Bronner, M. E. In Vivo Quantitative Imaging Provides Insights into Trunk Neural Crest Migration. *Cell Rep*. 26, (2019). DOI: 10.1016/j.celrep.2019.01.039

W.T participated in embryo slice culture experiments and visualization.

TABLE OF CONTENTS

LIST OF ILLUSTRATIONS, TABLES AND DATA

Table

Data file

NOMENCLATURE

Cardiac neural crest: delaminates from dorsal neural tube adjacent to mid-otic-somite 3.

Posterior vagal neural crest: delaminates from dorsal neural tube adjacent to somite 4-7.

Caudal hindbrain neural crest: refers to the population including cardiac neural crest and posterior vagal neural crest.

Sacral neural crest: delaminates from dorsal neural tube posterior to somite 28.

Dorsal root ganglia: a region of gathered sensory cell bodies adjacent to the spinal cord, derived from the neural crest.

Cranial nerve IX: the glossopharyngeal nerve, derived from the neural crest.

Pharyngeal arch arteries: refers to embryonic form of great arteries in the neck that undergo rearrangement during development. Cardiac and posterior vagal neural crest cells reside in this region during migration.

Cell lineage: tracing an individual cell or a group of cells from an early embryonic stage to assess the distribution of derived cells at later stages.

Clone, clonal relationship, clonal analysis: a clone is defined by a group of cells derived from a single progenitor cell. Such group of cells are clonally related. Clonal analysis is a study to retrieve clonal relationship between the cells.

Chapter I

THE NEURAL CREST

Part of this chapter was published as Tang, W. & Bronner, M. E. Neural crest lineage analysis: From past to future trajectory. *Development* 147, (2020). DOI: 10.1242/dev.193193

ABSTRACT

Since its discovery 150 years ago, the neural crest has intrigued investigators due to its remarkable developmental potential and extensive migratory ability. Cell lineage analysis has been an essential tool for exploring neural crest cell fate and migration routes. By marking progenitor cells, one can observe their subsequent locations and the cell types into which they differentiate. Here, we review major discoveries in neural crest lineage tracing from a historical perspective. We discuss how advancing technologies have refined lineage tracing studies, and how clonal analysis can be applied to questions regarding multipotency. We also highlight how effective progenitor cell tracing, when combined with recently developed molecular and imaging tools such as single-cell transcriptomics, single molecule fluorescence in situ hybridization and high-resolution imaging, can extend the scope of neural crest lineage studies beyond development to regeneration and cancer initiation. The context of Chapter I will be enriched by the following chapters, with a focus on retroviral lineage tracing techniques to conduct population level lineage tracing, clonal analysis in combination with time-lapse imaging, and single-cell transcriptomics.

1.1 A LONG-STANDING QUESTION IN NEURAL CREST CELL FATES

The neural crest is an embryonic stem cell population unique to vertebrates. In 1868, Wilhelm His first described the "Zwischenstrang" as a band of cells residing between the neural tube and epidermis that later migrates laterally to form the spinal ganglion[1]. Today, this cell population is known as the neural crest. Induced at the neural plate border, neural crest cells undergo an epithelial-to-mesenchymal transition (EMT) to leave the neural tube. They then migrate laterally and ventrally, eventually giving rise to cell types as diverse as cartilage of the head, connective tissue, pigment cells, cardiac outflow septum, and peripheral nervous system. As cells arising from different levels of the rostrocaudal body axis give rise to different cell types, the neural crest can be subdivided into cranial, vagal, trunk, and sacral subpopulations.

Although experimental embryologists over the past century have mapped neural crest cells at all these axial levels, recent studies using refined tools have revealed previously unrecognized neural crest derivatives and behaviors. Thus, there are many interesting open questions about neural crest development. For example, how do migrating neural crest cells interact with each other, both molecularly and mechanically? How are lineage decisions coupled with migration and how do neural crest cells interact with the rapidly developing surrounding tissue? Since neural crest cells have stem cell properties, what is their degree of fate restriction versus multipotency to form diverse cell types? How does this vary along the rostrocaudal body axis? In the adult, do neural crest-derived cells participate in tissue repair? How and why do things go wrong, resulting in neural crest-derived tumor formation? These

questions require means to indelibly label the progeny of single cells or specific groups of neural crest cells *in vivo*, while enabling assessment of their transcriptomic landscape, spatial characteristics, and cellular dynamics.

In this chapter, we describe how the neural crest was studied from a chronological perspective, beginning with methods for lineage tracing at a population level, followed by recent advances in clonal analysis to explore the developmental potential of individual cells. We comment on advantages and limitations of different approaches, and adaptation of new tools to questions in the field as technology proceeded. Lastly, we extend the discussion to the broader application of lineage tracing of neural crest-derived cells during regeneration and cancers.

1.2 WHERE DO THEY GO? WHAT DO THEY BECOME?

In the first half of the 20th century, the neural crest was studied intensely by experimental embryologists primarily using amphibian embryos taking advantage of vital dye labeling, interspecies/heterotopic grafting, and cell ablation techniques. In 1950, Sven Hörstadius presented a thorough overview of the state of knowledge regarding neural crest induction, migration, and differentiation. Although the neural crest then was "only sparsely treated by the authors of text books[2]", many of the results and perspectives in the book remain incredibly insightful. The broadness and accuracy of knowledge obtained by removing, grafting or rotating pieces of tissue is remarkable from today's perspective.

1.2.1 THE DAWN OF EXPERIMENTAL EMBRYOLOGY

One lineage tracing experiment Hörstadius addressed as "exceedingly beautiful" was performed by Ross Harrison in 1935. To understand whether neural crest cells contribute to the gill arch skeleton, Harrison exchanged hindbrain regions between two amphibian species, *Amb. punctatum* and *Amb. tigrinum* or *mexicanum*, whose gill arch sizes vary. After neural crest cells had migrated to the arch, the branchial arch itself — including both donor and host cells — was transplanted into another host of the same species. In this way, only branchial neural crest cells were derived from the donor. Gill size in the resulting chimera matched that of the donor on the transplanted side, suggesting that intrinsic information in the neural crest contributed to the arch skeleton[3] (Fig.1-1A). The migratory properties of neural crest cells were examined in a similar way by Victor Twitty, who interchanged trunk neural crest cells between two species of salamander, *Tr. rivularis* and *Tr. Torosus*, with distinct pigment patterns. He discovered that grafted cells undergo migratory patterns characteristic of the donor, indicating that intrinsic properties of the pigment cells, rather than the environment, affected cell migration[4] (Fig.1-1B). A caveat of such interspecific grafts, however, is that they may alter normal tissue interactions thus modulating signaling and timing events between donor and host tissues in unpredictable ways[2].

Thanks to the ability to combine different tissue types, grafting experiments have also provided insights into cell-cell interactions. To distinguish whether cranial neural crest cells can differentiate into cartilage autonomously, or if tissue interactions are required, Hörstadius and others transferred cranial neural crest cells into the trunk region[5]. Unless other

manipulations such as removing the somite or grafting endomesodermal cells from the gill arch were conducted concomitantly, cranial crest cells could not differentiate into cartilage in the trunk. This suggested that, at the stage grafted, neural crest cells were not yet fated toward chondrogenic lineages. Moreover, differentiation into cartilage required interaction with adjacent tissue at the cranial region or signals from the environment released at the wound where the somite was removed[5] (Fig.1-1C). Interestingly, these results differ from similar experiments carried out in birds, which suggest that some avian cranial neural crest cells can form cartilage nodules when transplanted to the trunk[6]. This may be due to species-specific differences or evolutionary changes that render the amniote cranial neural crest gene regulatory circuitry more hard-wired to form craniofacial cartilage[7].

While amphibian transplantations elegantly pioneered the field of neural crest experimental embryology, several controversies arose because only partial answers could be obtained, as acknowledged by the authors. In the following decades, neural crest researchers expanded lineage analysis methods to adapt to various model organisms. As predicted, these efforts greatly revolutionized the field by "attack(ing) the problems on sufficiently broad lines[2]".

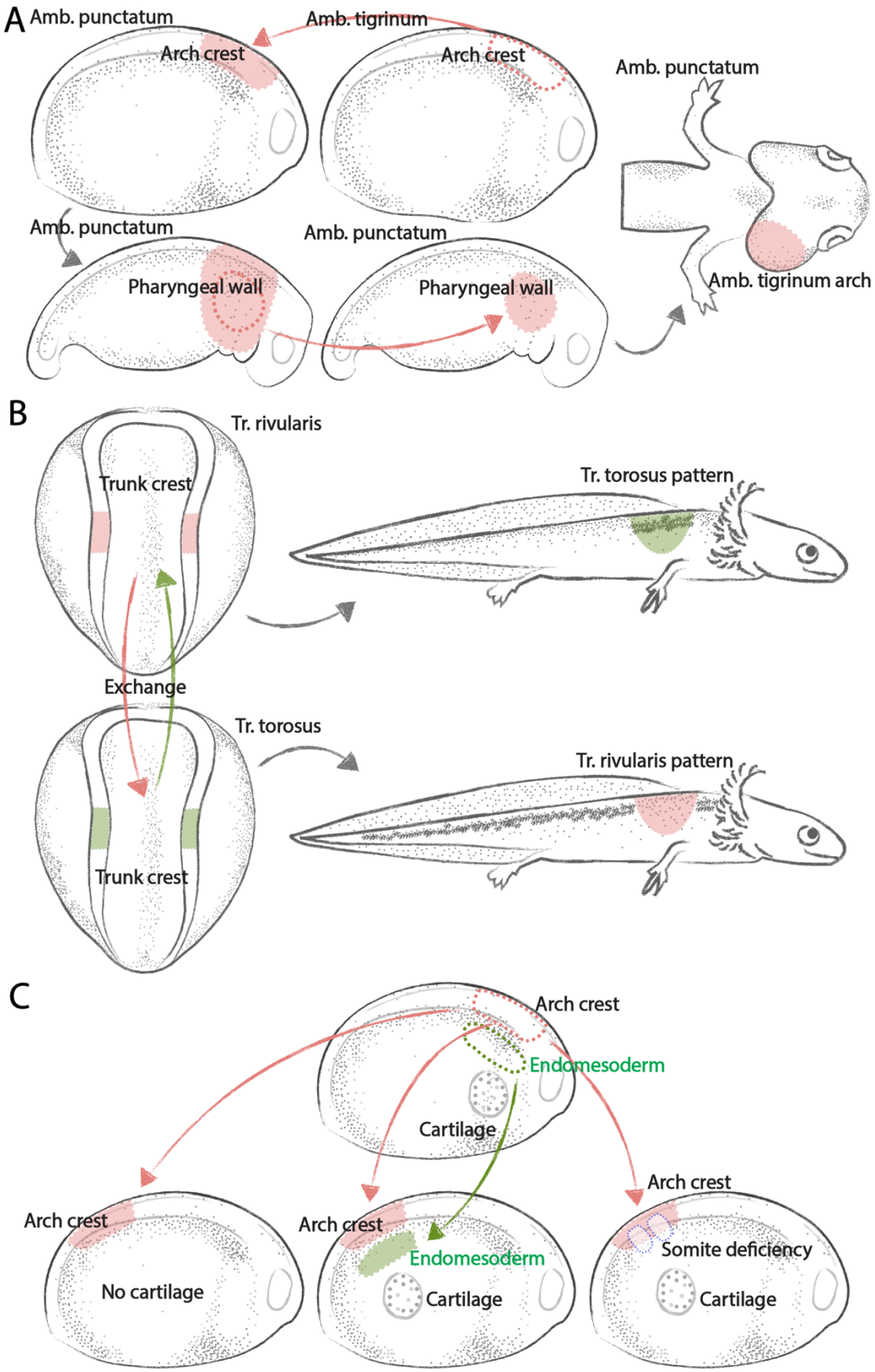
A
Amb. punctatum
Arch crest
Amb. tigrinum
Arch crest
Amb. punctatum
Amb. punctatum
Pharyngeal wall
Amb. punctatum
Pharyngeal wall
Amb. tigrinum arch
B
Tr. rivularis
Trunk crest
Tr. torosus pattern
Exchange
Tr. torosus
Tr. rivularis pattern
Trunk crest
C
Arch crest
Endomesoderm
Cartilage
Arch crest
Arch crest
No cartilage
Arch crest
Endomesoderm
Cartilage
Arch crest
Somite deficiency
Cartilage

Figure 1-1. Understanding neural crest development through transplantation experiments. (A) A neural crest contribution to the gill arch skeleton was mapped by interchanging hindbrain and ectoderm (arch crest, red) between *Amb. punctatum* and *Amb. tigrinum*. After migration, the pharyngeal wall (red) containing neural crest cells from the donor (*Amb. tigrinum*) was transplanted into another host. In the chimeric animal, gill arch skeleton on the transplanted side was larger than the host side due to different growth rates between the two species, demonstrating that the gill arch skeleton originates from hindbrain neural crest[3]. (B) Neural crest cells give rise to melanophores. To understand whether patterning information is intrinsic to neural crest cells or imparted by the environment, trunk neural crest was reciprocally exchanged between two species, *Tr. rivularis* (red) and *Tr. torosus* (green). When grafted into other species, pigment cells continued to form patterns characteristic of the donor, indicating that pigment distribution is dependent on the intrinsic ability of neural crest cells to migrate and aggregate[4]. (C) Heterotopic grafts were utilized to explore the role of tissue interactions during neural crest chondrogenesis. Usually, cranial neural crest (arch crest, red) cells cannot give rise to cartilage when grafted to the trunk. However, when endomesodermal cells (green) were grafted from the gill arch to the trunk, or when the somites in the trunk were removed (blue dashed lines), the grafted cranial crest cells differentiated into cartilage, suggesting that interaction with branchial endomesodermal cells, or signals released by somite removal, are required for chondrogenic differentiation[5]. Colored arrows represent grafting; grey arrows represent development.

1.2.2 QUAIL-CHICK AND OTHER CHIMERAE

Two decades after publication of Hörstadius' treatise on the development of amphibian neural crest, Nicole Le Douarin extended grafting techniques to avian models by taking advantage of the fact that quail and chick embryos resemble one another closely morphologically, but can be easily distinguished at the cellular level; quail cells have condensed heterochromatin in their nucleoli whereas chick cells are euchromatic such that cells of the two species can be distinguished by staining for DNA. In these chimerae, the

dorsal neural tube or neural folds from quail donors are grafted to replace chick host tissue of equivalent stages for lineage tracing, or different stages for exploring the developmental potential of the grafted cells. Utilizing this technique, Le Douarin and colleagues identified several populations of neural crest cells along the body axis. The most rostral "cranial" neural crest cells formed the dermis of the face and neck, large arteries, craniofacial bone and cartilage, as well as cranial ganglia[8]. Vagal neural crest from the caudal hindbrain formed the enteric neurons of the gut, including the large intestines and rectum[9]. Trunk neural crest cells formed dorsal root and sympathetic ganglia as well as contributing to the adrenal gland[6]. Like the vagal neural crest, the sacral neural crest also contributed to the enteric nervous system but was restricted to the post-umbilical region[9]. Neural crest from all axial levels were found to contribute to melanocytes[6].

Quail-chick chimerae were particularly useful for fine resolution fate mapping of the skull, revealing that cranial neural crest derived from each rhombomere contributed to distinct segments of the skull[10,11]. Similarly, the caudal hindbrain or "cardiac" neural crest was shown to contribute to the aorticopulmonary septum of the heart[12,13]. Moreover, surgical removal of the cardiac neural folds resulted in defects in the formation of the outflow tract septum, phenocopying the human congenital defect Persistent Truncus Arteriosus[14], which results in mixing of blood flowing to and from the lungs, and transposition of the vessels.

Quail-chick grafting approaches made it possible to challenge cells by exposing them to diverse environments at distinct times. To analyze the developmental potential of the cranial neural crest, Le Lievre and Le Douarin performed "back-transplantation" experiments by

placing pieces of the nodose ganglion, whose glia are neural crest-derived, onto the neural crest migration pathway of a younger chick embryo. The results showed that some quail cells resumed migration and contributed to autonomic structures, suggesting that environmental factors can turn back the differentiation clock[15]. Typically, the first neural crest cells to emigrate from the neural tube move the furthest ventrally, e.g. forming craniofacial cartilage whereas later migrating cells remain closer to the neural tube. However, when grafted to replace early migrating cells, late migrating cells still gave rise to jaw skeleton, thus demonstrating that the early and late migrating population have similar developmental potential[16]. Whereas these studies demonstrated developmental plasticity, others suggested that axial level-specific patterning information may be inherent to some neural crest populations prior to emigration. For example, in 1983, Drew Noden replaced cells that would normally migrate into second or third arches with cells of the first arch, resulting in ectopic beak formation, suggesting that some neural crest cells retain axial level-specific patterning information[17].

Neural crest formation is controlled by a feed-forward gene regulatory network (GRN) comprised of transcription factors and signaling pathways, partitioned into developmental module that control events from induction at the neural plate border to differentiation into a numerous cell types[18]. While all neural crest cells share common GRN components, there are also regional differences along the body axis. This raises the important question of what transcription factors underlie different neural crest axial identities as distinct as cranial, vagal or trunk? With recent progress in transcriptomics, it has been possible to revisit classical grafting techniques to identify axial level-specific GRNs that determine neural crest identity.

For example, trunk neural crest, when grafted in place of cranial or cardiac neural crest, maintains its original axial identity and cannot give rise to cranial cartilage or contribute to the cardiac outflow septum. However, when genes of a cranial-specific subcircuit of the GRN, namely Sox8, Tfap2b and Ets1, are expressed in the trunk neural tube, this is sufficient to activate a cranial-specific promoter in trunk neural crest cells. Moreover, when this "reprogrammed" trunk neural tube is grafted to the head, these cells can differentiate into cartilage, something that trunk neural crest cells normally cannot do[19]. Similarly, ectopic expression in the trunk neural tube of genes comprising a cardiac crest-specific subcircuit, Sox8, Tgif1 and Ets1, can redirect trunk neural crest cells grafted in place of ablated cardiac neural crest to migrate into the cardiac outflow tract, thus rescuing persistent truncus arteriosus[20]. These two examples demonstrate that subtle differences in gene regulatory architectures can alter neural crest cell fate and account for axial level-specific differences between neural crest subpopulations.

While quails and chicks were chosen for chimeric analyses due to their similarities, other chimeric combinations have been chosen for their distinct characteristics. For example, because ducks have different head and jaw structures compared to quails, the role of neural crest cells in morphogenesis of the cranial skeleton can be analyzed through quail-duck (quck) chimerae[21]. In these qucks, mesenchymal neural crest forms a beak[22] and branchial skeleton[23] characteristic of the donor. These results suggest that, despite environmental and tissue interactions, neural crest-derived cells follow the patterning information of the donor species. More recent studies using the quck chimeric system have explored molecular aspects

of species-dependent morphogenesis, including cell cycle regulators[24], rates of bone resorption[25], and FGF/TGFβ signaling[26].

The mouse-chick chimeric system offers a similar advantage to study morphological features, such as the development of teeth. Whereas teeth have many neural crest-derived components, including condensed dental mesenchyme, dental papilla, odontoblasts, and dentine matrix, chickens lack teeth. Interestingly, combining molar mesenchyme from the mouse with chick epithelium can trigger tooth development in the chick[27,28], suggesting that loss of odontogenesis during avian evolution is associated with the loss of a signal from the chick mesenchyme. Another advantage of rodent-avian chimerae is that this approach enables the use of mammalian genetics in a surgically accessible environment. For example, neural crest cells from splotch mutant mice can migrate normally after being grafted into chick embryos, suggesting that an abnormal tissue interaction is the underlying cause of defective neural crest migration in the mutant rather than a defect intrinsic to the neural crest[29]. Recently, rat-chick chimerae were utilized to study the developmental potential of enteric precursor cells[30]. By transplanting mouse hindgut into a chick-quail host before neural crest colonization, another study was able to show that components of the extracellular matrix, such as Collagen 18 and Agrin, secreted by enteric neural crest precursors direct their migration through a cell-specific microenvironment[31,32]. These methods have also revealed that a limited number of progenitor cells can give rise to a vast number of enteric neurons; enteric precursor cells were termed “superstars” due to their extensive proliferative and colonization ability[33].

Despite their utility, interspecies grafts have some disadvantages. For example, grafts require healing time, such that cell migration might be delayed, potentially causing some early-migrating neural crest derivatives to have been missed. In addition, differences in developmental timing and cellular environment between distinct, albeit related, species may change cell behavior. Thus, many interspecific chimerae have been or are being reproduced with intraspecific grafts using GFP chick donors to circumvent the challenges of using two different species. A useful complement to these experiments is the direct labelling of neural crest cells in situ through non-invasive approaches such as dye or viral labeling, as discussed below.

1.2.3 DYE LABELING

In the 1980s and 1990s, vital dyes such as fluorescent dextrans like lysinated rhodamine dextran (LRD) or the lipophilic dye DiI were widely used for labeling single or populations of neural crest cells. These approaches have the advantage of enabling direct observation of the labelled cell or population using a fluorescence microscope immediately after injection; however, these labels are transient, and the signal only remains visible for a few days due to progressive dilution as neural crest cells divide. Because vital dye is less invasive, flexible and requires almost no healing time compared with grafting experiments, it is an ideal tool to analyze early neural crest migration events. For example, using DiI injection, Serbedzija and coworkers traced dorsolateral and ventral pathways of trunk neural crest migration. By injecting at distinct time points, the authors concluded that cells that migrate first give rise to the most ventral structures[34]. Similarly, another study took advantage of focal injection into

a small group of cells to map the migration of cranial neural crest from particular rhombomeres into the branchial arches[35]. Combined with *ex utero* culturing technique, vital dye also has been applied to study trunk[36], cranial[37,38] and sacral[39] neural crest cells in mammalian systems.

Dye injection is an ideal complementary approach to other lineage tracing methods, such as grafting[40], retroviral lineage tracing[41], or neural crest-specific genetic lines[42]. For instance, one study combined the use of Wnt1-Cre mice with Dil injection at specific axial levels to study lineage contributions to craniofacial mesenchyme. The results showed that the frontal and parietal bones of the skull originate primarily from proliferation of cranial neural crest-derived cells, with only a minor contribution from the adjacent tissue[42].

1.2.4 RETROVIRUSES FOR LINEAGE TRACING

Genetic cell labelling via retroviral infection was developed in birds in the 1980s and 90s and was applied to studies of the central and peripheral nervous system[43]. To prevent horizontal infection of adjacent cells, envelop protein was removed from the viral genome, creating a recombinant replication incompetent retrovirus. By removing its ability to transmit infection to other cells, an infected progenitor cell can faithfully pass the reporter signal only to its descendants[44]. Using LacZ as a reporter, retroviral labelling studies have been applied to map the contributions of cardiac neural crest cells to smooth muscle and neurons of the cardiovascular system[45], and to study vagal neural crest migration into the enteric nervous system[46]. This type of lineage tracing also confirmed trunk neural crest contributions to the sympathetic chain ganglia and melanocytes[47], and colonization of sacral neural crest in the

post-umbilical bowel[34]. The results were consistent with those obtained through vital dye labeling and quail-chick chimera. Because retrovirus can permanently integrate reporters such as LacZ into the host genome, a unique advantage of this tool is that it supports long term analysis without signal dilution through time. On the other hand, retrovirus-based labelling is not ideal for short term analysis, because viral reporters require at least 12 hours after initial contact with the cells to be expressed at sufficient levels for detection.

1.2.5 NEURAL CREST-SPECIFIC DRIVER LINES

Unlike amphibians and birds, mammalian embryos are less accessible to surgical manipulations. On the other hand, injection and transplantation-based approaches only label a subpopulation of cells, leaving open the possibility that some contributions may have been missed. Using the power of genetics, the Cre-loxP system in combination with a neural crest-specific driver line was established to label the neural crest population in mammalian embryos for long term lineage analysis. Commonly used Cre-driver lines, recently reviewed in detail by Debbache et al[48]., include *P3Pro-Cre*[49] and *Wnt1-Cre*[50] for premigratory neural crest, and *Ht-PA-Cre*[51], *P0-Cre*[52], *Sox10-Cre*[53], and *Mef2c-F10N-Cre*[54] for migratory neural crest. Wnt1-Cre has been successfully utilized in fate mapping of cranial[55] and cardiac neural crest cells[56]. The comprehensive nature of *Wnt1-Cre* driver lines can uncover patterns of morphogenesis, which sparse labeling cannot achieve. For example, during tooth and mandibular development, *Wnt1-Cre* labelled neural crest cells are dynamically located at the chondrogenic front, while mesodermal tissue contributes to the interior of the cartilage[55]. To circumvent the potential caveat caused by *Wnt1-Cre* driver lines due to ectopic activation of

Wnt signaling pathway, a new *Wnt1-Cre2* transgenic mouse line was introduced to label the neural crest in a similar manner but without ectopic Wnt expression[57].

A number of reporter lines have also been developed to label neural crest cells in zebrafish. One such line that is widely utilized is *Tg(-4.9sox10:egfp)*[58], in which a *Sox10* regulatory element drives GFP in neural crest and otic placode cells[59,60]. *Foxd3* is also an early neural crest specifier essential for maintaining some neural crest fates[61,62]. Expressed in both cranial and vagal/trunk regions, its enhancers can be used to drive reporter expression in the entire neural crest lineage[63]. Additionally, *Snai1b*[64], *Crestin*[65], and *Fli1a*[66] reporter lines have been harnessed to understand neural crest-related events such as EMT, melanoma initiation, or ectomesenchymal fate decision, respectively.

Taken together, neural crest driver lines in mammalian and zebrafish models provide a stable and reproducible approach for lineage tracing. In addition, neural crest lines with inducible Cre allow for time-specific recombination and clonal analysis, as discussed in the following section. One issue, however, is that these lines can be "leaky" and thus prone to ectopic expression in some cases.

1.3 STEM CELL PROPERTIES OF THE NEURAL CREST: ARE THEY MULTIPOTENT?

Because neural crest cells are highly migratory, it is more challenging to determine whether individual progenitors can give rise to multiple cell types than in progenitors whose progeny remain in close proximity (e.g. neural tube cells). A question of interest has been whether

individual neural crest cells are multipotent (i.e. able to differentiate into several cell types) or restricted (i.e. only able to form single or limited cell types) prior to or during their migration. To distinguish between these possibilities, one needs to trace the progeny of individual progenitors at clonal resolution. In the following sections, we discuss both classical and recent methods for clonal analyses of neural crest stem cells.

1.3.1 IN VITRO CLONAL ANALYSIS

Neural crest clonal analysis was first performed by isolating quail neural crest cells that migrated away from neural tube explants, dissociating them into a single cell suspension, seeding them at low density into multi-well plates, and screening for wells with only one cell. Differentiation of clones was subsequently analyzed by immunostaining with cell fate markers. Using this approach, Sieber-Blum and Cohen showed that single neural crest progenitors give rise to three types of clones: pigmented clones differentiating into melanocytes, unpigmented clones giving rise to adrenergic cells, and mixed clones. Differentiation occurred without direct interaction with non-neural crest cells, suggesting intrinsic multipotency of these progenitors[67]. After 7-10 days in culture, clonal progeny exhibited migratory behavior and differentiation potential when injected back to chick embryos, suggesting that some progenitors remained multipotent[68].

In the early 1990s, Stemple and Anderson showed that individual mammalian neural crest cell clones *in vitro* were able to self-renew and give rise to both neuronal and glia fates[69]. However, single derivative clones were also isolated[70], with TrkC marking neuronal only clones while cKit marked melanocytic only clones[71]. Clonal analysis of quail cranial neural

crest cells revealed broad developmental potential into both neuronal (neurons, glia) and mesenchymal (cartilage, connective tissue) cells of the head[72,73]. This multipotent character was amplified by addition of Sonic hedgehog[72,73]. Taken together, these studies suggest that migratory neural crest cells in amniotes appear to consist of a mixture of multipotent progenitors and progenitors that contribute to a single derivative. Whether the latter were restricted to a particular fate (i.e. unipotent) is unclear since these experiments can only assay cell fate but not developmental potential. Moreover, multipotent premigratory neural crest cells could not be maintained long term until the discovery of neuroepithelial "crestospheres" obtained from neural tubes prior to neural crest emigration[74]. These culture conditions enable neural crest self-renewal and maintenance of multipotency for weeks. When placed in differentiation media or injected back into the embryo, crestosphere cells gave rise to all neural crest derivatives, including glia, neurons, smooth muscle, cartilage and melanocytes[74].

Given the limited tools available for clonal analysis within an embryo, these *in vitro* systems provided invaluable information about intrinsic neural crest stem cell properties. However, cultures are typically maintained in rich medium containing many growth factors as well as on extracellular matrix-rich substrates. Addition of certain grown factors can drive clones toward different pathways of differentiation, with NGF promoting neuronal fate and GGF/neuregulin promoting glial fate[67]. In serum-deprived medium, neural crest cells tend to differentiate towards neuronal fates, whereas the presence of serum facilitates proliferation[75]. The influence of such factors in the culture medium suggests that environmental cues may be important for cell fate determination, thus necessitating studying the stem cell properties and developmental potential of individual neural crest cells within an *in vivo* context.

1.3.2 VITAL DYE LABELING OF A SINGLE NEURAL CREST PROGENITOR

Using microinjection of vital dye into a single premigratory neural crest cell, researchers further extended clonal analysis from cell culture into the embryo. By injecting the fluorescent dextran LRD into individual dorsal neural tube cells as well as some early migrating cells of chick embryos, Bronner-Fraser and Fraser found that descendants of individual precursors localized to distinct sites and formed cell types ranging from sensory and sympathetic neurons to non-neuronal cells and melanocyte precursors. They concluded that some premigratory neural crest cells are multipotent and that multipotency is maintained at migratory stages[76,77]. Supporting results were also obtained from studies in Xenopus laevis[78] and mouse[79]. By adjusting the stage of vital dye injection, Serbedzija et al. showed that contributions to neural crest derivatives vary with time; earlier migrating cells gave rise to both dorsal and ventral structures, such as dorsal root ganglia, sympathetic ganglia and Schwann cells along the ventral root, while clones of late migrating cells were restricted to dorsal structures[79].

Vital dye injection into single progenitor cells was the first approach to provide clonal resolution *in vivo*. Although conceptually simple, this approach is technically challenging and has its limitations. For example, because a limited amount of dye is injected, the fluorescence signal becomes diluted by cell division and is undetectable after a few days. Additionally, for clonal analysis, only one cell is injected per embryo. Thus, it can be challenging to retrieve information since the injected cell may die in some cases or its progeny might be missed during tissue processing. As a result, there was a need for new tools

with increased ease of manipulation and ability to provide permanent labeling at a multiplex level. These shortcomings necessitated the genesis of genetic clonal analysis, as made possible by the advent of Confetti transgenic lines, multicolor retroviral analysis, and genome editing coupled with *in situ* hybridization.

1.3.3 CLONAL ANALYSIS USING MULTICOLOR REPORTERS

In genetic systems, clonal analysis can be achieved by site-specific recombination using neural crest lineage tracing lines that express Cre recombinase under the control of a neural crest-specific promoter, such as *Wnt1*, *Plp* or *Sox10*. When crossed with a reporter line, the genetic marker is permanently expressed in cells in which the promoter is active. Particularly useful for clonal analysis are inducible CreER lines that can be activated by tamoxifen treatment.

The multicolor *Brainbow* reporter[80], initially created for synaptic mapping in the brain, utilizes random recombination of three fluorescent proteins to generate more than 90 colors, each color uniquely assigned as a clone. This multicolor reporter, also called *Confetti*[81], has been broadly applied for clonal analysis in developmental and stem cell biology. By crossing inducible *Wnt1-CreERT* and *Sox10-CreERT2* with an *R26R-Confetti* reporter line, it was shown that premigratory and migratory trunk neural crest cells are multipotent, contributing to cell types as diverse as sensory neurons, sympathetic neurons, glia, and melanocytes within one clone[81]. In conjunction with this, the *Confetti* system has also uncovered clonal organization of cranial neural crest during craniofacial morphogenesis[82] and has revealed the

developmental potential of enteric precursor cells in the intestine to form neuronal-only, glial-only and neuronal-glial bipotent clones[83].

Subsequently, a zebrafish version of *Brainbow*, called *Zebrabow* became available[84]. Due to their transparency, quick development and accessibility, zebrafish embryos and larvae are ideal models in which to combine multicolor clonal analysis with dynamic imaging. Clonal analysis using *Zebrabow* has contributed to our understanding of various aspects of neural crest cell behavior, such as intercalation and oriented cell proliferation in Meckel's cartilage morphogenesis[85] and the role of Schwann cell precursors in cranial and trunk skeletal development[86]. Multicolor *Zebrabow* has also been adapted to explore coordinated cell death during brain development[87].

Brainbow has recently contributed greatly to our understanding of stem cells and regeneration in both fish and mice. For example, it has been used to elucidate the mechanism of aging through clonal selection of epidermal stem cells[88], ploidy reduction during liver regeneration[89], and dynamics in clonal complexity after rounds of muscle injury[90]. In addition, this transgenic system has been invaluable in cancer studies, revealing clonal outgrowth of colorectal cancer[91], clonal restriction in mammary tumors[92], and Lgr5+ intestinal cancer stem cell proliferation and transition to polyclonal clusters with tumor progression[93]. Despite its wide application, multicolor clonal analysis requires careful consideration. First, tamoxifen dosage has to be optimized to achieve the desired recombination frequency. Without titration, labeling density might be too low to visualize multicolor clones, or too high such that it renders clonal relationships hard to interpret. In

addition, the presence of multicolor fluorescent proteins that occupy imaging channels limits the number of antibodies that can be used for downstream analysis, which is also reflected by retroviral multicolor system described in the next section.

1.3.4 RETROVIRAL CLONAL ANALYSIS

Retroviruses can integrate several kilobases of sequence (e.g. encoding barcodes, histological markers, fluorescent proteins) into the host genome and thus are very useful for lineage tracing. Clonal resolution is achieved by sparse labeling of locally restricted clones such as in the retina[94–96] or multiple infection followed by barcode sequencing, more efficient for retrieving clonal information than sequencing for integration sites[97]. Combined with laser capture microscopy for spatially distinct cell populations, barcode-seq can provide highly complex lineage information through multiple infection with up to 105 tags. Accordingly, one study has shown that neural stem cells in mice become regionalized and diverge from other lineages by E11.5[98]. Although the method provides clonal resolution while preserving spatial information, laser capture microscopy can be time-consuming, thus limiting the number of samples that can be assayed.

In the neural crest field, histological markers and fluorescent proteins have been preferable because spatial information is essential for examining lineage relationships in this highly migratory cell type. Clonal analysis using replication incompetent avian (RIA) retroviruses (covered in detail in Chapter II-IV) was made possible by multiple simultaneous infection events, which occur very rarely. When a viral mixture infects the cells, the probability of a cell being infected by 2, 3, or 4 viral particles concomitantly can be calculated, assuming

each viral particle has equal opportunity to enter the cell[99]. As probability of multiple infections is extremely low, 2 or more viruses marking the same cell tends to occur once per embryo. Therefore, progeny carrying the same set of histological/fluorescent markers can be considered a clone. On this basis, Frank and Sanes used two viruses encoding LacZ in the cytosol or nucleus to map clonally related cells in the dorsal root ganglia, providing evidence for neural crest multipotency[100].

This method was recently extended by incorporating five fluorescent proteins, targeted to the nucleus, membrane, mitochondria or actin filaments, into RIA retroviruses, allowing multiplex clonal analysis of trunk neural crest cells[101]. Infection of a single cell by two or more viruses encoding unique colors and/or subcellular localizations yields easily uniquely identifiable clonal descendants. Applying this to trunk neural crest cells confirmed their multipotency, similar to results from single cell microinjections of LRD in chick and *Confetti* in the mouse[76,77,81,101]. Given that three different methods in two different species generated identical results, this is a nice example of "reproducibility" in science.

Retroviral cell labeling also can be used to achieve stable molecular perturbation. For instance, retroviral overexpression of Id2 was shown to convert ectodermal cells into neural crest cells, indicating that regulation of Id2 is required for maintaining ectodermal fate[102]. Progress in viral engineering enables combining molecular perturbations with clonal analysis to understand fate decisions within clonally related cells. Compared with the *Confetti* system, multicolor retroviral lineage analysis provides more flexible spatiotemporal control. However, one should note that most retroviruses can only infect actively dividing cells[103,104].

Additionally, as with tamoxifen titration in the *Confetti* system, precise titration is required to achieve the proper level of coinfection to guarantee clonality.

1.3.5 SINGLE-CELL SPATIAL TRANSCRIPTOMICS AND GENOME EDITING-BASED LINEAGE RECONSTRUCTION

All clonal analysis approaches mentioned so far obtain clonal information based on cell counts, locations and cell fates observed at the last time point, thus providing a single snapshot of cell fate. However, a complete lineage tree delineating each branching point or round of cell division is far more complex than that observed at the endpoint. Much of the information occurring during neural crest induction, delamination, migration, condensation, differentiation and morphogenesis is therefore lost. This contrasts with elegant lineage analysis in C. elegans by Sulston and colleagues, which allowed direct visualization of the entire cell lineage of the organism[105].

Single-cell spatial transcriptomics, by dissecting cell trajectories at spatiotemporal level, aims to identify transient states and branch points in early cell fate decision[106]. Using this approach, Soldatov et al. identified transcription factors that bias neural crest cells towards sensory versus other cells fates, autonomic versus mesenchymal fates across multiple axial levels and migration states, therefore providing a comprehensive spatiotemporal map of murine neural crest fate decisions[106].

Another approach termed ‘memory by engineered mutagenesis with optical *in situ* readout’ (MEMOIR) holds the promise of achieving complete lineage reconstruction in complex

systems[107]. In this approach, CRISPR-Cas9 randomly deletes a series of barcoded sequences during cell division. The deletion is inherited by all daughter cells, with each daughter cell undergoing another round of random deletion and so forth. In this way, a cell-specific deletion signature will record lineage information within its genome, which subsequently can be detected by single molecule fluorescence in situ hybridization (smFISH). As proof of principle, this method was applied in embryonic stem cells and was shown to be compatible with simultaneous detection of the pluripotency regulator Esrrb[107]. Prior to the development of MEMOIR, a technique called 'genome editing of synthetic target arrays for lineage tracing' (GESTALT) utilized DNA/RNA sequencing to retrieve edited barcodes and reconstructed a lineage tree with about 200, 000 cells in zebrafish embryos[108]. Based on a similar principle, another approach used CRISPR-Cas9 to generate random insertions and deletions in tandem GFP or RFP sequences, which can be retrieved with single-cell RNA sequencing to obtain developmental history[109,110]. However, these approaches require generation of a transgenic line prior to lineage analysis. Recently, a new method has been developed to identify and edit endogenous 5'G sequence in non-functional genomic region for CRISPR-Cas9-based phylogenetic fate mapping. This approach is useful in species in which transgenic animals cannot be easily obtained[111].

It is worth noting that, GESTALT and other methods based on deep sequencing obtain clonal information of a large number of cells at the expense of spatial information. Unfortunately, such spatial information is essential for neural crest lineage tracing. Thus, MEMOIR, although tracking fewer clones and genes, is complementary to sequencing-based GESTALT. Built upon MEMOIR, a technique termed ZOMBIE combines the advantage of

high-density barcoding through *in vitro* transcription with preservation of spatial information[112]. Future efforts toward a complete neural crest lineage tree hold the promise of applying these genome editing methods to uncover previously inaccessible information, including but not limited to: How do neural crest precursors make lineage choices? Which derivatives are clonally diverse, and which are derived from a limited number of progenitor cells? Is there a clonal selection process after neural crest cells aggregate to form derivatives like ganglia or cartilage?

1.4 TISSUE-SPECIFIC ROLES: TRACING NEURAL CREST CELLS IN ADULTS

Although the neural crest is a transient structure during development, neural crest-derived cells persist throughout life[113]. In addition, neural crest-derived cells that harbor stem cell properties reside within many adult tissues[113]. This raises the possibility that their unique developmental history can be harnessed in the adult during injury or disease. Neural crest-derived cells in the adult encompass could either be undifferentiated cells or differentiated ones with plasticity to dedifferentiate under some circumstances. Here, we use two examples — the adult heart and cancer — to demonstrate how lineage tracing tools can help uncover the role of neural crest cells beyond embryogenesis. While heart regeneration and NF1-associated tumor formation both suggest a role for already differentiated cells, the function of undifferentiated neural crest cells remains to be explored and may be important in other situations.

1.4.1 HEART DEVELOPMENT AND REGENERATION

The adult zebrafish heart has the remarkable capacity to regenerate when up to 20% of the ventricle is surgically removed[114], generating great interest regarding gene regulation and cell lineage decisions contributing to new cardiomyocytes during repair. A key question is whether new cardiomyocytes derive from a resident stem cell population, or from dedifferentiation of existing cardiomyocytes. Using the inducible transgenic line *tg-cmlc2a-cre-Ert2:tg-cmlc2a-LnL-GFP* to trace cardiomyocytes, Jopling et al. discovered that new cardiomyocytes are derived by dedifferentiation and proliferation of pre-existing cardiomyocytes[115]. But whether dedifferentiation-proliferation was restricted to a specific subpopulation of cardiomyocytes remained unclear. Multiple lineage analyses suggest that the adult zebrafish ventricle is indeed heterogeneous, comprised of multiple subpopulations with distinct developmental origins. For example, in addition to the first and second heart fields, which are derived from mesoderm, neural crest cells migrate into the bulbus arteriosus, atrium and ventricle, as shown by uncaging fluorescein[116,117], cell transplantation of fluorescently injected donors, and laser induction of hsp70-eGFP zebrafish[81]. This result was recently confirmed using advanced genetic lines, specifically *NC:NfsB-mCherry* for short term and *Tg(NC:mCherry)* for long term tracing[118]. This cardiac neural crest contribution is essential for normal heart function, as surgical ablation of the neural crest in zebrafish leads to decreased stroke volume, ejection fraction, and cardiac output[80]. In addition, genetically induced removal of neural crest-derived cardiomyocytes causes hypertrophic cardiomyopathy[119]. Together, these results demonstrate that zebrafish neural crest-derived cardiomyocytes are functionally important in the heart.

There is also evidence suggesting a neural crest contribution to the mammalian heart, which exhibits limited regeneration during a narrow window up to postnatal day 7[120]. Cardiospheres isolated from mammalian hearts, when injected into chick embryos, migrate like neural crest cells into the cardiac outflow tract[114]. Another study, using *cKitCreERT2/+* and *Wnt1::Flpe* mouse lineage tracing lines, showed that neural crest cells give rise to a cKit+ stem cell population in the heart[121]. Analysis of the *P0Cre-GFP* transgenic mouse line also showed the presence of neural crest-derived cells as ventricular cardiomyocytes[122]. Moreover, these cells migrated toward the injury site through MCP-1 mediated chemoattraction[123], indicating a role for cardiac neural crest-derived cells in heart repair.

Recently, the contribution of neural crest cells to heart repair in amniotes was confirmed using *Wnt1-Cre* mice and retroviral lineage analysis in chick embryos[124] (Fig.1-2A). Consistent with this, genetic ablation of cardiac neural crest cells in zebrafish impairs heart regeneration*125*. Sox10 and other neural crest GRN components are upregulated upon injury [124,125](Fig.1-2B, C), suggesting that neural crest-derived cardiomyocytes contribute to heart regeneration. Future studies will elucidate the mechanisms underlying migration and proliferation of neural crest-derived cells during heart regeneration. Molecularly, CXCL2a expressed in the epicardium can chemoattract cardiac neural crest-derived cardiomyocytes through the receptor CXCR4[128], making this a candidate ligand-receptor pair worthy of further analysis. Other examples implicating neural crest-derived cells in regeneration include a role for Schwann cell precursors (SCPs) in limb regeneration[126] and chromaffin cell formation[127].

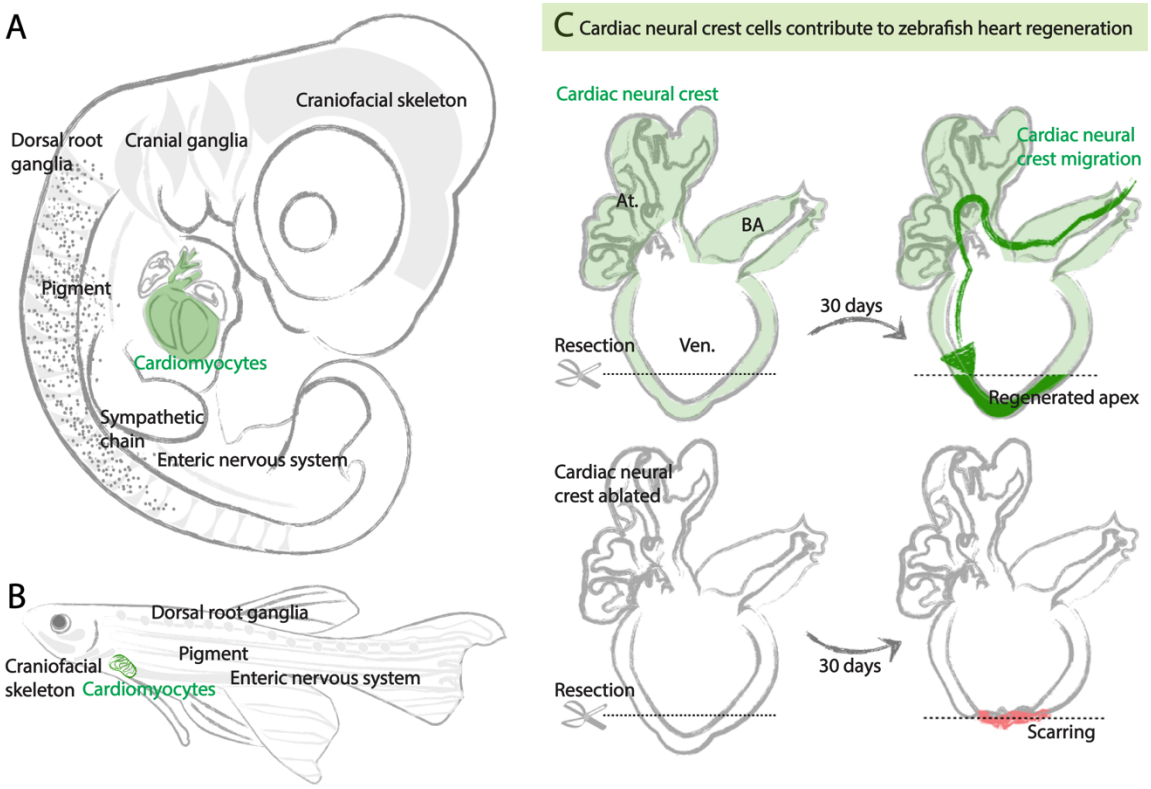

Figure 1-2. Neural crest-derived cardiomyocytes contribute to zebrafish heart regeneration. (A, B) Neural crest-derived cells persist as differentiated or stem cells residing in multiple organs, such as the craniofacial skeleton, peripheral nervous system, pigment of the skin (grey), and cardiovascular systems (green) in both amniotes (A, embryonic day (E) 5 chick) and fish (B, adult). (C) In the normal zebrafish heart, neural crest cells give rise to heart muscle (green) in the bulbus arteriosus (BA), atria (At.) and ventricles (Ven.). When the apex is surgically removed, these neural crest-derived cells participate in heart regeneration by migrating towards the injury site and redeploying genes that regulate neural crest development such as Sox10. Genetic ablation of these cardiac neural crest cells disrupts heart regeneration, leading to scarring (red)[124,125]. Grey arrows represent regeneration period.

1.4.2 TUMOR DEVELOPMENT

Neural crest-derived cells, including melanocytes and cells of the peripheral nervous system (PNS), can develop into benign or malignant tumors upon genetic mutation (Fig.1-3A). Neurofibromatosis type 1 (NF1), characterized by café-au-lait spots, plexiform or cutaneous neurofibromas, gliomas, and cardiovascular abnormalities, is caused by loss of *Nf1*, which encodes a tumor suppressor in the Ras signaling pathway. A longstanding question is whether tumor forming cells arise from undifferentiated neural crest stem cells or differentiated PNS cells. Conditional deletion of *Nf1* in the PNS (*P0a-Cre: Nf1fl/-*) suggested that tumors formed from differentiated neural crest-derived Schwann cells[129]. Similarly, *Nf1*-deficient neural crest stem cells developed into normal PNS derivatives, but tumors occurred later in the abnormally differentiated Remak bundle[130]. Taken together, the results suggest that *Nf1* deficiency predisposes neural crest progenitor cells to tumor development after differentiation (Fig.1-3B), highlighting the role of differentiated cells in tumor formation. Finally, using a Schwann cell precursor (SCP) driver line (*Dhh-Cre*) to delete *Nf1* in SCPs resulted in plexiform neurofibroma, thus narrowing down the embryonic origin of neurofibroma-forming cells to SCPs[131], with *PLP-CreERT* revealing the most susceptible time window of *Nf1* loss to before SCP maturation[132]; these neurofibroma-forming SCPs are localized in the dorsal root ganglia[133].

Embryonic neural crest cells share many properties with cancer cells, including multipotency, migratory ability, general invasiveness, and transcriptional/epigenetic signatures[134,135]. A recent study used the *Crestin:EGFP* reporter line to create a zebrafish

model of melanoma initiation in which neural crest cells could be visualized and compared during embryogenic development and melanoma initiation. In *BRAF* mutant and *p53*-deficient cancerized fish, *Sox10* expression correlates with melanoma formation, activating the same regulatory elements as in neural crest cells[65] (Fig.1-3C). In another zebrafish model, mcr:NRAS, the melanoma gene expression pattern was highly reminiscent of embryonic neural crest cells, as shown by upregulation of *crestin*, *sox10*, and *dlx2a*[136]. *Yy1*, transcription factor that regulates both neural crest development and melanoma initiation via regulating MITF and c-MYC expression[137]. A mutant model of melanoma developed in *Xiphophorus* hybrids, which form malignant melanoma under the control of oncogenic *Xmrk*, has provided insight into the signaling pathways and adhesion molecules involved in melanoma, especially in comparison to human skin cancer[138–140]. Exploring similarities and differences between normal developmental processes and tumor formation can inform upon ontogeny of neural crest-derived tumors. Thus, neural crest lineage tracing is an indispensable approach to identify tumor initiating cells that are only transiently present and challenging to detect.

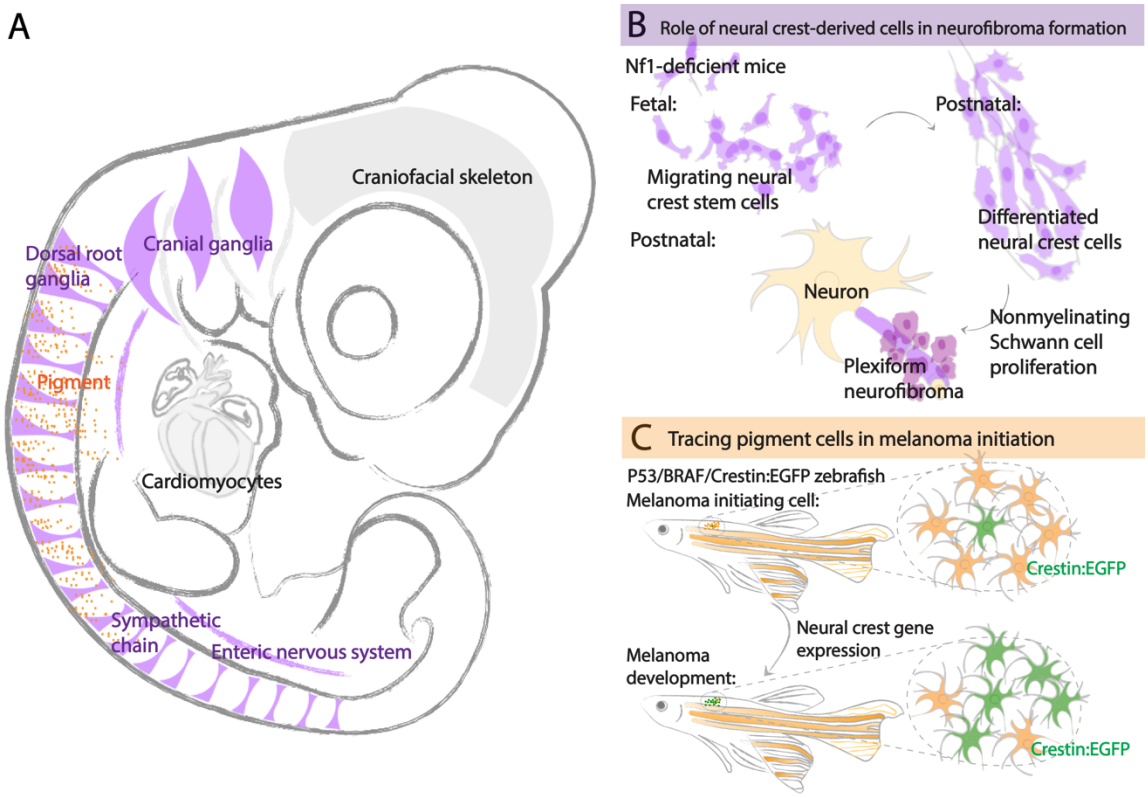

Figure 1-3. Tracing neural crest cells in tumor development. (A) Neural crest-derived cells contribute to the peripheral nervous system (PNS, purple) and pigment of the skin (orange), as illustrated in a chick embryo at E5. (B) Plexiform neurofibroma is a tumor of the PNS caused by mutations in the tumor suppressor gene *Nf1*. By tracing neural crest cells throughout the tumorigenesis process in Nf1 knockout mice, studies found that *Nf1*-deficient neural crest cells differentiate normally. Tumors subsequently form by proliferation of differentiated Schwann cells. Thus, neural crest stem cells are not directly responsible for plexiform neurofibroma[129,130]. (C) Neural crest lineage tracing helps identify early signs of melanoma. In a zebrafish model with oncogenic mutations in *P53* and *BRAF*, melanoma initiation is characterized by a normal pigment cell (orange) re-expressing neural crest-related genes, visualized by *crestin:EGFP* (green). This particular cell transforms into a neural crest progenitor-like fate and later expands into a tumor[65]. Grey arrows represent development.

1.5 CONCLUSIONS

Lineage tracing at the population and clonal level has made essential contributions to discoveries in the neural crest field by application to a multitude of vertebrate embryos. While several reports have shown that many newly formed neural crest cells at cranial and trunk levels are multipotent, it is likely that that they become progressively fate restricted as they migrate and reach their final destinations[106]. Thus, the embryonic neural crest is a transient stem cell type. Interestingly, neural crest-derived cells persist into adulthood and may have important roles in tissue regeneration. On the other hand, abnormalities in these cells can lead to birth defects and several adult cancers. Thus, improved lineage tracing methods can extend knowledge of the neural crest from the early embryo to disease and injury models.

It is worth noting that only vertebrates have *bona fide* neural crest cells. However, neural crest-like cells have been identified in non-vertebrate chordates like ascidians which have pigment cells[141] and peripheral neuroendocrine cells[142]. Even the basal chordate amphioxus has migratory ectodermal cells[143] though not derived from the neural tube or neural plate borders. A major difference is that the precursors of these chordate cells tend to give rise to single cell types rather than being multipotent. In contrast, basal jawless vertebrates like the sea lamprey have migratory and multipotent neural crest cells albeit less regionalized along the body axis than in jawed vertebrates. Accordingly, the lamprey neural crest GRN is most similar to the trunk neural crest GRN of amniotes. Indeed, region-specific neural crest GRN

components appear to have been progressively added to the neural crest GRN during the course of vertebrate evolution[7].

All lineage tracing methods described herein can be mixed and matched (Fig.1-4), making the advantages adaptable to numerous model systems (Table 1-1). Future studies are likely to refine current tools towards ever higher resolution and hold the promise of providing transcriptional and spatial lineage information coupled with identifying clonal relationships. Through genome editing or barcoding, clonal analysis approaches can be combined with RNA-seq to understand changes in transcriptional landscapes during critical cell fate decisions. Clonal analysis coupled with molecular perturbations will provide a deeper understanding of the ways that differential gene expression can drive clonal diversification. At the same time, high-resolution imaging can be used to dynamically assess cell behavior during clonal expansion, providing new opportunities to manipulate cell fates in stem cell, regenerative and cancer studies. These combined approaches are likely to fulfill Hörstadius' expectations some 70 years ago that[2] "further investigations with a variety of methods and giving due consideration to possible sources of error will certainly give us a deeper insight into… the developing neural crest."

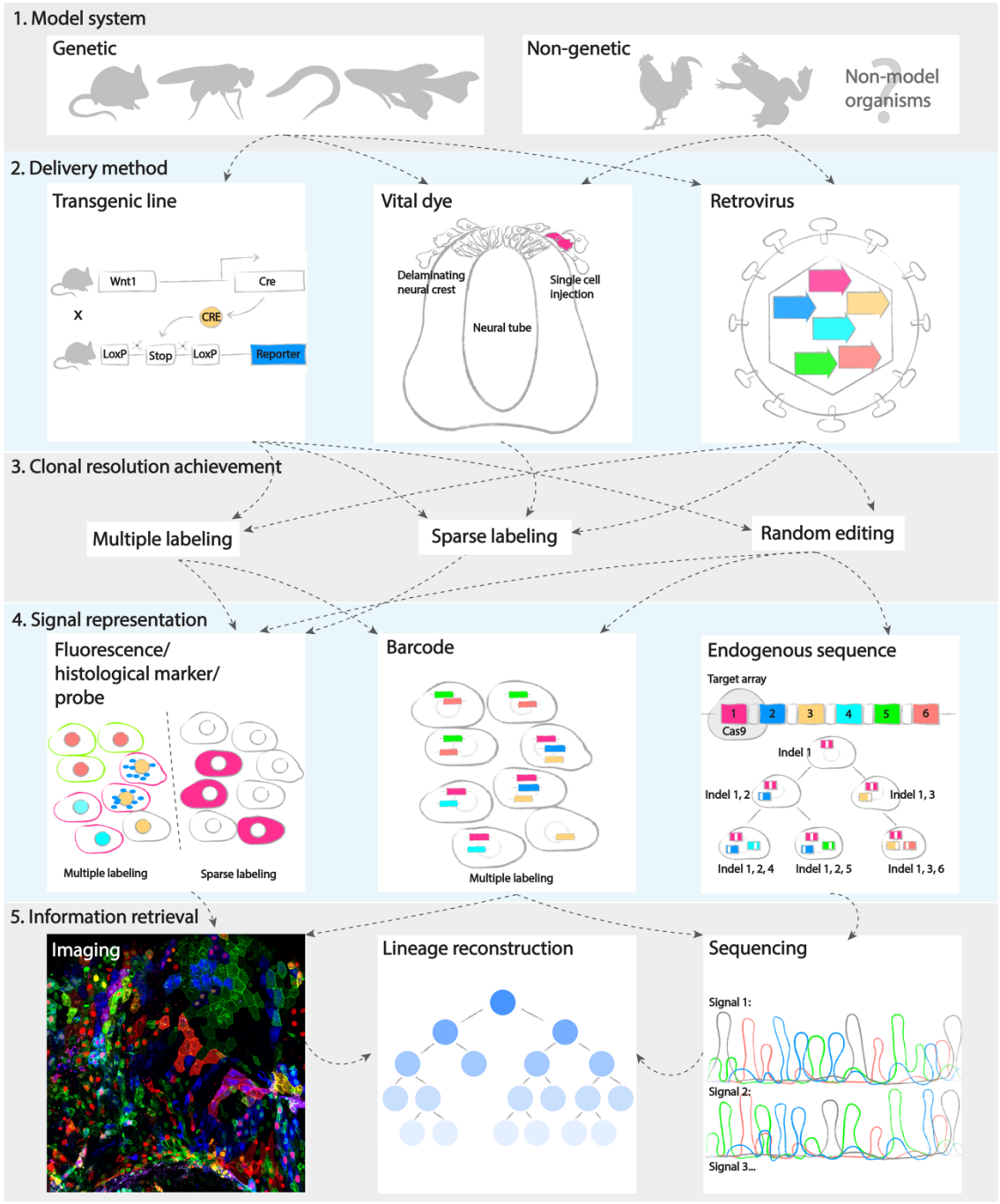

Figure 1-4. Conceptual summary of clonal analysis workflow. Clonal analysis approaches can involve the following five elements: model systems (1), delivery methods (2), ways to achieve clonal resolution (3), signal representation, and information retrieval approaches (5). (1, 2) Stable transgenic lineage tracing lines can only

be obtained with genetic systems. However, non-genetic and new model organisms are also accessible through vital dye injection and retroviral transduction. (3) Clonal resolution is achieved by rare events such as multiple labeling, sparse labeling and random editing with CRISPR/Cas9 system. (4) Depending on how clonal resolution is achieved, one can utilize imageable materials such as fluorescent proteins, histological markers, probes, or sequences such as barcodes and endogenous CRISPR/Cas9 target arrays for downstream analysis. (5) All imaging and sequencing-based methods can obtain endpoint lineage information. Phylogenetic lineage reconstruction can be provided by multiplexed genome editing. Sets of fluorescent markers, barcodes and endogenous target arrays are color-coded to indicate heterogeneity (magenta, blue, yellow, cyan, green, red). Dashed arrows suggest available choices in the following step.

Table 1. Tools for neural crest lineage tracing and their advantages

Tools/advantages	Vital dye	Transplantation	Genetic line	Retrovirus	Genome editing
Clonal resolution	Yes	Yes (combined with electroporation of *Brainbow* construct)	Yes	Yes	Yes
Flexibility to change environment	No	Yes	No	No	No
Non-invasive	Yes	No	Yes	Yes	Yes
Temporal control	Yes	Yes	Yes	Yes	Yes
Long term	No	Yes	Yes	Yes	Yes
Multiplexed	No	Yes	Yes	Yes	Yes
Lineage tree reconstruction	No	No	No	No	Yes
Non-accessible models	No	No	Yes	No	Yes

A summary of each lineage-tracing method covered in this Review.
Clonal resolution, the ability to follow clonal relationships between cells; flexibility to change environment, being able to challenge a cell by moving it into regions that are distinct from its origin; non-invasive, to conduct experiments with the endogenous environment undisrupted; temporal control, being able to initiate/terminate experiments at desired time points; long term, supports analysis into late developmental stages and adulthood; multiplexed, the ability to obtain multiple readouts within an individual embryo, a property associated with clonal analysis; lineage tree reconstruction, allows the recording of each round of cell division; non-accessible models, can be applied to embryos *in utero*.

Table 1-1. Advantages of tools for neural crest lineage tracing. Table summarizes advantages of each lineage tracing method covered in Chapter I. Definition of terms: clonal resolution, ability to follow clonal relationship between cells; flexibility to change environment, being able to challenge a cell by moving it into regions distinct from its origin; non-invasive, to conduct experiments with endogenous environment undisrupted; temporal control, being able to initiate/terminate experiments at desired timepoints; long term, supports analysis into late developmental stages and adulthood; multiplexed, ability to obtain multiple readouts within an individual embryo, a property associated with clonal analysis; lineage tree reconstruction, information allows recording each round of cell division; non-accessible models, tools available for embryos that develop *in utero*.

ACKNOWLEDGEMENT

We thank Dr. Victoria Prince for valuable discussions and suggestions on the original manuscript. This work was supported by NIHR01DE027568, NIHRO1HL14058, and NIH DE027568 to M.E.B.

1.6 ORGANIZATION OF THE THESIS

The key question we address in the thesis is whether neural crest cells are a group of multipotent cells capable of giving rise to a wide range of cell types, or are some fate-determined cells. The thesis follows a storyline of first introducing the question, advantages and limitations of previously used techniques (Chapter I). Second, we develop a new retroviral tool (RIAs) that combines several advantages such as its usage in non-genetic models, ability to perform targeted infection, multiplexing, and ability to retain the signal in the long term (Chapter II). We then apply single-color RIAs to population level lineage tracing (Chapter III) and multicolor RIAs to combinatorial clonal analysis accompanied by time-lapse imaging (Chapter IV), leading to a conclusion in Chapter V.

1.7 REFERENCES

1. His, W. (1868). Untersuchungen über die erste Anlage des Wirbelthierleibes: die erste Entwickelung des Hühnchens im Ei.

2. Hörstadius, S. (1950). The neural crest, its properties and derivatives in the light of experimental research. *Oxford University Press.*

3. Harrison, R. (1935). Heteroplastic grafting in embryology. *Harvey Lect. Balt*. 29.

4. Twitty, V. C. (1945). The developmental analysis of specific pigment patterns. *J. Exp. Zool*. 100, 141–178.

5. Hörstadius, S. & Sellman, S. (1946). Experimentelle Untersuchungen über die Determination des knorpeligen Kopfskelletes bei Urodelen. *Stockholm: Almquist & Wiksell*.

6. Le Douarin, N. & Kalcheim, C. (1999). The Neural Crest. *Cambridge University Press*.

7. Martik, M. L. et al. (2019). Evolution of the new head by gradual acquisition of neural crest regulatory circuits. *Nature* 574, 675–678.

8. Le Lièvre, C. S. & Le Douarin, N. M. (1975). Mesenchymal derivatives of the neural crest: Analysis of chimaeric quail and chick embryos. *J Embryol Exp Morphol.* 34, 125-54.

9. Le Douarin, N. M. & Teillet, M. A. (1973). The migration of neural crest cells to the wall of the digestive tract in avian embryo. *J. Embryol. Exp. Morphol*. 30, 31–48.

10. Couly, G. F., Coltey, P. M. & Le Douarin, N. M. (1993). The triple origin of skull in higher vertebrates: A study in quail-chick chimeras. *Development* 117(2): 409-29.

11. Kontges, G. & Lumsden, A. (1996). Rhombencephalic neural crest segmentation is preserved throughout craniofacial ontogeny. *Development* 122(10): 3229-42.

12. Phillips, M. T., Kirby, M. L. & Forbes, G. (1987). Analysis of cranial neural crest distribution in the developing heart using quail-chick chimeras. *Circ. Res.* 60, 27–30.

13. Miyagawa-Tomita, S., Waldo, K., Tomita, H. & Kirby, M. L. (1991). Temporospatial study of the migration and distribution of cardiac neural crest in quail-chick chimeras. *Am. J. Anat.* 192, 79–88.

14. Kirby, M. L., Gale, T. F. & Stewart, D. E. (1983). Neural crest cells contribute to normal aorticopulmonary septation. *Science* 220 (4601):1059-61.

15. Ayer-Le Lievre, C. S. & Le Douarin, N. M. (1982). The early development of cranial sensory ganglia and the potentialities of their component cells studied in quail-chick chimeras. *Dev. Biol.* 94, 291–310.

16. Baker, C. V., Bronner-Fraser, M., Le Douarin, N. M. & Teillet, M. A. (1997). Early- and late-migrating cranial neural crest cell populations have equivalent developmental potential in vivo. *Development* 124(16): 3077-87.

17. Noden, D. M. (1983). The role of the neural crest in patterning of avian cranial skeletal, connective, and muscle tissues. *Dev. Biol.* 96, 144–165.

18. Sauka-Spengler, T. & Bronner-Fraser, M. (2008). A gene regulatory network orchestrates neural crest formation. *Nature Reviews Molecular Cell Biology* 9, 557–568.

19. Simoes-Costa, M. & Bronner, M. E. (2016). Reprogramming of avian neural crest axial identity and cell fate. *Science* 352 (6293):1570-3.

20. Gandhi, S., Ezin, M. & Bronner, M. E. (2020). Reprogramming axial level identity to rescue neural-crest-related congenital heart defects. *Dev. Cell* 53, 300-315.e4.

21. Lwigale, P. Y. & Schneider, R. A. (2008). Chapter 3 other chimeras: quail-duck and mouse-chick. *Methods in Cell Biology* 87, 59–74.

22. Schneider, R. A. & Helms, J. A. (2003). The cellular and molecular origins of beak morphology. *Science* 299 (5606):565-8.

23. Tucker, A. S. & Lumsden, A. (2004). Neural crest cells provide species-specific patterning information in the developing branchial skeleton. *Evol. Dev*. 6, 32–40.

24. Hall, J. et al. (2014). Evolution of a developmental mechanism: Species-specific regulation of the cell cycle and the timing of events during craniofacial osteogenesis. *Dev. Biol*. 385, 380–395.

25. Ealba, E. L. et al. (2015). Neural crest-mediated bone resorption is a determinant of species-specific jaw length. *Dev. Biol*. 408, 151–163.

26. Woronowicz, K. C., Gline, S. E., Herfat, S. T., Fields, A. J. & Schneider, R. A. (2018). FGF and TGFβ signaling link form and function during jaw development and evolution. *Dev. Biol*. 444, S219–S236.

27. Kollar, E. J. & Fisher, C. (1980). Tooth induction in chick epithelium: Expression of quiescent genes for enamel synthesis. *Science* 207 (4434):993-5.

28. Mitsiadis, T. A., Chéraud, Y., Sharpe, P. & Fontaine-Pérus, J. (2003). Development of teeth in chick embryos after mouse neural crest transplantations. *Proc. Natl. Acad. Sci*. U. S. A. 100, 6541–6545.

29. Serbedzija, G. N. & McMahon, A. P. (1997). Analysis of neural crest cell migration in splotch mice using a neural Crest-Specific LacZ reporter. *Dev. Biol*. 185, 139–147.

30. White, P. M. & Anderson, D. J. (1999). In vivo transplantation of mammalian neural crest cells into chick hosts reveals a new autonomic sublineage restriction. *Development* 126(19): 4351-63.

31. Nagy, N. & Goldstein, A. M. (2006). Intestinal coelomic transplants: A novel method for studying enteric nervous system development. *Cell Tissue Res*. 326, 43–55.

32. Nagy, N. et al. (2018). Collagen 18 and agrin are secreted by neural crest cells to remodel their microenvironment and regulate their migration during enteric nervous system development. *Development* 145(9): dev160317.

33. Cheeseman, B. L., Zhang, D., Binder, B. J., Newgreen, D. F. & Landman, K. A. (2014). Cell lineage tracing in the developing enteric nervous system: Superstars revealed by experiment and simulation. *J. R. Soc. Interface* 11, 20130815.

34. Serbedzija, G. N., Bronner-Fraser, M. & Fraser, S. E. (1989). A vital dye analysis of the timing and pathways of avian trunk neural crest cell migration. *Development* 106(4):809-16.

35. Lumsden, A., Sprawson, N. & Graham, A. (1991). Segmental origin and migration of neural crest cells in the hindbrain region of the chick embryo. *Development* 113(4): 1281-91.

36. Serbedzija, G. N., Fraser, S. E. & Bronner-Fraser, M. (1990). Pathways of trunk neural crest cell migration in the mouse embryo as revealed by vital dye labelling. *Development* 108 (4): 605-12.

37. Serbedzija, G. N., Bronner-Fraser, M. & Fraser, S. E. (1992). Vital dye analysis of cranial neural crest cell migration in the mouse embryo. *Development* 116 (2): 297-307.

38. Trainor, P. A., Sobieszczuk, D., Wilkinson, D. & Krumlauf, R. (2002). Signalling between the hindbrain and paraxial tissues dictates neural crest migration pathways. *Development* 129(2): 433-42.

39. Serbedzija, G. N., Burgan, S., Fraser, S. E. & Bronner-Fraser, M. (1991). Vital dye labelling demonstrates a sacral neural crest contribution to the enteric nervous system of chick and mouse embryos. *Development* 111(4):857-66.

40. Krotoski, D. M., Fraser, S. E. & Bronner-Fraser, M. (1988). Mapping of neural crest pathways in Xenopus laevis using inter- and intra-specific cell markers. *Dev. Biol*. 127, 119–132.

41. Pomeranz, H. D., Rothman, T. P. & Gershon, M. D. (1991). Colonization of the post-umbilical bowel by cells derived from the sacral neural crest: Direct tracing of cell migration

using an intercalating probe and a replication-deficient retrovirus. *Development* 111(3): 647-55.

42. Yoshida, T., Vivatbutsiri, P., Morriss-Kay, G., Saga, Y. & Iseki, S. (2008). Cell lineage in mammalian craniofacial mesenchyme. *Mech. Dev.* 125, 797–808.

43. Sanes, J. R. (1989). Analysing cell lineage with a recombinant retrovirus. *Trends. Neurosci.* 12, 21–28.

44. Chen, C. M. et al. (1999). Production and design of more effective avian replication-incompetent retroviral vectors. *Dev. Biol.* 214, 370–84.

45. Poelmann, R. E., Mikawa, T. & Groot, A. C. G. (1998). Neural crest cells in outflow tract septation of the embryonic chicken heart: Differentiation and apoptosis. *Dev. Dyn*. 212, 373–384.

46. Epstein, M. L., Mikawa, T., Brown, A. M. C. & McFarlin, D. R. (1994). Mapping the origin of the avian enteric nervous system with a retroviral marker. *Dev. Dyn*. 201, 236–244.

47. Stocker, K. M., Brown, A. M. C. & Ciment, G. (1993). Gene transfer oflacZ into avian neural tube and neural crest cells by retroviral infection of grafted embryonic tissues. *J. Neurosci. Res.* 34, 135–145.

48. Debbache, J., Parfejevs, V. & Sommer, L. (2018). Cre-driver lines used for genetic fate mapping of neural crest cells in the mouse: An overview. *Genesis* 56, e23105.

49. Li, J., Chen, F. & Epstein, J. A. (2000). Neural crest expression of Cre recombinase directed by the proximal Pax3 promoter in transgenic mice. *Genesis* 26, 162–164.

50. Danielian, P. S., Muccino, D., Rowitch, D. H., Michael, S. K. & McMahon, A. P. (1998). Modification of gene activity in mouse embryos in utero by a tamoxifen-inducible form of Cre recombinase. *Curr. Biol*. 8, 1323–1326.

51. Pietri, T., Eder, O., Blanche, M., Thiery, J. P. & Dufour, S. (2003). The human tissue plasminogen activator-Cre mouse: A new tool for targeting specifically neural crest cells and their derivatives in vivo. *Dev. Biol*. 259, 176–187.

52. Yamauchi, Y. et al. (1999). A novel transgenic technique that allows specific marking of the neural crest cell lineage in mice. *Dev. Biol*. 212, 191–203.

53. Matsuoka, T. et al. (2005). Neural crest origins of the neck and shoulder. *Nature* 436, 347–355.

54. Aoto, K. et al. (2015). Mef2c-F10N enhancer driven β-galactosidase (LacZ) and Cre recombinase mice facilitate analyses of gene function and lineage fate in neural crest cells. *Dev. Biol*. 402, 3–16.

55. Chai, Y. et al. (2000). Fate of the mammalian cranial neural crest during tooth and mandibular morphogenesis. *Development* 127, 1671–9.

56. Jiang, X., Rowitch, D. H., Soriano, P., McMahon, A. P. & Sucov, H. M. (2000). Fate of the mammalian cardiac neural crest. *Development* 127, 1607–16.

57. Lewis, A. E., Vasudevan, H. N., O'Neill, A. K., Soriano, P. & Bush, J. O. (2013). The widely used Wnt1-Cre transgene causes developmental phenotypes by ectopic activation of Wnt signaling. *Dev. Biol*. 379, 229–234.

58. Carney, T. J. et al. (2006). A direct role for Sox10 in specification of neural crest-derived sensory neurons. *Development* 133, 4619–4630.

59. Betancur, P., Bronner-Fraser, M. & Sauka-Spengler, T. (2010). Genomic code for Sox10 activation reveals a key regulatory enhancer for cranial neural crest. *Proc. Natl. Acad. Sci. U. S. A*. 107, 3570–3575.

60. Betancur, P., Sauka-Spengler, T. & Bronner, M. (2011). A sox10 enhancer element common to the otic placode and neural crest is activated by tissue-specific paralogs. *Development* 138, 3689–3698.

61. Teng, L., Mundel, N. A., Frist, A. Y., Wang, Q. & Labosky, P. A. (2008). Requirement for Foxd3 in the maintenance of neural crest progenitors. *Development* 135, 1615–1624.

62. Lukoseviciute, M. et al. (2018). From Pioneer to Repressor: Bimodal foxd3 activity dynamically remodels neural crest regulatory landscape in vivo. *Dev. Cell* 47, 608-628.e6.

63. Simões-Costa, M. S., McKeown, S. J., Tan-Cabugao, J., Sauka-Spengler, T. & Bronner, M. E. (2012). Dynamic and differential regulation of stem cell factor FoxD3 in the neural crest is encrypted in the genome. *PLoS Genet*. 8(12): e1003142.

64. Jimenez, L. et al. (2016). Phenotypic chemical screening using a zebrafish neural crest EMT reporter identifies retinoic acid as an inhibitor of epithelial morphogenesis. Dis. Model. Mech. 9, 389–400.

65. Kaufman, C. K. et al. (2016). A zebrafish melanoma model reveals emergence of neural crest identity during melanoma initiation. *Science* 351(6272): aad2197.

66. Das, A. & Crump, J. G. (2012). Bmps and Id2a Act Upstream of Twist1 to restrict ectomesenchyme potential of the cranial neural crest. *PLoS Genet*. 8, e1002710.

67. Sieber-Blum, M. & Cohen, A. M. (1980). Clonal analysis of quail neural crest cells: They are pluripotent and differentiate in vitro in the absence of noncrest cells. *Dev. Biol*. 80, 96–106.

68. Bronner-Fraser, M., Sieber-blum, M. & Cohen, A. M. (1980). Clonal analysis of the avian neural crest: Migration and maturation of mixed neural crest clones injected into host chicken embryos. *J. Comp. Neurol*. 193, 423–434.

69. Stemple, D. L. & Anderson, D. J. (1992). Isolation of a stem cell for neurons and glia from the mammalian neural crest. *Cell* 71, 973–985.

70. Ito, K., Morita, T. & Sieber-Blum, M. (1993). In Vitro clonal analysis of mouse neural crest development. *Dev. Biol*. 157, 517–525.

71. Luo, R., Gao, J., Wehrle-Haller, B. & Henion, P. D. (2003). Molecular identification of distinct neurogenic and melanogenic neural crest sublineages. *Development* 130, 321–330.

72. Calloni, G. W., Glavieux-Pardanaud, C., Le Douarin, N. M. & Dupin, E. (2007). Sonic Hedgehog promotes the development of multipotent neural crest progenitors endowed with both mesenchymal and neural potentials. *Proc. Natl. Acad. Sci. U. S. A*. 104, 19879–19884.

73. Dupin, E., Calloni, G. W. & Le Douarin, N. M. (2010). The cephalic neural crest of amniote vertebrates is composed of a large majority of precursors endowed with neural, melanocytic, chondrogenic and osteogenic potentialities. *Cell Cycle* 9, 238–249.

74. Kerosuo, L., Nie, S., Bajpai, R. & Bronner, M. E. (2015). Crestospheres: Long-term maintenance of multipotent, premigratory neural crest stem cells. *Stem Cell Reports* 5, 499–507.

75. Ziller, C., Dupin, E., Brazeau, P., Paulin, D. & Le Douarin, N. M. (1983). Early segregation of a neuronal precursor cell line in the neural crest as revealed by culture in a chemically defined medium. *Cell* 32, 627–638.

76. Bronner-Fraser, M. & Fraser, S. (1989). Developmental potential of avian trunk neural crest cells in situ. *Neuron* 3, 755–66.

77. Fraser, S. E. & Bronner-Fraser, M. (1991). Migrating neural crest cells in the trunk of the avian embryo are multipotent. *Development* 112(4):913-20.

78. Collazo, A., Bronner-Fraser, M. & Fraser, S. E. (1993). Vital dye labelling of Xenopus laevis trunk neural crest reveals multipotency and novel pathways of migration. *Development* 118(2):363-76.

79. Serbedzija, G. N., Bronner-Fraser, M. & Fraser, S. E. (1994). Developmental potential of trunk neural crest cells in the mouse. *Development* 120(7): 1709-18.

80. Livet, J. et al. (2007). Transgenic strategies for combinatorial expression of fluorescent proteins in the nervous system. *Nature* 450, 56–62.

81. Baggiolini, A. et al. (2015). Premigratory and migratory neural crest cells are multipotent in vivo. *Cell Stem Cell* 16, 314–322.

82. Kaucka, M. et al. (2016). Analysis of neural crest–derived clones reveals novel aspects of facial development. *Sci. Adv*. 2, e1600060.

83. Lasrado, R. et al. (2017). Lineage-dependent spatial and functional organization of the mammalian enteric nervous system. *Science* 356, 722–726.

84. Albert Pan, Y. et al. (2013). Zebrabow: Multispectral cell labeling for cell tracing and lineage analysis in zebrafish. *Development* 140, 2835–2846.

85. Rochard, L. J., Ling, I. T. C., Kong, Y. & Liao, E. C. (2015). Visualization of chondrocyte intercalation and directional proliferation via zebrabow clonal cell analysis in the embryonic Meckel's cartilage. *J. Vis. Exp*. (105):e52935.

86. Xie, M. et al. (2019). Schwann cell precursors contribute to skeletal formation during embryonic development in mice and zebrafish. *Proc. Natl. Acad. Sci. U. S. A*. 116, 15068–15073.

87. Brockway, N. L. et al. (2019). Multicolor lineage tracing using in vivo time-lapse imaging reveals coordinated death of clonally related cells in the developing vertebrate brain. *Dev. Biol.* 453, 130–140.

88. Liu, N. et al. (2019). Stem cell competition orchestrates skin homeostasis and ageing. *Nature* 568, 344–350.

89. Matsumoto, T., Wakefield, L., Tarlow, B. D. & Grompe, M. (2020). In vivo lineage tracing of polyploid hepatocytes reveals extensive proliferation during liver regeneration. *Cell Stem Cell* 26, 34-47.e3.

90. Tierney, M. T., Stec, M. J., Rulands, S., Simons, B. D. & Sacco, A. (2018). Muscle stem cells exhibit distinct clonal dynamics in response to tissue repair and homeostatic aging. *Cell Stem Cell* 22, 119-127.e3.

91. Lamprecht, S. et al. (2017). Multicolor lineage tracing reveals clonal architecture and dynamics in colon cancer. *Nat. Commun*. 8, 1–9.

92. Rios, A. C. et al. (2019). Intraclonal plasticity in mammary tumors revealed through large-scale single-cell resolution 3D Imaging. *Cancer Cell* 35, 618-632.e6.

93. Yanai, H. et al. (2017). Intestinal cancer stem cells marked by Bmi1 or Lgr5 expression contribute to tumor propagation via clonal expansion. *Sci. Rep*. 7, 1–10.

94. Khalili, S. et al. (2018). Induction of rod versus cone photoreceptor-specific progenitors from retinal precursor cells. *Stem Cell Res*. 33, 215–227.

95. Turner, D. L. & Cepko, C. L. (1987). A common progenitor for neurons and glia persists in rat retina late in development. *Nature* 328, 131–6.

96. Fields-Berry, S. C., Halliday, A. L. & Cepko, C. L. (1992). A recombinant retrovirus encoding alkaline phosphatase confirms clonal boundary assignment in lineage analysis of murine retina. *Proc. Natl. Acad. Sci. U. S. A*. 89, 693–7.

97. Adair, J. E. et al. (2020). DNA barcoding in nonhuman primates reveals important limitations in retrovirus integration site analysis. *Mol. Ther. Methods. Clin. Dev*. 17, 796–809.

98. Fuentealba, L. C. et al. (2015). Embryonic origin of postnatal neural stem cells. *Cell* 161, 1644–1655.

99. Figliozzi, R. W., Chen, F., Chi, A. & Hsia, S.-C. V. (2016). Using the inverse Poisson distribution to calculate multiplicity of infection and viral replication by a high-throughput fluorescent imaging system. *Virol. Sin*. 31, 180–3.

100. Frank, E. & Sanes, J. R. (1991). Lineage of neurons and glia in chick dorsal root ganglia: analysis in vivo with a recombinant retrovirus. *Development* 111(4), 895–908.

101. Tang, W., Li, Y., Gandhi, S. & Bronner, M. E. (2019). Multiplex clonal analysis in the chick embryo using retrovirally-mediated combinatorial labeling. *Dev. Biol*. 450, 1–8.

102. Martinsen, B. J. & Bronner-Fraser, M. (1998). Neural crest specification regulated by the helix-loop-helix repressor Id2. *Science* 281(5379):988-91.

103. Temin, H. M. & Rubin, H. (1958). Characteristics of an assay for Rous sarcoma virus and Rous sarcoma cells in tissue culture. *Virology* 6, 669–688.

104. Yamashita, M. & Emerman, M. (2006). Retroviral infection of non-dividing cells: Old and new perspectives. *Virology* 344, 88–93.

105. Sulston, J. E. (1983). Neuronal cell lineages in the nematode Caenorhabditis elegans. *Cold Spring Harb. Symp. Quant. Biol.* 48 Pt 2, 443–52.

106. Soldatov, R. et al. (2019). Spatiotemporal structure of cell fate decisions in murine neural crest. *Science* 364(6444):eaas9536.

107. Frieda, K. L. et al. (2017). Synthetic recording and in situ readout of lineage information in single cells. *Nature* 541, 107–111.

108. McKenna, A. et al. (2016). Whole-organism lineage tracing by combinatorial and cumulative genome editing. *Science* 353(6298):aaf7907.

109. Alemany, A., Florescu, M., Baron, C. S., Peterson-Maduro, J. & Van Oudenaarden, A. (2018). Whole-organism clone tracing using single-cell sequencing. *Nature* 556, 108–112.

110. Spanjaard, B. et al. (2018). Simultaneous lineage tracing and cell-type identification using CrIsPr-Cas9-induced genetic scars. *Nat. Biotechnol*. 36, 469–473.

111. Cotterell, J., Vila-Cejudo, M., Batlle-Morera, L. & Sharpe, J. (2020). Endogenous CRISPR/Cas9 arrays for scalable whole-organism lineage tracing. *Development* 147(9):dev184481.

112. Askary, A. et al. (2020). In situ readout of DNA barcodes and single base edits facilitated by in vitro transcription. *Nat. Biotechnol*. 38, 66–75.

113. Achilleos, A. & Trainor, P. A. (2012). Neural crest stem cells: Discovery, properties and potential for therapy. *Cell Research* 22, 288–304.

114. Poss, K. D., Wilson, L. G. & Keating, M. T. (2002). Heart regeneration in zebrafish. *Science* 298(5601):2188-90.

115. Jopling, C. et al. (2010). Zebrafish heart regeneration occurs by cardiomyocyte dedifferentiation and proliferation. *Nature* 464, 606–609.

116. Li, Y.-X. et al. (2003). Cardiac neural crest in zebrafish embryos contributes to myocardial cell lineage and early heart function. *Dev. Dyn*. 226, 540–50.

117. Sato, M. & Yost, H. J. (2003). Cardiac neural crest contributes to cardiomyogenesis in zebrafish. *Dev. Biol.* 257, 127–39.

118. Cavanaugh, A. M., Huang, J. & Chen, J.-N. (2015). Two developmentally distinct populations of neural crest cells contribute to the zebrafish heart. *Dev. Biol*. 404, 103–12.

119. Abdul-Wajid, S., Demarest, B. L. & Yost, H. J. (2018). Loss of embryonic neural crest derived cardiomyocytes causes adult onset hypertrophic cardiomyopathy in zebrafish. *Nat. Commun.* 9, 1–11.

120. Porrello, E. R. et al. (2011). Transient regenerative potential of the neonatal mouse heart. *Science* 331(6020):1078-80.

121. Hatzistergos, K. E. et al. (2015). CKit+ cardiac progenitors of neural crest origin. *Proc. Natl. Acad. Sci. U. S. A.* 112, 13051–13056.

122. Tomita, Y. et al. (2005). Cardiac neural crest cells contribute to the dormant multipotent stem cell in the mammalian heart. *J. Cell Biol*. 170, 1135–46.

123. Tamura, Y. et al. (2011). Neural crest–derived stem cells migrate and differentiate into cardiomyocytes after myocardial infarction. *Arterioscler. Thromb. Vasc. Biol*. 31, 582–589.

124. Tang, W., Martik, M. L., Li, Y. & Bronner, M. E. (2019). Cardiac neural crest contributes to cardiomyocytes in amniotes and heart regeneration in zebrafish. *Elife* 8.

125. Sande-Melón, M. et al. (2019). Adult sox10+ cardiomyocytes contribute to myocardial regeneration in the zebrafish. *Cell Rep*. 29, 1041-1054.e5.

126. Kumar, A., Godwin, J. W., Gates, P. B., Garza-Garcia, A. A. & Brockes, J. P. (2007). Molecular basis for the nerve dependence of limb regeneration in an adult vertebrate. Science 318(5851):772-7.

127. Furlan, A. et al. (2017). Multipotent peripheral glial cells generate neuroendocrine cells of the adrenal medulla. *Science* 357(6346):eaal3753.

128. Itou, J. et al. (2012). Migration of cardiomyocytes is essential for heart regeneration in zebrafish. *Development* 139, 4133–4142.

129. Joseph, N. M. et al. (2008). The loss of Nf1 transiently promotes self-renewal but not tumorigenesis by neural crest stem cells. *Cancer Cell* 13, 129–140.

130. Zheng, H. et al. (2008). Induction of abnormal proliferation by nonmyelinating Schwann cells triggers neurofibroma formation. *Cancer Cell* 13, 117–128.

131. Wu, J. et al. (2008). Plexiform and dermal neurofibromas and pigmentation are caused by Nf1 loss in Desert Hedgehog-expressing cells. *Cancer Cell* 13, 105–116.

132. Le, L. Q. et al. (2011). Susceptible stages in Schwann cells for NF1-associated plexiform neurofibroma development. *Cancer Res.* 71, 4686–4695.

133. Chen, Z. et al. (2014). Cells of origin in the embryonic nerve roots for NF1-associated plexiform neurofibroma. *Cancer Cell* 26, 695–706.

134. Angeles Rabadán, M., Usieto, S., Lavarino, C. & Martí, E. (2013). Identification of a putative transcriptome signature common to neuroblastoma and neural crest cells. *Dev. Neurobiol*. 73(11):815-27.

135. Dravis, C. et al. (2018). Epigenetic and transcriptomic profiling of mammary gland development and tumor models disclose regulators of cell state plasticity. *Cancer Cell* 34, 466-482.e6.

136. McConnell, A. M. et al. (2019). Neural crest state activation in NRAS driven melanoma, but not in NRAS-driven melanocyte expansion. *Dev. Biol*. 449, 107–114.

137.Varum, S. et al. (2019). Yin Yang 1 orchestrates a metabolic program required for both neural crest development and melanoma formation. *Cell Stem Cell* 24, 637-653.e9.

138. Schartl, A., Malitschek, B., Kazianis, S., Borowsky, R. & Schartl, M. (1995). Spontaneous melanoma formation in nonhybrid Xiphophorus. *Cancer Res.* 55, 159–65.

139. Schartl, M. (2014). Beyond the zebrafish: Diverse fish species for modeling human disease. *Disease Models and Mechanisms* 7, 181–192.

140. Lu, Y. et al. (2018). Comparison of Xiphophorus and human melanoma transcriptomes reveals conserved pathway interactions. *Pigment Cell Melanoma Res*. 31, 496–508.

141. Jeffery, W. R., Strickler, A. G. & Yamamoto, Y. (2004). Migratory neural crest-like cells form body pigmentation in a urochordate embryo. *Nature* 431, 696–699.

142. Powell, J. F. F. et al. (1996). Two new forms of gonadotropin-releasing hormone in a protochordate and the evolutionary implications. *Proc. Natl. Acad. Sci. U. S. A*. 93, 10461–10464.

143. Holland, N. D., Panganiban, G., Henyey, E. L. & Holland, L. Z. (1996). Sequence and developmental expression of AmphiDll, an amphioxus Distal-less gene transcribed in the ectoderm, epidermis and nervous system: Insights into evolution of craniate forebrain and neural crest. *Development* 122, 2911 LP – 2920.

Chapter II

MULTIPLEX CLONAL ANALYSIS IN THE CHICK EMBRYO USING RETROVIRALLY-MEDIATED COMBINATORIAL LABELING

Part of this chapter was published as Tang, W., Li, Y., Gandhi, S. & Bronner, M. E. Multiplex clonal analysis in the chick embryo using retrovirally-mediated combinatorial labeling. *Dev. Biol*. 450, (2019). DOI: 10.1016/j.ydbio.2019.03.007

ABSTRACT

Lineage analysis plays a central role in exploring the developmental potential of stem and progenitor cell populations. In higher vertebrates, a variety of techniques have been used to label individual cells or cell populations, including interspecies grafting, intracellular microinjection, and Cre-mediated recombination. However, these approaches often suffer from difficulties in progenitor cell targeting, low cellular resolution and/or ectopic labeling. To circumvent these issues, here we utilize replication incompetent avian (RIA) retroviruses to deliver combinations of fluorescent proteins into distinct cellular compartments in chick embryos. In particular, RIA-mediated lineage tracing is optimal for long term mapping of dispersing cell populations like the neural crest. Using this tool, we confirm that trunk neural crest cells are multipotent. Furthermore, our RIA vector is engineered to be fully adaptable for other purposes such as cell fate analysis, gene perturbation studies and time-lapse imaging. Taken together, we present a novel approach of multiplex lineage analysis that can be applied to normal and perturbed development of diverse cell populations in avian embryos.

2.1 INTRODUCTION

A fundamental challenge in developmental biology is to determine the range of cell types that can arise from single embryonic cells. Whereas the fertilized egg or embryonic stem cells are totipotent, other embryonic cell types may be multipotent, bipotent or unipotent. Distinguishing between these possibilities requires methods that enable analysis of a cell's developmental history. In organisms like *C. elegans*, cell lineage analysis has been elegantly done by visually mapping the progeny of each cell division (Sulston, 1983). While this was a technical *tour de force* in a simple organism, it is not feasible in more complex and/or opaque organisms. Analysis of cell lineage is particularly challenging in vertebrate embryos. In the past decades, various techniques have been developed to follow and analyze cell fates that greatly expanded our understanding of both embryogenesis and organogenesis. One approach is to directly inject single cells with fluorescent dyes that are large and thus cannot pass through gap junctions (Bronner-Fraser & Fraser, 1988). A second approach involves virally-mediated lineage analysis using β-galactosidase (Frank & Sanes, 1991; Sanes, 1989) or barcoded libraries (Gerrits et al., 2010). Third, quail-chick chimeric grafts have been a well-established tool for understanding the contribution of neural crest in avian embryos (Ayer-Le Lievre & Le Douarin, 1982). Finally, transgenic *Confetti* and *Brainbow* technology in mice and zebrafish, respectively, have been used to express fluorescent proteins at specific time points, enabling clonal analysis using high resolution imaging (Cai et al., 2013; Livet et al., 2007). A complication of the latter, however, is that it is difficult to establish clonality as it involves sophisticated statistical analysis of rare color combinations (Baggiolini et al., 2015). Moreover, this technology is not easily applicable to non-genetic organisms and is

particularly challenging for cell types that are migratory and thus disperse widely in the embryo.

One example of such a cell type is the neural crest. Neural crest cells originate within the closing neural tube but then migrate to diverse locations in the embryo and form diverse cell types (Ayer-Le Lievre & Le Douarin, 1982). Despite the broad range of the neural crest derivatives at a population level, there are conflicting views in the literature regarding the degree of multipotency of individual neural crest cells. Single cell lineage analysis using microinjection of fluorescent dyes suggested that trunk neural crest cells in avian embryos are multipotent at both premigratory (Bronner-Fraser and Fraser, 1988) and migratory (Bronner-Fraser and Fraser, 1989) stages. In the mouse, Sommer and colleagues (Baggiolini et al., 2015) found similar results using *R26R-Confetti* technology. However, other studies have suggested that neural crest cells are restricted in their fate, even before emigration from the neural tube (Krispin et al., 2010; Weston & Thiery, 2015). Thus, further analysis of neural crest lineage is warranted, particularly since little is known about their developmental potential at axial levels other than the trunk region.

The chick embryo has been an excellent system for neural crest biology. As amniotes, chick embryos develop similar to humans at stages of neural crest migration, but are cost-effective compared with mice. Moreover, their ability to develop outside of the mother facilitates not only genetic and surgical manipulations but also dynamic imaging (Benazeraf et al., 2010). Recently, we have applied RIA-mediated lineage analysis to chick cartilage to understand how sister cells rearrange within a constrained region surrounded by extracellular matrix (Li et al., 2017). Here, we expand the repertoire of colors and subcellular localizations of these reagents and demonstrate their utility for defining clonal relationship of other cell types,

including those that disperse widely in the embryo, like neural crest cells. As proof of principle, we confirm the multipotent property of trunk neural crest cells. Thus, our study enriches the toolkit for cell lineage analysis in a non-genetic model organism.

2.2 RESULTS AND DISCUSSION

2.2.1 OPTIMIZATION AND *IN VITRO* VALIDATION OF REPLICATION-INCOMPETENT AVIAN (RIA) RETROVIRUSES FOR MULTIPLEX CLONAL ANALYSIS

RIA retrovirus has been employed widely for lineage tracing in chick embryos (Chen et al., 1999). After stably integrating into host genome, RIA DNA is faithfully and equally passaged to daughter cells during cell division. In contrast to replication-competent avian (RCAS) virus (Fig. 2-1A), RIA does not synthesize its own envelope (ENV) protein and thus cannot horizontally transfer into neighboring cells. As a result, all descendants of an RIA infected cell are permanently labeled with a unique common signature, representing an isogenic clone. This feature offers several advantages over other approaches for lineage analysis: first, it is less invasive compared to quail-chick grafts, marking endogenous host cells without the necessity for surgery or combining tissue from different species; second, compared with progressively diluting vital dyes, the integrated RIA transgene enables indelible marking of host cells and their progeny (Li et al., 2018); finally, compared to *Confetti* mouse and zebrafish labeling, RIA ensures specific targeting of progenitor cells through focal injection, avoiding the general challenges faced by the Cre-lox systems that are dependent upon the choice of promoters (Lewis et al., 2013).

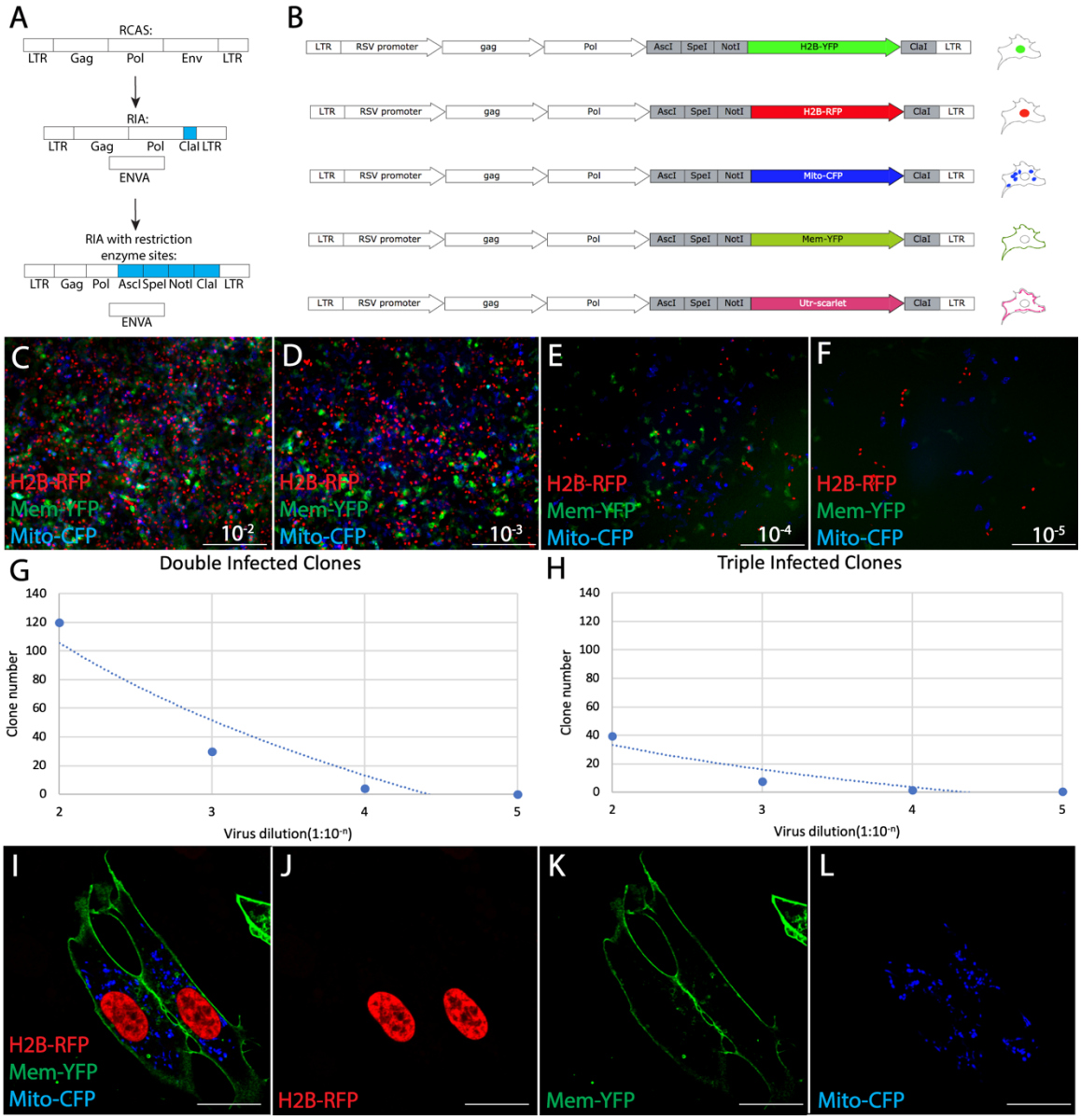

Figure 2-1. Validating RIA-mediated multicolor clonal analysis in cell culture. (A) Construct map of RCAS, RIA, and modified RIA with restriction enzyme sites (blue). (B) Transgenes encoding fluorescent proteins targeted to specific subcellular regions were cloned into the RIA vector. Note the maps in (A) and (B) are not to scale. (C-F) Equal mixture of three viruses (H2B-RFP, Mem-YFP, Mito-CFP) was serially diluted and infected into DF1 cells. (G, H) The number of double and triple-infected clones showed an inverse relationship to viral titer. (I-L) High magnification imaging on infected cells with 63x objective lens confirmed specific subcellular targeting of fluorescent proteins. Scale bars: C-F 100μm, I-L 10μm.

Previous studies have used RIA viruses to resolve clonal boundaries in cartilage, tendon, perichondrium and retina (Li et al., 2017; Pearse et al., 2007). One common characteristic of all these tissues is that they are comprised of coherent clones with regular morphology. To extend this analysis to broader types of tissues, we have optimized this approach and expanded its application to cells that migrate extensively and actively rearrange.

To this end, we modified the previous version of the RIA vector (Chen et al., 1999) by adding three unique restriction enzyme sites (AscI, SpeI, NotI) in the upstream of the common cloning site ClaI. The AscI and SpeI sites were preserved for expanding the application of this viral vector for future research, such as, creating fusion proteins and bicistronic systems to visualize protein dynamics and perform gene functional study, respectively. For the purpose of lineage tracing in wild-type chick embryos in this study, we generated five distinct viruses by inserting *H2B-YFP, H2B-RFP, Mito-CFP, Membrane-YFP (Mem-YFP), Utrophin-Scarlet (Utr-Scarlet)* between NotI and ClaI sites (Fig. 2-1B). Clonality assessment was based on three criteria: a complex color combination created by multiple (two or more) infections of a single progenitor cell; similar signal intensity, based on numbers of copies integrated and/or insertion location in the host genome; distinct subcellular localizations of fluorescent proteins. Taken together, these improvements in the complexity of viral infection enable spatial resolution of individual clones.

We performed a careful characterization of this novel cell-tagging reagent *in vitro* before applying it to *in vivo* systems. First, we showed these viruses can label clones in cell culture by introducing serial dilutions of an equal mixture of three viruses (H2B-RFP, Mem-YFP, Mito-CFP) into DF1 cells. As dilution factor increased (Fig. 2-1C-F), the numbers of double and triple-colored cell clusters decreased logarithmically (Fig. 2-1G, H); such a pattern was

expected if infection with a viral particle is an independent event (Turner, 1987). Second, we performed high magnification imaging to confirm the fidelity of the subcellular localization of distinct fluorescent proteins and excluded the possible effects of optical bleed-through (Fig. 2-1I-L).

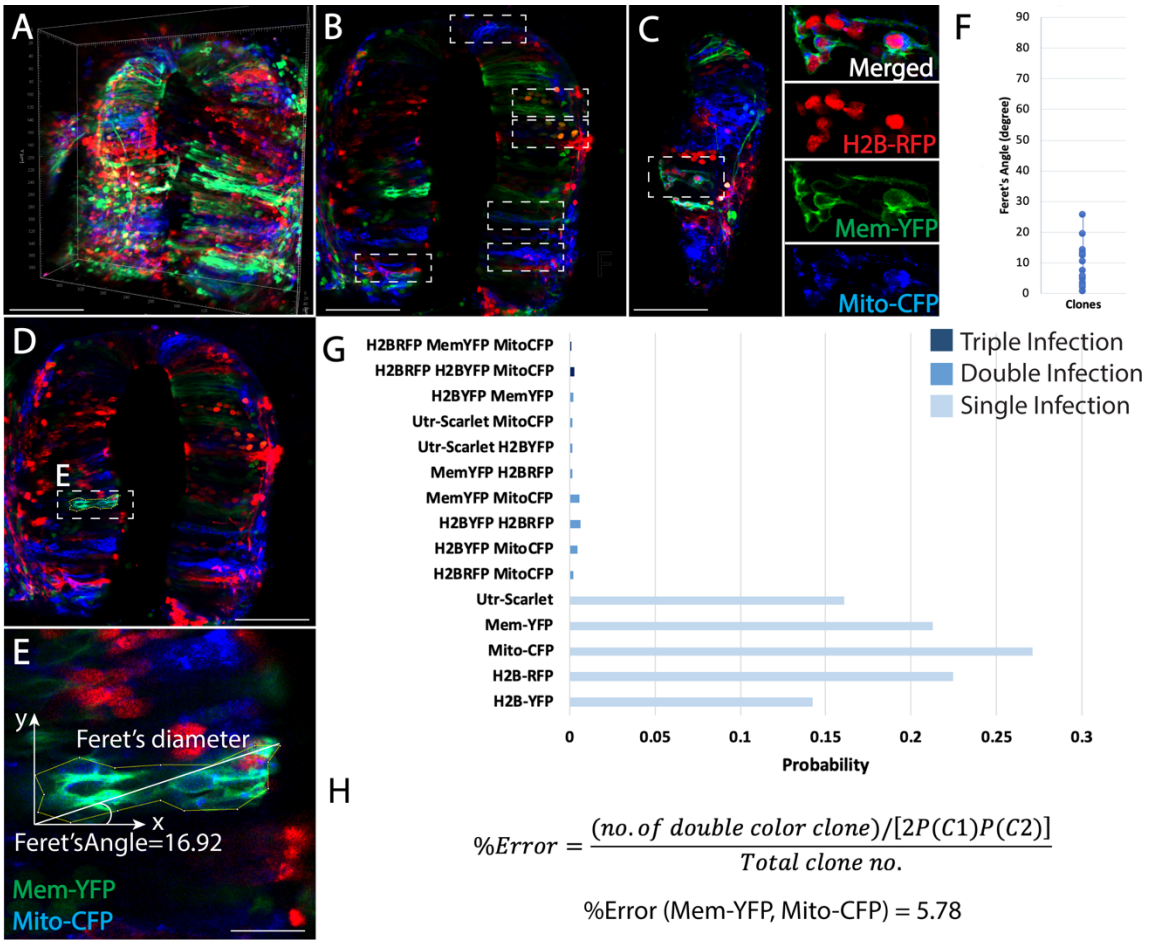

Figure 2-2. RIA-mediated multicolor clonal analysis reveals coherent clonal structure in the neural tube (A) Three-dimensional (3D) view of a chick neural tube infected with viral mixture. (B) In one selected slice of the same tissue in (A), clones (dashed white boxes) appeared to arrange parallelly to the horizontal axis of the tissue. (C) In one representative clone (zoom in view), all the cells expressed three fluorescent proteins in distinct cellular compartments. (D-F) Quantitative analysis reveals lateral distribution of clones. As an example, a double color clone (D) was manually segmented and its Feret's angle was measured (E); in most cases of the

16 clones analyzed, this angle was less than 20 degree (F). (G) Experimental probability of double and triple-infections are low. (H) Percent error as a result of viral aggregation is about 5.78% for Mem-YFP/Mito-CFP, the most frequent occurring double-infected clone. Scale bars: A-D 100μm, E 20μm.

2.2.2 CLONAL RELATIONSHIPS WITHIN THE NEURAL TUBE

To extend our analysis *in vivo*, we used our recombinant virus to confirm the spatial arrangement of clones in the neural tube. A previous study using time-lapse imaging revealed that these cells undergo oriented division, and in turn, form laterally distributed clusters (Tawk et al., 2007), providing a simple *in vivo* system to validate our reagents. As such, we injected a mixture containing equal amounts of five distinct RIA viruses into the lumen of the neural tube at Hamburger and Hamilton (HH) stage 11 (n=6), and harvested the embryos 48 hours-post infection for imaging thick slices in transverse orientation (Fig. 2-2A). In a single orthogonal slice, we identified six clones according to the criteria established above; all the clones appeared to align orthogonal to the elongation axis of the neural tube (Fig. 2-2B, C, Movie 2-1). We segmented these clones and enclosed them with a polygon using FIJI to measure their Feret's angle, the angle between the maximum diameter of the polygon and the lateral axis of the neural tube (see details in Methods) (Fig. 2-2D, E). This endpoint analysis revealed an average Feret's angle of about 10 degrees, consistent with the model of lateral clonal expansion suggested by previous longitudinal analyses (Fig. 2-2F) (Tawk et al., 2007). Both double and triple infection events were rare, with probabilities $p < 0.01$ (Fig. 2-2G). To rule out the possibility that clonal assessment could be biased if viral aggregates infected adjacent progenitor cells in neural tube, we calculated the error rate of the most

frequent doubly infected clone expressing both Mem-YFP and Mito-CFP with the formula previously described (Fields-berry et al., 1992):

$$\%Error = \frac{no.of\ double\ infected\ clone/[2P(C1)P(C2)]}{Total\ clone\ no.}$$

in which *P(C1)* is the probability of being infected by Mem-YFP virus and *P(C2)* is the probability of being infected by Mito-CFP virus; both are equal to 1/5 because the same amounts of five viruses were applied. In this particular case, 3 clones with this color combination were identified out of the total 648 clones, leading to an error rate of 5.78% (Fig. 2-2H), corresponding to a high confidence level in defining clonal boundaries of this combination as well as all other putative clones (Fields-berry et al., 1992).

RIA viruses employed in previous research encoded a single histological marker such as β-galactosidase or alkaline phosphatase, necessitating the need to use highly diluted virus and wide dispersion since individually labeled clones must be separated in order to verify clonality (Fields-berry et al., 1992). As a result, large number of embryos were required for statistical analysis. In contrast, our multicolor toolkit enables combinatorial tagging and determination of many individual clones within the same tissue preparation, avoiding heterogeneity issues raised from numerous samples and developmental stages.

2.2.3 MULTIPLEX ANALYSIS CONFIRMS MULTIPOTENCY OF TRUNK NEURAL CREST CELLS

We next applied this approach to investigate the clonal relationship of cells that migrate extensively and disperse widely throughout the embryo. The trunk neural crest is such an example as it contributes to several tissues along the dorsoventral axis, including dorsal root ganglia (DRG), sympathetic ganglia (SG), and cells along the ventral root (VR) (Bronner-Fraser and Fraser, 1989). The viral mixture described above was introduced into the entire trunk neural tube of chick embryos at Hamburger and Hamilton (HH) stage 11, when trunk neural crest cells are about to emigrate. The embryos were allowed to develop until HH21 (n=10) when neural crest cells complete migration and begin to differentiate at their final destinations. For live imaging using confocal microscopy, we dissected a thick transverse section (500μm in thickness) at the forelimb level (Fig. 2-3A, B) (Li et al., 2019). To capture all the clones within several embryos, we used the tile function of Zeiss LSM 800 to visualize the region from the dorsal neural tube to the dorsal aorta (800μm x 1600μm x 150μm), encompassing most territories through which trunk neural crest cells migrate.

Within individual slices, we observed clonally related cells residing in distinct sites, including the dorsal neural tube (dNT), DRG, SG, and VR (Fig. 2-3C, DE, double infected clone; FG, triple infected clone). The results suggest that DRG and SG are more clonally associated with each other than with cells along the VR (Fig. 2-4B). This may be due to the fact that the VR is a smaller tissue, so that cells have less chance to condense within it. Alternatively, cells along the VR may be more developmentally restricted at the time of condensation, or derived from a limited number of progenitor cells.

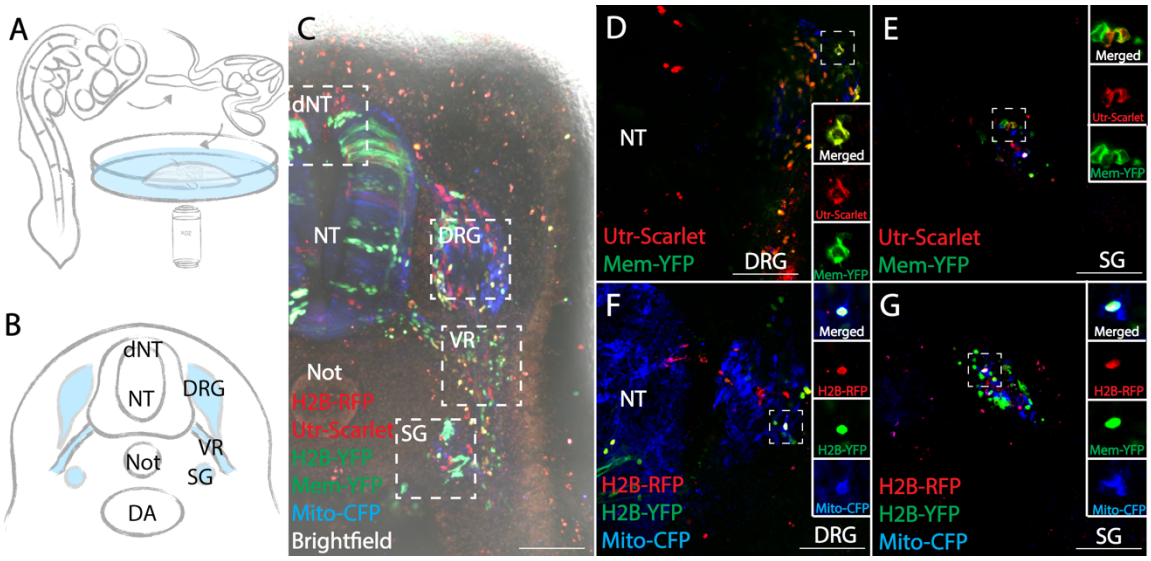

Figure 2-3. RIA-mediated multicolor clonal analysis confirms multipotency of trunk neural crest cells. (A) Schematic diagram of experimental procedure. A transverse slice at forelimb level was cut, embedded in 1% agarose for live imaging. (B) Schematic of trunk neural crest derivatives (NT, neural tube; Not, notochord; DA, dorsal aorta; dNT, dorsal neural tube; DRG, dorsal root ganglia; SG, sympathetic ganglia; VR, ventral root; neural crest-derived structures in light blue). (C) A representative transverse view of an infected chick embryo. Regions inside white dashed boxes indicate neural crest-derivatives. (D, E) A double-labeled clone in DRG and SG (Utr-Scarlet, red; Mem-YFP, green) in the same tissue slice. (F, G) A triple-labeled clone in DRG and SG (H2B-RFP, red; H2B-YFP, green; Mito-CFP, blue) in the same tissue slice. Scale bars: C 200μm; D-G100μm.

2.2.4 PROBABILITY CALCULATION CONFIRMS THE RELIABILITY OF COINFECTION-BASED CLONAL RELATIONSHIP

Given that many cells with identical color/subcellular localization combinations dispersed across a single embryonic slice at the trunk level (Fig. 2-4A), we sought to quantitatively verify their clonality. We have demonstrated that in both cell culture and in neural tube (Fig. 2-1, 2-2), infection with multiple viruses is a rare process; the lower the probability of co-infection, the greater the likelihood that cells bearing the same combined color combination

are derived from the same precursor. Since migrating neural crest cells are heterogeneous with respect to cell cycle progression and anatomic location, it is challenging to accurately estimate the number of cells infected at time 0. Therefore, we determined the coinfection efficiency by calculating the upper bound of the probability of multiple infection, independent of the initial number of infected progenitor cells. When a given titer of virus is allowed to infect a cell population, each viral particle entering an individual cell can be defined as an independent event. To this end, we estimated the probability of an individual cell being infected with a given number of viruses using a Poisson distribution, which describes discrete events that occur in a fixed time interval and/or space (Figliozzi et al., 2016):

$$P\{n\} = \frac{m^n e^{-m}}{n!}$$

where P{n} is the probability of infection by n viral particles; m is the multiplicity of infection (MOI), the average number of viral particles per cell. We first measured the titer of the virus to determine the MOI. In a typical experiment, about 0.5µl of viral mixture with a titer of 1 x 10^7 pfu/ml per embryo was injected into the trunk segment, suggesting that ~5,000 particles were injected. Next, we estimated the total number of cells in a segment of the neural tube using DAPI. Among these cells, only a portion are premigratory neural crest cells. This is highlighted by expression of the molecular marker Pax7, which marks the premigratory domain (Fig. 2-4D), though not all Pax7 expressing cells depart from the neural tube. The number of particles that "premigratory" neural crest cells absorb then can be deduced by the total particle number multiplied by the ratio of neural crest to neural tube (approximately 1:5). Taking all these factors into account, the MOI is approximately 0.2

(calculated from an average of 5000 premigratory neural crest cells and 25,000 neural tube cells at the trunk region of interest). The probability of a premigratory neural crest cell in the Pax7 domain being infected with one virus (*P{1}*) is 0.16, with two viruses (*P{2}*) is 0.016, with three viruses (*P{3}*) is 0.001 (Fig. 2-4C, D). Using the way in which clonality was determined in *Confetti* mouse as a reference (Bagglioni et al., 2015), double and triple infections in our case were rare events. Statistical evaluation under experimental conditions further shows that this probability is close to the theoretical value, despite some variations between *P{1} and P{2}* for different viruses or color combinations. This disparity is possibly due to slight differences in virus titer, or intrinsic variation between the fluorescent protein that affects infection efficiency or expression level, and is also seen in the *Confetti* mouse (Fig. 2-4E). On this basis, we conclude that cells bearing two to three distinct viral integrations are derived from a single progenitor. Cells bearing similar multiple color combinations can be used as an optical readout of a clone.

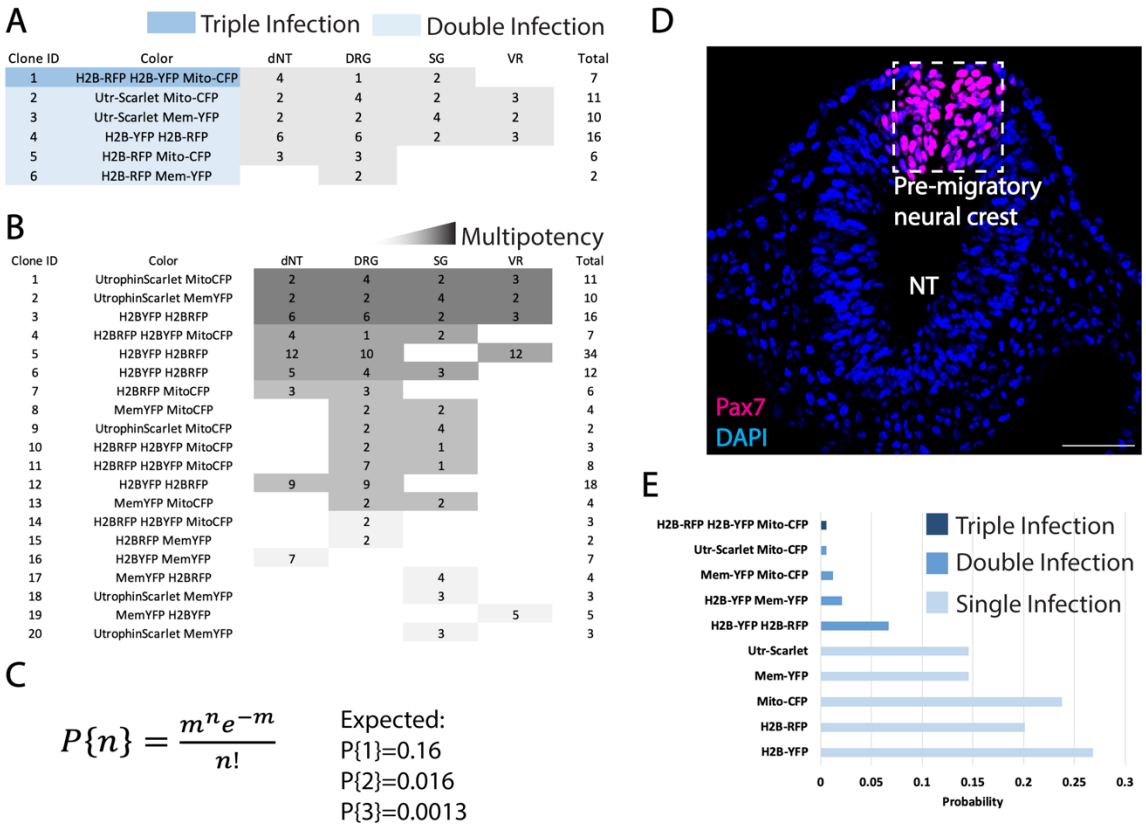

Figure 2-4. Probability calculation of viral co-infection efficiency confirms that double/triple infected clones are rare. (A) An example of clones identified in one embryo. 6/6 of the clones were found in more than one neural crest-derived regions, suggesting multipotency of the progenitor cells. (B) An overview of all the clones identified in multiple embryos (n=4). 13/20 clones were multipotent. Shade of grey represents the number of places where cells of a particular clone were observed, indicating degree of multipotency. (C) Multiple infection can be portrayed as a Poisson distribution, where the probability of single infection is 0.16, double infection is 0.016, and triple infection is 0.001. (D) Pax7 (Magenta) and DAPI (blue) staining were used to estimate the efficiency of viral infection in (C). (E) Experimentally obtained coinfection index agrees with the theoretical values, demonstrating that double and triple infections are low probability events. Scale bar: 100μm.

Given the fact that RIA viral DNA only integrates into the host genome during metaphase, non-uniform distribution of cell-cycle stages of the infected cells will influence the timing of

transgene expression. For cells in metaphase, broken nuclear membrane allows viral integration into the host chromosome; for cells in G1 phase, the viral DNA will stay in the cytoplasm until metaphase; if there are post-mitotic cells in the dorsal neural tube, the viral genes will not express. These factors influence the timing of transgene expression and the estimation of initial viral infection, but also present an opportunity to enhance clonal complexity, as this mosaic context will result in different signal intensity based on the timing of viral DNA integration.

Our result revealing trunk neural crest multipotency is remarkably similar to previous findings based on vital dye injection into individual dorsal neural tube cells in chick (Bronner-Fraser and Fraser, 1989) as well as *Wnt1-CreERT* and *Sox10-CreERT* driven *R26R-Confetti* mouse (Bagglioni et al., 2015). Whereas dye labeling experiments require single cell injection which is technically challenging and the signal becomes diluted with cell division, viral infection is simple and the fluorescent proteins are stably expressed. Importantly, we can identify multiple clones in a single embryo, as each clone displays a unique color combination resulting from co-infection of two to three viruses (Fig. 2-3D-G). Compared with *Confetti* system in mice, our approach is significantly more cost-effective and applicable to the chick, the most widely used animal model for neural crest research. Thus, our newly developed RIA-mediated method is an effective albeit much simpler alternative for clonal analysis on dispersed cell populations.

2.2.5 COMBINED CLONAL AND CELL FATE ANALYSIS BEYOND THE TRUNK NEURAL CREST

The ultimate goal of lineage analysis is to explore the developmental potential of individual progenitor cells in order to determine their degree of multipotency or lineage restriction. For instance, if neural crest cells acquire their identities early during migration, clonally related cells may express uniform cell fate; alternatively, if cells remain multipotent, and do not commit to a cell fate until they reach the final destination, cells within a clone may disperse and form heterogeneous derivatives. Gaining insights into the latter case requires the ability to examine diverse cell morphologies, localizations, and identities within the same clone. To achieve this goal, lineage tracing needs to be coupled with cell fate analysis.

To test the possibility of combining lineage analysis with cell fate markers, we injected a mixture of viruses in the neural tube adjacent to somites 1-3. Neural crest cells that emerge from this axial level migrate into branchial arches 4 and 6 (Kirby et al., 1983). Embryos were allowed to develop until HH21 and processed for sectioning and immunohistochemistry. Using immunofluorescence, we found that cells labelled with native fluorescent proteins acquired distinct cell fates differentiating into neurons (HuC/D, Fig. 2-5A, A'), including primary sensory or motor neuron (E1.9, Fig. 2-5B, B'), as well as smooth muscle (SMA, Fig. 2-5C, C'). Taken together, our results show that RIA-mediated lineage analysis is compatible with post-processing such as paraformaldehyde fixation, cryo-sectioning and antibody staining, while the endogenous fluorescence signal is well-preserved.

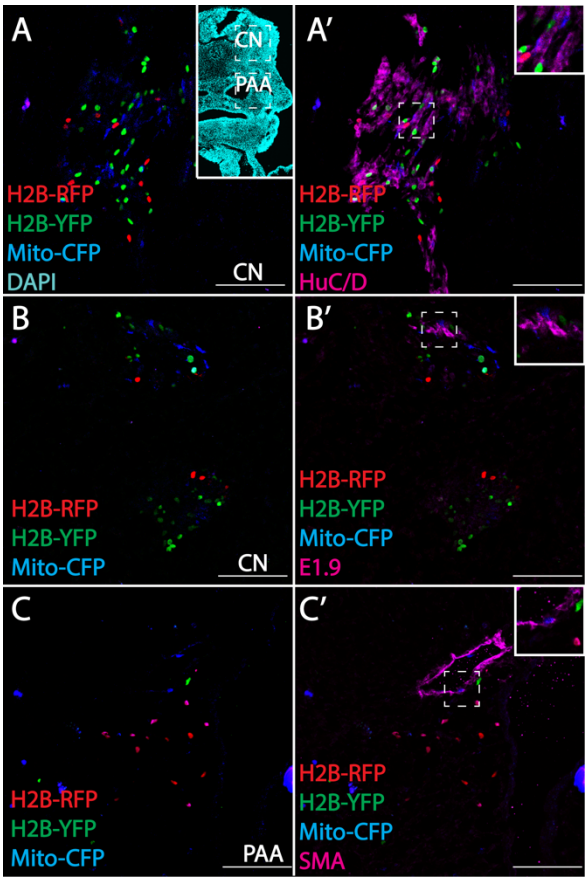

Figure 2-5. RIA-mediated clonal analysis can be combined with cell fate studies. A representative transverse section of the virally infected hindbrain was processed for antibody staining. Fluorescently labeled progenies in cranial nerve-IX (CN) and pharyngeal arch arteries (PAA) were indicated with dashed boxes in (A) (DAPI, Cyan). In cranial nerve-IX, neural crest derived cells expressed a neuronal (HuC/D, Magenta) (A, A') or sensory/motor neuron marker (E1.9, Magenta) (B, B'); some of their siblings can migrate more ventrally into the pharyngeal arch arteries (PAA) and differentiated into smooth muscle (SMA, Magenta) (C, C'). Scale bars: 100μm.

2.3 CONCLUSION

In summary, by modifying RIA viruses to enable simultaneous expression of different fluorophores, we present a useful means to orthogonally detect multiple clones in single

avian embryos. We demonstrate the utility of this approach in cell culture, the neural tube and neural crest. Our results on migrating neural crest cells confirm the multipotency of this cell population that has been demonstrated previously by other complementary techniques (Bronner-Fraser and Fraser, 1988; Bagglioni et al., 2015). Moreover, our RIA virus constructs are designed to enable co-expression of fluorophores and proteins that function either normally or as mutants (Gandhi et al., 2017; Li et al., 2017) for the purpose of gene perturbation experiments or time-lapse imaging (Li et al., 2015) at clonal level. This approach simplifies clonal analysis in avian embryos and broadens the range of cell types to which cell lineage analysis can be applied.

2.4 MATERIALS AND METHODS

Molecular cloning and virus preparation

The original RIA vector (Chen et al., 1999) was modified by inserting AscI, SpeI, NotI upstream of existing ClaI digestion site. H2B-YFP (#96893), H2B-RFP (#92398), Mito-CFP (#36208), Membrane-YFP (#56558) and Utrophin-Scarlet (#26739) were obtained from Addgene, and were subsequently subcloned into the modified RIA vector. ENV-A plasmid encoding the Envelope A protein was a gift from Dr. Connie Cepko and colleagues (Chen et al., 1999). ENV-A plasmid was co-transfected with recombinant RIA plasmids into chick DF1 cells to pseudotype RIA virus (ATCC, Manassas, VA; #CRL-12203, Lot number 62712171, Certificate of Analysis with negative mycoplasma testing available at ATCC website) in 15 cm culture dishes using standard transfection protocols. 24 hours post-transfection, the cell culture medium was harvested twice per day for four days, and

concentrated at 26,000 rpm for 1.5 hr. The pellet was dissolved in 20-30 µl of DMEM to achieve the titer of 1 x 10^7 pfu/ml. The viral aliquots were stored in -80°C until injection.

Virus titering and clonal analysis in DF1 cells

Concentrated virus was serially diluted at 1:10^4, 1:10^5, 1:10^6, and 1:10^7, respectively, in 200µl of DMEM. The diluted viral solution was added to chick DF1 cells in 24-well-plates. Cells were incubated at 38°C for two hours to permit viral infection. Another 800 µl DMEM was subsequently added and infected cells were incubated for 72 hours to allow for the expression of fluorescent proteins, which was used as a readout for functional recombinant virus. The number of cell clusters was quantified under an epifluorescence microscope. Typically, within a well of cells infected with the virus at 1:10^7 dilution, one positive cluster was observed, meaning the viral titer is around 1 x 10^7 pfu/ml. For clonal analysis in DF1 cells, a mixture of H2B-RFP, Mem-YFP and Mito-CFP viruses was serially diluted and infected DF1 cells as above. The number of cell clusters (clones) with distinct color(s) in a given field of view (n=3) was quantified using image software FIJI.

Viral injection and chick embryology

Equal amounts of RIA viruses encoding H2B-YFP, H2B-RFP, Mito-CFP, Membrane-YFP and Utrophin-Scarlet were mixed. A working solution was made at 1:2 dilution of the viral mixture with Ringer's solution (0.9% NaCl, 0.042%KCl, 0.016%$CaCl_2 \bullet 2H_2O$ wt/vol, pH7.0), and supplemented with 0.3µl of 2% food dye (Spectral Colors, Food Blue 002, C.A.S# 3844-45-9) as an indicator. About 1µl of working solution was injected into the

lumen of the neural tube posterior to somite 3 in HH11 chicken embryos. The embryos were sealed with surgical tape, incubated at 37°C for 2 days. Embryos were harvested at HH21 (n=16), dissected and a 500 μm thick transverse slice at forelimb region was cut for imaging analysis (detailed procedure in Li et al., 2019). For immunohistochemistry, embryos were fixed in 4% PFA in PBS for 30 mins at 4°C, embedded in Tissue-Tek O.C.T compound (Sakura #4583) and sectioned (*Microm* HM550 cryostat).

Immunohistochemistry and imaging analysis

Frozen tissue sections were incubated in 1xPBS at room temperature to remove O.C.T, permeabilized with 0.3% vol/vol Triton-X100 in 1xPBS. Primary and secondary antibodies were diluted in blocking buffer (1xPBS with: 5% vol/vol normal donkey serum, 0.3% vol/vol Triton-X100). Sections were stained with primary antibody at 4°C overnight (primary antibody dilutions: 1:500 Mouse anti-smooth muscle actin, Sigma-Cat# F1840-200uG; 1:500 Mouse antiHuC/D IgG2b, Invitrogen-Cat#A21271; 1:10 E1.9 primary sensory and motor neuron marker, DSHB). The next day, sections were washed with 1xPBS, and treated with secondary antibody for 1 hour at room temperature. The following secondary antibodies were used: 1:1000 donkey anti-mouse IgG 647, 1:1000 goat anti-mouse IgM 647, 1:1000 goat anti mouse IgG2b 647, Molecular Probes. Sections were imaged using a Zeiss AxioImager.M2 with Apotome.2 and Zeiss LSM 800 confocal microscope. The number of infected cells displaying single color was quantified with thresholding followed by automated particle analysis using FIJI software. The number of doubly and triply infected cells was counted manually. For Feret's angle analysis of clonal orientation, a cell cluster

with identical double-or triple- color was identified. Subsequently, a polygon was drawn along the boundary of the clone and the angle of the polygon was automatically measured by FIJI.

ACKNOWLEDGEMENT

We thank Alison Koontz for providing insightful suggestions on probability calculation, and Can Li, Felipe Vieceli, David Miller for technical support. We thank the Carlos Lois Laboratory and Caltech Biological Imaging Facility for sharing equipment. This work was supported by NIHR01DE027568 and NIHRO1HL14058 to M.E.B and American Heart Association predoctoral fellowship 18PRE34050063 to S.G.

2.5 REFERENCES

Ayer-Le Lievre and Le Douarin, 1982 C.S. Ayer-Le Lievre, N.M. Le Douarin

The early development of cranial sensory ganglia and the potentialities of their component cells studied in quail-chick chimeras

Dev. Biol., 94 (2) (1982), pp. 291-310

Baggiolini et al., 2015 A. Baggiolini, S. Varum, J.M. Mateos, D. Bettosini, N. John, M. Bonalli, et al.

Premigratory and migratory neural crest cells are multipotent in vivo

Cell Stem Cell, 16 (3) (2015), pp. 314-322

Bénazéraf et al., 2010 B. Bénazéraf, P. Francois, R.E. Baker, N. Denans, C.D. Little, O. Pourquié

A random cell motility gradient downstream of FGF controls elongation of an amniote

embryo

Nature, 466 (7303) (2010), pp. 248-252

Bronner-Fraser and Fraser, 1989 M. Bronner-Fraser, S. Fraser

Developmental potential of avian trunk neural crest cells in situ

Neuron, 3 (6) (1989), pp. 755-766

Bronner-Fraser and Fraser, 1988 M. Bronner-Fraser, S.E. Fraser

Cell lineage analysis reveals multipotency of some avian neural crest cells

Nature, 335 (6186) (1988), pp. 161-164

Cai et al., 2013 D. Cai, K.B. Cohen, T. Luo, J.W. Lichtman, J.R. Sanes

Improved tools for the Brainbow toolbox

Nat. Methods, 10 (6) (2013), pp. 540-547

Chen et al., 1999 C. Chen, D. Smith, M. Peters, M. Samson, J. Zitz, C. Tabin, C. Cepko

Production and design of more effective avian replication-incompetent retroviral vectors

Dev. Biol., 214 (2) (1999), pp. 370-384

Fields-Berry et al., 1992 S.C. Fields-Berry, A.L. Halliday, C. Cepko

A recombinant retrovirus encoding alkaline phosphatase confirms clonal boundary assignment in lineage analysis of murine retina

Proc. Natl. Acad. Sci. Unit. States Am., 89 (1992), pp. 693-697

Figliozzi et al., 2016 R.W. Figliozzi, F. Chen, A. Chi, S.-C.V. Hsia

Using the inverse Poisson distribution to calculate multiplicity of infection and viral replication by a high-throughput fluorescent imaging system

Virol. Sin., 31 (2) (2016), pp. 180-183

Frank and Sanes, 1991 E. Frank, J.R. Sanes

Lineage of neurons and glia in chick dorsal root ganglia: analysis in vivo with a recombinant retrovirus

Development (Cambridge, England), 111 (4) (1991), pp. 895-908

Gandhi et al., 2017 S. Gandhi, M.L. Piacentino, F.M. Vieceli, M.E. Bronner

Optimization of CRISPR/Cas9 Genome Editing for Loss-Of-Function in the Early Chick Embryo

Dev Biol., 432 (1) (2017), pp. 86-97

Gerrits et al., 2010 A. Gerrits, B. Dykstra, O.J. Kalmykowa, K. Klauke, E. Verovskaya, Broekhuis, G. de Haan, L.V. Bystrykh

Cellular barcoding tool for clonal analysis in the hematopoietic system

Blood, 115 (13) (2010), pp. 2610-2618

Kirby et al., 1983 M.L. Kirby, T.F. Gale, D.E. Stewart

Neural crest cells contribute to normal aorticopulmonary septation

Science (New York, N.Y.), 220 (4601) (1983), pp. 1059-1061

Krispin et al., 2010 S. Krispin, E. Nitzan, Y. Kassem, C. Kalcheim

Evidence for a dynamic spatiotemporal fate map and early fate restrictions of premigratory avian neural crest

Development (Cambridge, England), 137 (4) (2010), pp. 585-595

Lewis et al., 2013 A.E. Lewis, H.N. Vasudevan, A.K. O'Neill, P. Soriano, J.O. Bush

The widely used Wnt1-Cre transgene causes developmental phenotypes by ectopic activation of Wnt signaling

Dev. Biol., 379 (2) (2013), pp. 229-234

Li et al., 2015 Y. Li, V. Trivedi, T.V. Truong, D.S. Koos, R. Lansford, C.M. Chuong, D. Warburton, R.A. Moats, S.E. Fraser

Dynamic imaging of the growth plate cartilage reveals multiple contributors to skeletal morphogenesis

Nat. Commun., 6 (2015), p. 6798, 10.1038/ncomms7798

Li et al., 2017 Y. Li, A. Li, J. Junge, M. Bronner

Planar cell polarity signaling coordinates oriented cell division and cell rearrangement in clonally expanding growth plate cartilage

ELife, 6 (2017), p. e23279

Li et al., 2018 Y. Li, J.A. Junge, J.H. Miner, D.B. Arnold, S.E. Fraser

Discs large 1 controls daughter cell polarity after cytokinesis during skeletal formation

Proc. Natl. Acad. Sci. Unit. States Am., 115 (46) (2018), pp. E10859-E10868

1713959115

Li et al., 2019 Y. Li, F.M. Vieceli, W.G. Gonzalez, A. Li, W. Tang, C. Lois, M.E. Bronner

In vivo quantitative imaging provides insights into trunk neural crest migration

Cell Rep., 26 (6) (2019), pp. 1489-1500 e3

Livet et al., 2007 J. Livet, T.A. Weissman, H. Kang, R.W. Draft, J. Lu, R.A. Bennis, J.R. Sanes, J.W. Lichtman

Transgenic strategies for combinatorial expression of fluorescent proteins in the nervous system

Nature, 450 (7166) (2007), pp. 56-62

Pearse et al., 2007 R.V. Pearse, P.J. Scherz, J.K. Campbell, C.J. Tabin

A cellular lineage analysis of the chick limb bud

Dev. Biol., 310 (2) (2007), pp. 388-400

Sanes, 1989 J.R. Sanes

Analysing cell lineage with a recombinant retrovirus

Trends Neurosci., 12 (1) (1989), pp. 21-28

Sulston, 1983 J.E. Sulston

Neuronal cell lineages in the nematode Caenorhabditis elegans

Cold Spring Harbor Symp. Quant. Biol., 48 (Pt 2) (1983), pp. 443-452

Tawk et al., 2007 M. Tawk, C. Araya, D.A. Lyons, A.M. Reugels, G.C. Girdler, P.R. Bayley, D.R. Hyde, M. Tada, J.D.W. Clarke

A mirror-symmetric cell division that orchestrates neuroepithelial morphogenesis

Nature, 446 (7137) (2007), pp. 797-800

Turner and Cepko, 1987 D.L. Turner, C.L. Cepko

A common progenitor for neurona and glia persists in rat retina late in development

Nature, 328 (1987), pp. 131-136

Weston and Thiery, 2015 J.A. Weston, J.P. Thiery

Pentimento: neural crest and the origin of mesectoderm

Dev. Biol., 401 (1) (2015), pp. 37-61

Chapter III

CARDIAC NEURAL CREST CONTRIBUTES TO CARDIOMYOCYTES IN AMNIOTES

Part of this chapter was published as Tang, W.*, Martik, M. L.*, Li, Y. & Bronner, M. E. Cardiac neural crest contributes to cardiomyocytes in amniotes and heart regeneration in zebrafish. *Elife* 8, (2019). DOI: 10.7554/eLife.47929

ABSTRACT

Cardiac neural crest cells contribute to important portions of the cardiovascular system including the aorticopulmonary septum and cardiac ganglion. Using replication incompetent avian retroviruses for precise high-resolution lineage analysis, we uncover a previously undescribed neural crest contribution to cardiomyocytes of the ventricles in *Gallus gallus*, supported by *Wnt1-Cre* lineage analysis in *Mus musculus*. The results suggest that neural crest cells contribute to many cardiovascular structures including cardiomyocytes across vertebrates.

3.1 INTRODUCTION

The neural crest is an important stem cell population characterized by its multipotency, migratory behavior, and broad ability to differentiate into derivatives as diverse as elements of the cardiovascular system, craniofacial skeleton, and peripheral nervous system. However, not all neural crest cells are alike, with distinct populations existing along the body axis. One of the most unique neural crest populations is the “cardiac neural crest” that contributes to the outflow septum and smooth muscle of the outflow tract of the heart. Ablation studies in chick embryos show that removal of the cardiac crest results in a broad range of defects,

including persistent truncus arteriosus, abnormal myocardium function, and misalignment of the arch arteries[1,2,3]. These defects are highly reminiscent of some of the most common human congenital heart defects. Importantly, other neural crest populations cannot rescue the effects of cardiac neural crest ablation, even when grafted in its place, exemplifying the uniqueness of this population[4].

Classically, quail-chick transplantation experiments have been used to uncover contributions of the cardiac neural crest to the heart, with some more recent attempts using antibody staining of migratory neural crest cells or LacZ retroviral lineage analysis as well as transgenic lines such as *Wnt1-Cre* driven β-galactosidase in mammals[1,5-7]. The results suggest that the cardiac neural crest contributes to smooth muscle cells lining the great arteries, outflow tract septum and valves, mesenchyme that remodels pharyngeal arch arteries, and parasympathetic innervation of the heart, such as the cardiac ganglion. However, inconsistencies remain between different lineage approaches, most of which suffer from high background and low cellular resolution.

To reconcile these differences, here, we use a multi-organismal approach to examine the lineage contributions of cardiac neural crest to the heart. Using a novel retroviral labeling approach in chick and confirmed by *Wnt1-Cre* reporter lines in mouse, we reveal a previously undetected contribution of the amniote cardiac neural crest to the trabecular myocardium of the ventricles, a derivative previously thought to be confined to non-amniotic vertebrates[8-10]. Taken together, these results demonstrate an evolutionarily conserved contribution of neural crest cells to cardiomyocytes across vertebrates.

3.2 RESULTS AND DISCUSSION

3.2.1 LABELING THE CHICK CARDIAC NEURAL CREST USING REPLICATION INCOMPETENT AVIAN RETROVIRUS

To specifically label cardiac neural crest cells prior to their emigration from the neural tube and identify novel progeny of chick cardiac crest, we use a replication-incompetent avian retrovirus (RIA) that indelibly and precisely marks neural crest progenitors for long term lineage analysis at single cell resolution and without the need for tissue grafting. To this end, the post-otic neural tube of the hindbrain adjacent to somites 1-3 was injected at Hamburger and Hamilton (HH) stage 9-10 with high-titer (1x107 ifu/mL) RIA (Fig3-1A), which drives expression of nuclear localized H2B-YFP under control of a constitutive RSV promoter [11-15]. At this stage in the development, premigratory cardiac neural crest cells are positioned within the dorsal neural tube and about to emigrate. Accordingly, this labeling approach solely marks hindbrain neural tube cells including premigratory cardiac neural crest cells that subsequently delaminate from the dorsal neural tube during a two-hour time window when the virus remains active.

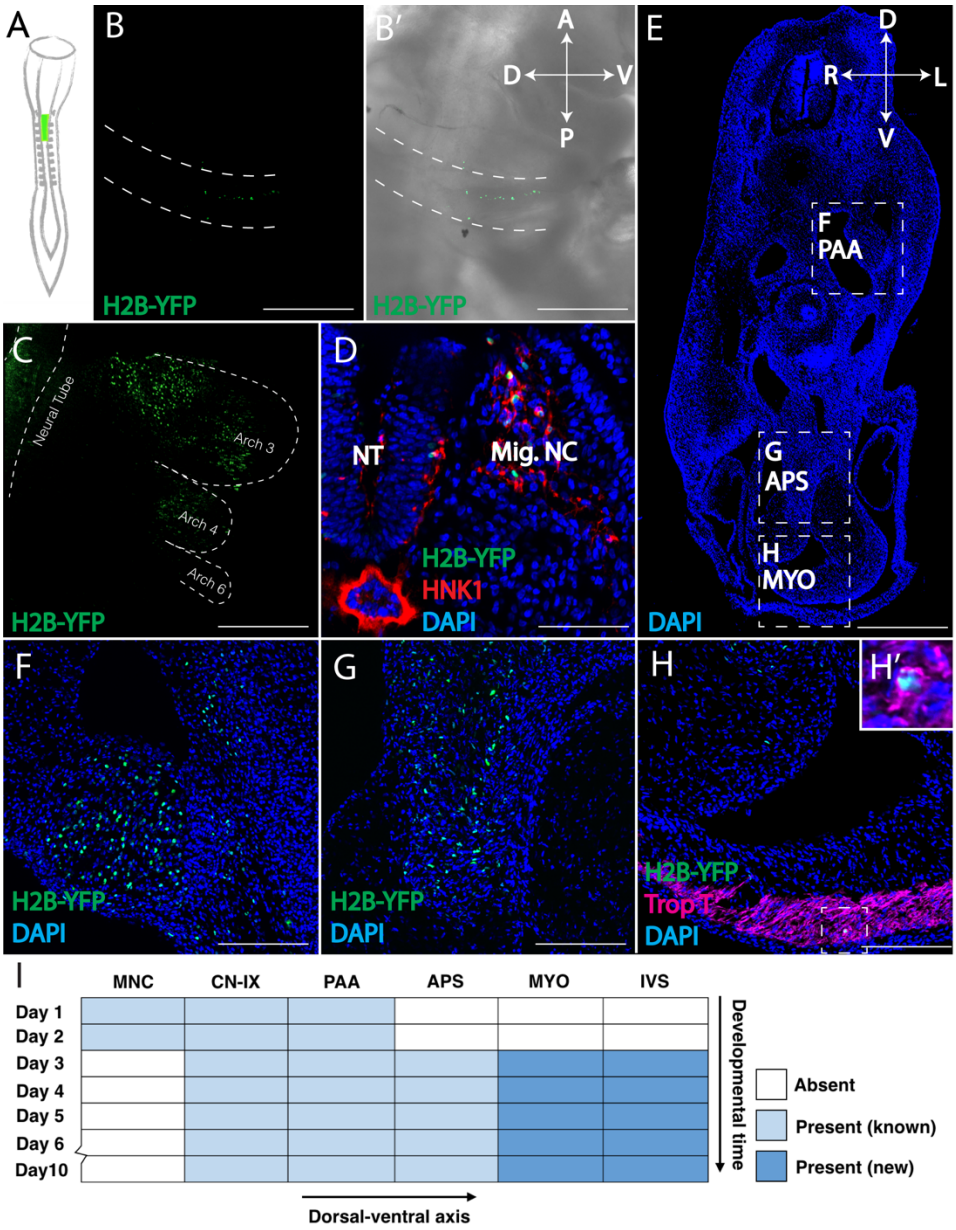

Figure 3-1. Retrovirally mediated fate mapping of cardiac neural crest reveals novel derivatives. (A) Schematic diagram of the approach: Replication Incompetent Avian (RIA) retrovirus encoding nuclear H2B-YFP was injected into the lumen of the hindbrain from which cardiac neural crest arises. (B) One day post-infection (HH14), whole mount image (lateral view) showing virally labelled progeny (green) in the cardiac migration stream en route to pharyngeal arch 3. (B') Brightfield image to show anatomical information. A, anterior; P, posterior; D, dorsal; V, ventral. (C) Two days post-infection (HH18), virally labelled cardiac crest has populated

pharyngeal arches 3, 4 and 6, highlighted with dashed line. (D) Transverse section showing that labelled cardiac crest expresses neural crest marker HNK-1 (red). D, dorsal; V, ventral; L, left; R, right. (E) Low magnification transverse section of an E6 embryo (DAPI, blue). Dashed boxes show relative positions of cardiac crest-derived populations. (F-H) High magnification image of selected regions in E: pharyngeal arch arteries (F); aorticopulmonary septum (G); Neural crest derivatives located in the outflow tract express Troponin T (magenta), a myocardium marker (H, H'). (I) Temporal map of the establishment of distinct cardiac neural crest derivatives. Labelled cells initially are in the migration stream, cranial nerve IX (CN-IX) and mesenchyme around pharyngeal arch arteries (PAA). Subsequently, they populate the aorticopulmonary septum (APS), myocardium (MYO) and interventricular septum (IVS). Separate channels are displayed in supplementary figure 3-1. Light blue indicates known neural crest derivatives. Dark blue reflects newly discovered neural crest derivatives. Scale bars: B, C, E 400μm; D, F, G, H 100μm.

Virally infected embryos were then allowed to develop for 1-9 days post injection, cryo-sectioned, and analyzed using confocal microscopy. One day after injection, whole mount imaging revealed RIA-labeled cells migrating in a stream along pharyngeal arch 3 (Fig 3-1B,B'), that subsequently accumulated in pharyngeal arches 3, 4, and 6 two days after infection (Fig 3-1C). Next, we confirmed that all labeled cells in the periphery co-localized with the migratory neural crest marker, HNK-1, demonstrating that the neural crest is the only population labeled with H2B-YFP outside the neural tube, thus verifying specificity of infection (Fig 3-1D, Supplementary figuer3-1 A). With time, labeled cardiac crest cells were observed in numerous and diverse derivatives, populating the cardiovascular system in a proximal to distal progression (Fig 3-1E-I). Consistent with quail-chick chimera, we observed RIA-labeled cells adjacent to and within the walls of pharyngeal arch arteries, in the aorticopulmonary septum, outflow tract, and cardiac cushion. Moreover, we definitively observed YFP-labeled cells in the superior interventricular septum, a site for which the neural

crest contribution has been controversial, although ventricular septal defects are common after cardiac neural crest ablation[16]. The cells of the outflow tract septum and pharyngeal arch arteries differentiated into smooth muscle actin (SMA) positive cells on embryonic day (E) 5 (Fig 3-2A,B).

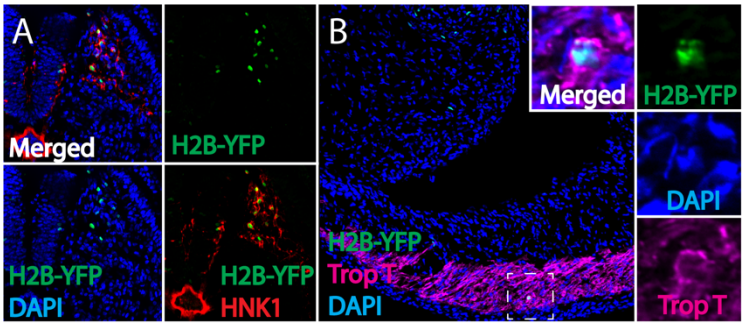

Supplementary figure 3-1: Separate channels for retroviral lineage analysis and immunohistochemistry. (A) Separate channels of Figure 1D. All H2B-YFP labelled cells that migrate out of the neural tube are HNK1-positive cardiac neural crest cells (H2B-YFP, green; HNK1, red; DAPI, blue). (B) Separate channels of Figure 3-1H. H2B-YFP labelled cardiac neural crest is present in myocardium of the outflow tract (H2B-YFP, green; Troponin T, magenta; DAPI, blue).

Importantly, by E3 and onward, virally labeled neural crest cells were observed in the myocardium of both the outflow tract and the ventricles, where they expressed the myocardial markers, Troponin T and Myosin Heavy Chain (Fig 3-1H, Supplementary figuer3-1 B, outflow tract; Fig 3-2 C,D, Supplementary figure 3-2 A,B, ventricles). These neural crest-derived cardiomyocytes were not actively undergoing cell division or programmed cell death (Fig 3-2E,F), consistent with the stable presence of cells observed over time (Fig 3-1I). Supplementary file 3-1a and 1b present quantification of contributions of virally labeled cells in the chick ventricular myocardium. While previous lineage tracing

experiments in zebrafish showed that a stream of neural crest cells integrate into the myocardium of the primitive heart tube to give rise to cardiomyocytes, our results present the first evidence of a homologous neural crest contribution to cardiomyocytes in chick embryos [8-10].

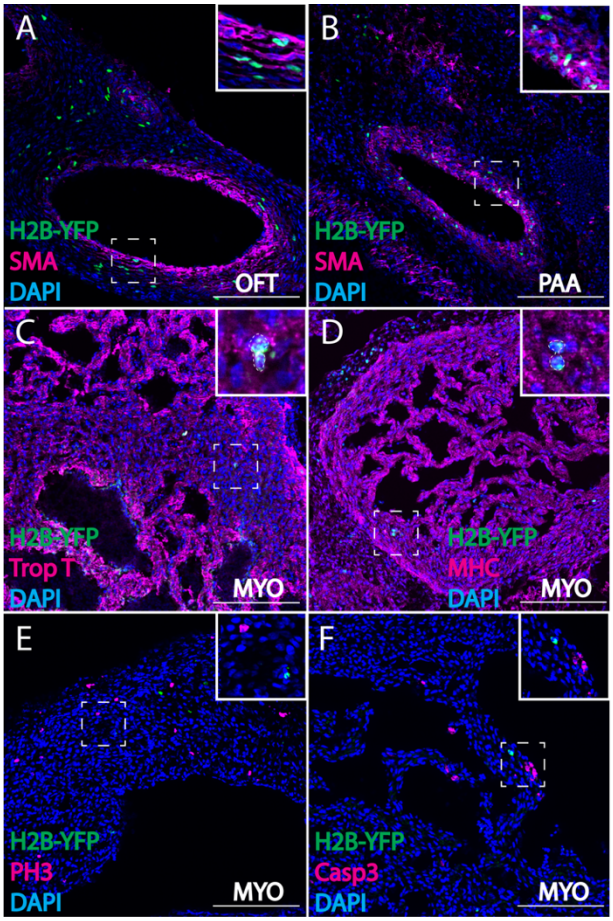

Figure 3-2. Cardiac crest-derived cells differentiate into smooth muscle and cardiomyocytes in avian embryos. (A, B) Retrovirally labelled cardiac crest cells (H2B-YFP, green) that migrate into the outflow tract (A, OFT) and pharyngeal arch arteries (B) express smooth muscle actin (SMA, magenta) marker. (C, D) Labeled cardiac crest cells that enter the ventricle express myocardial marker Troponin T (magenta) (C), and myocardial terminal differentiation marker Myosin Heavy Chain (MHC, magenta) (D) enclosed in dashed line. (E, F) Neural crest-derived cardiomyocytes are not actively dividing or undergoing apoptosis, as demonstrated by

phosphohistone H3 staining (PH3, magenta) (E) and Caspase 3 staining (magenta) (F). Transverse view of HH28 embryos. Separate channels are displayed in supplementary figure 3-2. Scale bars: 100μm.

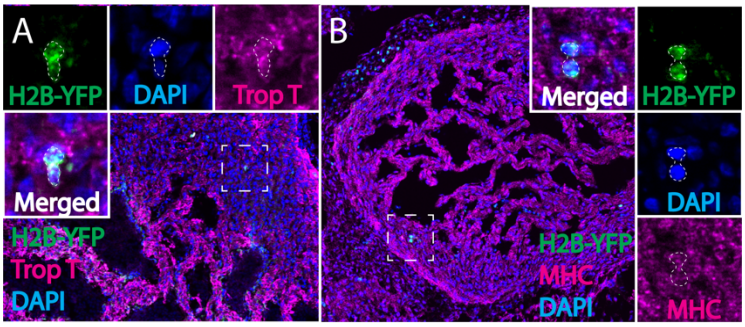

Supplementary figure 3-2: Separate channels for retroviral lineage analysis and immunohistochemistry. (A) Separate channels of Figure 2C. H2B-YFP virus labelled cardiac neural crest is present in myocardium of the ventricle and expresses cardiomyocyte marker Troponin T (H2B-YFP, green; Troponin T, magenta; DAPI, blue; enclosed in dashed line). (B) Separate channels of Figure 2D. H2B-YFP virus labelled cardiac neural crest is present in myocardium of the ventricle and expresses cardiomyocyte terminal differentiation marker myosin heavy chain (MHC) (H2B-YFP, green; MHC, magenta; DAPI, blue; enclosed in dashed line).

Supplementary File 1a

Quantification of cardiac neural crest contribution to the heart in chick and mouse

Wnt1-ZsGreen Chick retroviral lineage tracing

Stage	MNC	CN-IX	PAA	Cardiovascular structure		
				APS (%)	MYO (%)	IVS (%)
Day 1	15	12	22			
Day 2	38	36	199			
Day 3			112	16	7	
Day 4			64	65 (73.9)	11 (12.5)	12(13.6)
Day 5			270	197 (90.4)	6 (2.8)	15 (6.8)
Day 6			199	80 (84.2)	7 (7.4)	8 (8.4)
Day 10				201 (84.5)	12 (5)	25 (10.5)
E 15.5				169 (58.1)	95 (32.6)	27 (9.3)

Abbreviations: MNC, migratory neural crest; CN-IX, cranial nerve nine; PAA, pharyngeal arch arteries; APS, aorticopulmonary septum; MYO, myocardium of ventricle; IVS, interventricular septum.

Supplementary File 1b
Quantification of cardiac neural crest contribution to the heart in chick and mouse

	MNC	CN-IX	PAA	APS	MYO	IVS
D1 E1	7	11	20			
D1 E2	31	14	22			
D1 E3	5	14	26			
D1 E4	10	15	19			
D1 E5	24	6	22			
D2 E1	45	49	36			
D2 E2	63	73	195			
D2 E3	21	23	53			
D2 E4	27	15	517			
D2 E5	34	21	190			
D3 E1			82	9	12	
D3 E2			88	24	7	
D3 E3			49	17	7	
D3 E4			228	15	1	
D4 E1			46	129	20	7
D4 E2			49	11	7	0
D4 E3			44	35	11	26
D4 E4			115	85	6	15
D5 E1			265	446	7	8
D5 E2			270	144	7	3
D5 E3			227	97	6	18
D5 E4			316	99	5	31
D6 E1			106	48	6	16
D6 E2			211	117	9	8
D6 E3			282	61	5	0
D6 E4			198	92	6	9
D10 E1				77	7	32
D10 E2				422	18	26
D10 E3				51	13	23
D10 E4				254	8	19
E15.5 Wnt1-Zsgreen E1				146	86	32
E15.5 Wnt1-Zsgreen E2				149	80	33
E15.5 Wnt1-Zsgreen E3				212	145	35
E15.5 Wnt1-Zsgreen E4				170	70	8

Abbreviations: MNC, migratory neural crest; CN-IX, cranial nerve nine; PAA, pharyngeal arch arteries; APS, aorticopulmonary septum; MYO, myocardium of ventricle; IVS, interventricular septum.

Supplementary File 3-1 a, b: Quantification of cardiac neural crest contribution to the heart in chick and mouse. Table presents virally labelled cardiac neural crest derivatives at MNC (migratory neural crest), CN-IX (cranial nerve nine), PAA (pharyngeal arch arteries), APS (aorticopulmonary septum), MYO (myocardium of ventricle) and IVS (interventricular septum) at day 1-6 and day 10 post injection in chick. The bottom part presents number of Wnt1+ cells in E15.5 *Wnt1-Cre* mouse. Percentage in parentheses represents the proportion of the population among all NC-derived cells in cardiovascular structure (including MYO, APS, and IVS). % Neural crest contribution to ventricle, the proportion of Wnt1+ cells (including MYO and IVS) among all cells in the ventricle is about 16.8%. Supplementary File 3-1b shows the raw data of each embryo from which data in Supplementary File 3-1a was generated.

3.2.2 LINEAGE ANALYSIS IN THE MOUSE EMBRYO

To test whether the contribution of cardiac neural crest cells to the myocardium was conserved in mammals, we examined *Wnt1-Cre;ZsGreenfl/fl* transgenic mice in which neural crest cells were labeled with cytoplasmic GFP[17]. Embryos were fixed at E15.5 (similar to E7 in chick). Analogous to the results in chick embryos, we observed a large number of ZsGreen-positive myocardial cells in the outflow tract and ventricles, as confirmed by Troponin T expression (Fig 3-3A-C). To avoid ectopic expression that has been associated with the *Wnt1-Cre;ZsGreenfl/fl* transgenic line due to endogenous *Wnt1* activation caused by in-frame ATG located upstream of *Wnt1* start codon, we tested an improved *Wnt1* line (*Wnt1-Cre2+; R26mTmG* mouse line) without ectopic activation of canonical Wnt/β-catenin pathway[18]. The results were similar to those observed with the *Wnt1-Cre;ZsGreenfl/fl* transgenic mice (Fig 3-3D,E). As in the chick embryos, murine neural crest derived cells were present in the outflow tract, interventricular septum, and myocardium of both ventricles.

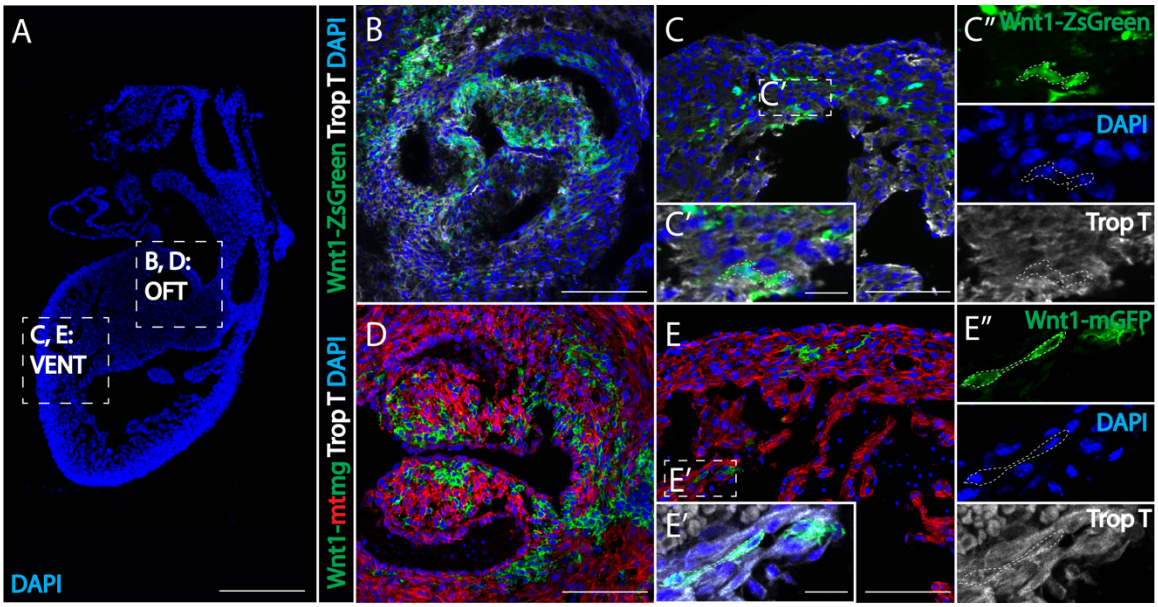

Figure 3-3. *Wnt1-Cre* fate mapping in mice confirms the presence of cardiac crest-derived myocardium. (A) Low magnification image to show the relative anatomical positions of a mouse heart at E15.5 (sagittal view, DAPI-blue). (B, C) In *Wnt1-Cre; ZsGreenfl/fl* mice, neural crest-derived cells (green, *Wnt1-Cre* driven ZsGreen expression is abbreviated as Wnt1-ZsGreen, enclosed in dashed line) were observed in myocardium (Troponin T, grey) of the outflow tract (B), and ventricle (VENT) (C, C'': separate channels of inset C'). (D, E) Similar results were obtained from *Wnt1-Cre2+; R26mTmG* mice (*Wnt1-Cre2+* driven replacement of membrane localized tdTomato (mT) by EGFP (mG) (abbreviated as Wnt1-mtmg), where cardiac crest-derived cells (green, enclosed in dashed line) were present in myocardium of the outflow tract (D) and ventricle (Troponin T, grey) (E, E'': separate channels of inset E'). Transverse view. Scale bars: A 400μm; B-E 100μm; C', E' 10μm.

The numbers of neural crest-derived cells appear to decrease with distance along the proximal-to-distal axis (Fig 3-4A), such that no neural crest-derived cardiomyocytes were observed in the apex of the heart (Fig3-4 D,E). As in the chick, the numbers of Wnt1+ cells remain stable with time, and the cells do not appear to undergo active cell division or apoptosis (Fig3-4 B,B',C,C'). This contribution persists postnatally, as Wnt1+ cells are

present at postnatal day 2 (Fig3-4 F-H). These results are consistent with previous studies using less specific *P0-Cre* lines and demonstrate that comparable cardiac crest contributions occur in birds and mammals[19-20]. Quantification of numbers of neural crest lineage labeled cells in the trabeculated myocardium of mice reveals that they represent approximately 17% of the population in the proximal half of the ventricle (Supplementary file 3-1a).

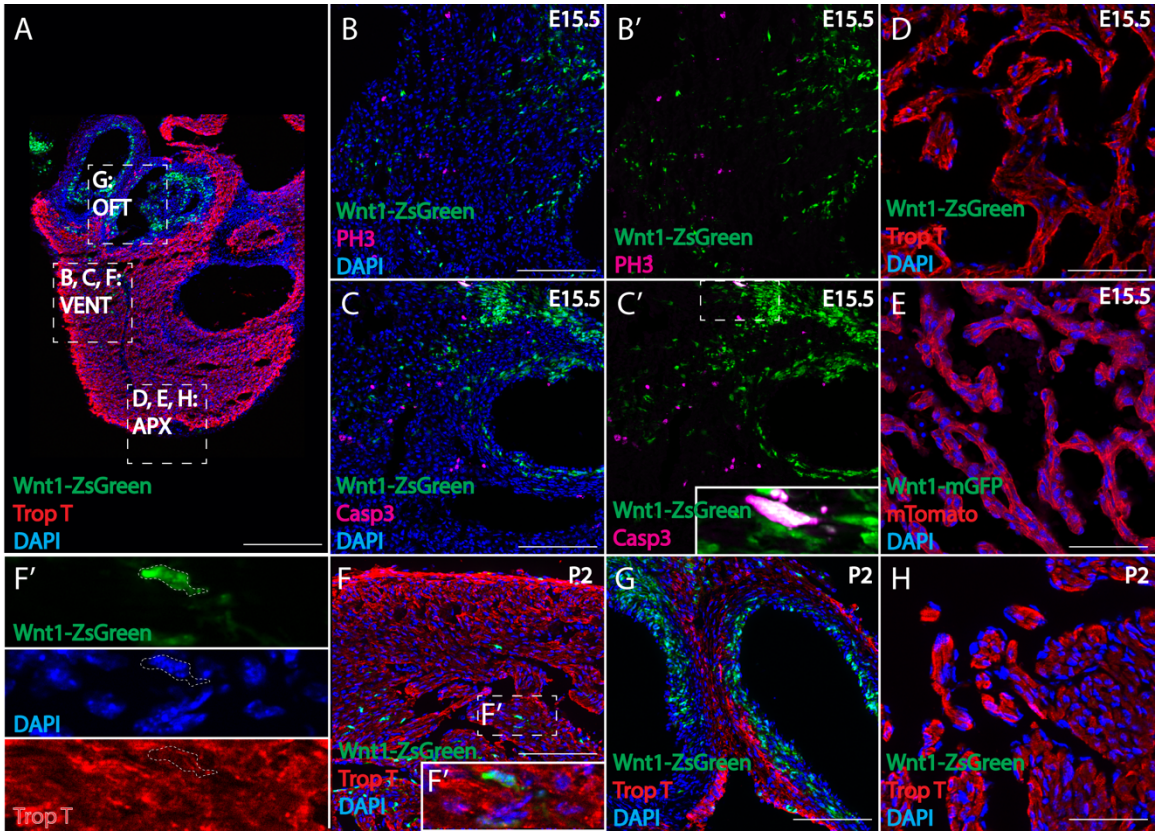

Figure 3-4. Spatial-temporal distribution of neural crest-derived cardiomyocytes in *Wnt1-Cre* mouse. (A) In E15.5 *Wnt1-Cre; Zsgreenfl/fl* mouse heart, cardiac neural crest progenies were distributed in the outflow tract, valves and myocardium of both ventricles. Density of Zsgreen+ cells decreased along the proximal-to-distal axis, thus no cell contributed to the apex (Wnt1-Zsgreen, green; Troponin T, red; DAPI, blue). (B) Proliferation marker PH3 did not selectively colocalize with Zsgreen+ cells (PH3, magenta; B', separate channels for colocalization). (C) Apoptosis marker Caspase3 was not selectively expressed in Zsgreen+ cells (Caspase 3,

magenta; C', separate channels for colocalization). (D) Cardiac neural crest did not contribute to apical myocardium in *Wnt1-Cre; Zsgreenfl/fl* mouse (Wnt1-Zsgreen, green; Troponin T, red; DAPI, blue), or (E) *Wnt1-Cre; R26mtmg* mouse (Wnt1-membrane GFP, green; membrane Tomato, red; DAPI, blue). (F-H) On postnatal day 2, cardiac neural crest progenies in *Wnt1-ZsGreen* mouse persisted in the myocardium of the ventricle (F) (separate channels in F'), outflow tract (G), but not the apex (H) (Wnt1-Zsgreen, green; Troponin T, red; DAPI, blue), similar to what was observed in E15.5 hearts. Scale bars: A 400μm; B, C, F, G 100μm; D, E, H 160μm.

3.2.3 DISCUSSION

Our cell lineage labeling results provide direct evidence for a neural crest contribution to the myocardium of the amniote heart. Why was the contribution of neural crest cells to cardiomyocytes in amniotes previously missed? Interspecific quail-chick chimera are generated via transplantation of donor tissue into the host, which requires time to heal[1]. If the neural crest cells that migrate to the ventricles are the earliest migrating cells, this population may have been delayed after grafting due to wound healing and hence unable to migrate as far. Alternatively, the labeled cells may have been missed since it can be challenging to identify a small population of dispersed quail cells amongst many more numerous chick cells. Furthermore, cell behavior might be altered when transplanted quail cells are introduced into a chick environment. Our retroviral lineage labeling circumvents these issues by indelibly labeling an endogenous neural crest population without the need for grafting. Moreover, the labeled cells are easily detectable due to their fluorescent readout. For lineage labeling in mice, there were hints in the literature regarding a possible neural crest contribution to cardiomyocytes. However, the experiments were either indirect or used lineage tracing techniques that were not specific to the neural crest. For example, Tomita et

al. showed that cells isolated from "cardiospheres" can behave like neural crest cells when injected into chick embryos[20]. In addition, lineage analysis in mouse using a *P0-Cre* line revealed EGFP-positive cells in the myocardium that gather at the ischemic border upon injury[20]. However, *P0* is not a neural crest specific marker, making these results inconclusive at the time. In contrast, *Wnt1* is the "gold standard" for neural crest labeling and the improved *Wnt1* line (*Wnt1-Cre2+; R26mTmG*) corrects possible ectopic expression problematic in the original *Wnt1-Cre;ZsGreen* line[7,17,18].

In chick and mouse, neural crest-derived cells comprise a significant portion (~17%) of the trabeculated myocardium in the proximal part of both ventricles. Interestingly, this percentage is similar to what has been reported in zebrafish[10,21]. In amniotes, we find that the density of the cells decreases along the proximal-distal axis and appears to be stable through time (Fig3-1I, Supplemental file 1-1a,b).

3.3 CONCLUSION

In summary, the present results show, for the first time, the common ability of cardiac neural crest cells across diverse vertebrates to contribute to heart muscle. Moreover, according to the published paper where this chapter was adapted from, these cells appear to be critical for cardiac regeneration in zebrafish. If the results extrapolate to other species, the mechanisms that control the normal development of the neural crest into cardiomyocytes may be harnessed to stimulate these cells to proliferate and regenerate new cardiomyocytes, thus offering potential therapeutic approaches to repair heart damage in mammals including humans.

3.4 MATERIALS AND METHODS

Cell culture and retrovirus preparation

Using a standard transfection protocol, chick DF1 cells (ATCC, Manassas, VA; #CRL-12203, Lot number 62712171, RRID:CVCL_0570, Certificate of Analysis with negative mycoplasma testing at the ATCC website) were transfected with RIA-H2B-YFP plasmid (RRID:Addgene_96893) and ENV-A plasmid in 15 cm culture dishes. Cell culture medium was collected 24 hours post-transfection, and twice per day for four days, then centrifuged at 26,000 rpm for 1.5 hr. The supernatant was dried with aspiration, and the pellet was dissolved in 20-30 µl of DMEM to a final titer of 1 x 10^7 ifu/mL. Viral aliquots were stored in -80°C until the time of injection.

Chick embryo processing and viral injection

Viral stock was diluted 1:2 with Ringer's solution (0.9% NaCl, 0.042%KCl, 0.016%$CaCl_2 \bullet 2H_2O$ wt/vol, pH7.0) to generate the working solution, which was mixed with 0.3µl of 2% food dye (Spectral Colors, Food Blue 002, C.A.S# 3844-45-9) as indicator. The lumen of the neural tube adjacent to the middle of the otic vesicle to the level of somite 3 was injected with 0.2µl of working in HH8-10 chicken embryos. Embryos were sealed with surgical tap and incubated at 37°C for 1-10 days, harvested at HH14 (n=5), HH18 (n=5), HH21 (n=4), HH25 (n=4), HH28 (n=4), HH32 (n=4) and E10 (n=4). At the time of harvesting, chick embryos were dissected, fixed in 4%PFA in PBS for 30 mins at 4°C, then embedded in gelatin and sectioned (*Microm* HM550 cryostat).

***Wnt1-Cre* mouse and tissue preparation**

The *Wnt1-Cre; ZsGreen*$^{fl/fl}$ mice described in Chai *et al*., 2000 (gift from Drs. Xia Han and Yang Chai at University of Southern California, Center for Craniofacial Molecular Biology) were harvested and fixed at E15.5 (n=8) and P2 (n=2). The hearts were dissected, fixed in 4%PFA in PBS for 30mins at 4°C. E15.5 *Wnt1-Cre2+; R26mTmG* mice (Lewis *et al*.,2013) (129S4-Tg(Wnt1-cre)1Sor/J, gift from Dr. Jeffrey Bush at University of California, San Francisco, n=3) were fixed with 4% PFA overnight before dissection. The hearts were embedded in gelatin, and sectioned.

Quantification of neural crest contributions to the ventricular myocardium

To quantify RIA-labeled cells in chick embryos, three consecutive sections of the same axial level were imaged per embryo. The number of YFP-positive cells was averaged to account for variability due to sampling. n=4-6 embryos were analyzed at each stage as biological replicates. The results are presented as presence or absence of virally labelled cardiac neural crest derivatives at different anatomical locations in Fig. 3-1I and supplementary file 3-1a, 1b. To quantify Wnt1-Zsgreen+ cells in E15.5 mouse heart, three consecutive sections of the same axial level were imaged per embryo (n=4). Automated particle analysis was conducted with FIJI program to estimate the total number of Zsgreen+ cells in the image. For the percentage of neural crest-derived cells in the ventricle, the same procedure was performed with the DAPI channel which represents total cell population. % Zsgreen/DAPI was calculated, and averaged to the result presented in the text of supplementary file 3-1a.

Immunohistochemistry and image analysis

After cryosectioning, slides were incubated in 1xPBS at 42°C to remove gelatin. 0.3% vol/vol Triton-X100in 1xPBS was used to permeabilize the tissue. Sections were incubated with primary antibody underneath a parafilm layer at 4°C overnight (primary antibody dilutions: 1:10 Troponin T CT3, DSHB (RRID:AB_528495); 1:10 Myosin Heavy Chain ALD58, DSHB (RRID:AB_528361); 1:10 Myosin Heavy Chain F59, DSHB (RRID:AB_528373); 1:500 Mouse anti-smooth muscle actin, Sigma-Cat# A5228-200uG; 1:500 Mouse anti phospho-histone H3, Abcam-ab14955; 1:500 rabbit anti caspase-3,R&D Systems # AF835; 1:500 goat anti GFP, Abcam Cat#ab6673, all in blocking reagent 1xPBS with: 5% vol/vol normal donkey serum, 0.3% vol/vol Triton-X100). Subsequently, sections were washed for 3 times with 1xPBS, incubated with secondary antibody for 40 mins at room temperature and counterstained with DAPI. Secondary antibodies include: Goat anti-mouse IgG2a Alexa-568 (RRID:AB_2535773), Goat anti-mouse IgG1 Alexa-568(RRID:AB_2535766), Goat anti-rabbit IgG Alexa-568(RRID:AB_2534121), Donkey anti-goat IgG Alexa-488(RRID:AB_2534102); 1:1000, Molecular Probes. Zeiss AxioImager.M2 with Apotome.2 and Zeiss LSM 800 confocal microscope were utilized for imaging. Images were cropped, rotated, and intensity was linearly adjusted for visualization.

ACKNOWLEDGMENT

We would like to thank Drs. Xia Han and Yang Chai at University of Southern California, Center for Craniofacial Molecular Biology for being extremely supportive and kindly providing *Wnt1-Cre; ZsGreen*$^{fl/fl}$ cardiac tissue. Many thanks to Dr. Jeffrey Bush at

University of California, San Francisco who generously sent us *Wnt1-Cre2+; R26mTmG* mouse embryos. We thank Joanne Tan-Cabugao and Constanza Gonzalez for technical assistance, and Beckman Institute Biological Imaging Facility for equipment. This work was supported by NIHR01DE027568 and NIHRO1HL14058 to MEB and a Helen Hay Whitney Post-doctoral Fellowship to MLM.

3.5 REFERENCES

1. Kirby M, Gale T, Stewart D (1983) Neural crest cells contribute to normal aorticopulmonary septation. *Science* 220(4601):1059-1061.

2. Waldo K, Zdanowicz M, Burch J, et al (1999) A novel role for cardiac neural crest in heart development. *J Clin Invest* 103(11):1499-1507.

3. Bockman DE, Redmond ME, Waldo K, Davis H, Kirby ML (1987) Effect of neural crest ablation on development of the heart and arch arteries in the chick. *Am J Anat.* 180(4):332-341.

4. Kirby ML (1989) Plasticity and predetermination of mesencephalic and trunk neural crest transplanted into the region of the cardiac neural crest. *Dev Biol.* 134(2):402-412.

5. Kuratani SC, Kirby ML (1991) Initial migration and distribution of the cardiac neural crest in the avian embryo: an introduction to the concept of the circumpharyngeal crest. *Am J Anat.* 191(3):215-227.

6. Boot MJ, Gittenberger-De Groot AC, Van Iperen L, Hierck BP, Poelmann RE (2003) Spatiotemporally separated cardiac neural crest subpopulations that target the outflow tract septum and pharyngeal arch arteries. *Anat Rec A Discov Mol Cell Evol Biol.* 275(1):1009-1018.

7. Jiang X, Rowitch DH, Soriano P, McMahon AP, Sucov HM (2000) Fate of the mammalian cardiac neural crest. *Development* 127(8):1607-1616.

8. Sato M, Yost HJ. Cardiac neural crest contributes to cardiomyogenesis in zebrafish (2003) *Dev Biol.* 257(1):127-139.

9. Li Y-X, Zdanowicz M, Young L, Kumiski D, Leatherbury L, Kirby ML (2003) Cardiac neural crest in zebrafish embryos contributes to myocardial cell lineage and early heart function. *Dev Dyn.* 226(3):540-550.

10. Cavanaugh AM, Huang J, Chen J-N (2015) Two developmentally distinct populations of neural crest cells contribute to the zebrafish heart. *Dev Biol.* 404(2):103-112.

11. Li Y, Li A, Junge J, Bronner M (2017) Planar cell polarity signaling coordinates oriented cell division and cell rearrangement in clonally expanding growth plate cartilage. *Elife* 6.

12. Tang W, Li Y, Gandhi S, Bronner ME (2019) Multiplex clonal analysis in the chick embryo using retrovirally-mediated combinatorial labeling. *Dev Biol.* 450(1):1-8.

13. Fields-Berry SC, Halliday AL, Cepko CL (1992) A recombinant retrovirus encoding alkaline phosphatase confirms clonal boundary assignment in lineage analysis of murine retina. *PNAS* 89(2):693-697.

14. Chen CM, Smith DM, Peters MA, et al (1999) Production and design of more effective avian replication-incompetent retroviral vectors. *Dev Biol.* 214(2):370-384.

15. Hamburger V, Hamilton HL (1951) A series of normal stages in the development of the chick embryo. *J Morphol.* 88(1):49-92.

16. Kirby ML, Turnage KL, Hays BM (1985) Characterization of conotruncal malformations following ablation of “cardiac” neural crest. *Anat Rec*. 213(1):87-93.

17. Chai Y, Jiang X, Ito Y, et al (2000) Fate of the mammalian cranial neural crest during

tooth and mandibular morphogenesis. *Development* 127(8):1671-1679.

18. Lewis AE, Vasudevan HN, O'Neill AK, Soriano P, Bush JO (2013) The widely used Wnt1-Cre transgene causes developmental phenotypes by ectopic activation of Wnt signaling. *Dev Biol.* 379(2):229-234.

19. Tomita Y, Matsumura K, Wakamatsu Y, et al (2005) Cardiac neural crest cells contribute to the dormant multipotent stem cell in the mammalian heart. *J Cell Biol.* 170(7):1135-1146.

20. Tamura Y, Matsumura K, Sano M, et al (2011) Neural crest-derived stem cells migrate and differentiate into cardiomyocytes after myocardial infarction. *Arterioscler Thromb Vasc Biol.* 31(3):582-589.

21. Abdul-Wajid S, Demarest BL, Yost HJ (2018) Loss of embryonic neural crest derived cardiomyocytes causes adult onset hypertrophic cardiomyopathy in zebrafish. *Nat Commun.* 9(1):4603.

Chapter IV

CLONAL ANALYSIS AND DYNAMIC IMAGING IDENTIFY MULTIPOTENCY OF INDIVIDUAL GALLUS GALLUS CAUDAL HINDBRAIN NEURAL CREST CELLS TOWARD CARDIAC AND ENTERIC FATES

Part of this chapter was published as Tang, W., Li, Y., Li, A. & Bronner, M. E. Clonal analysis and dynamic imaging identify multipotency of individual Gallus gallus caudal hindbrain neural crest cells toward cardiac and enteric fates. *Nat. Commun*. 12, (2021). DOI: 10.1038/s41467-021-22146-8

ABSTRACT

Neural crest stem cells arising from caudal hindbrain (often called cardiac and posterior vagal neural crest) migrate long distances to form cell types as diverse as heart muscle and enteric ganglia, abnormalities of which lead to common congenital birth defects. Here, we explore whether individual caudal hindbrain neural crest precursors are multipotent or predetermined toward these particular fates and destinations. To this end, we perform lineage tracing of chick neural crest cells at single-cell resolution using two complementary approaches: retrovirally mediated multiplex clonal analysis and single-cell photoconversion. Both methods show that the majority of these neural crest precursors are multipotent with many clones producing mesenchymal as well as neuronal derivatives. Time-lapse imaging demonstrates that sister cells can migrate in distinct directions, suggesting stochasticity in choice of migration path. Perturbation experiments further reveal guidance cues acting on cells in the pharyngeal junction can influence this choice;

loss of CXCR4 signaling results in failure to migrate to heart but no influence on migration toward the foregut, whereas loss of RET signaling does the opposite. Taken together, the results suggest that environmental influences rather than intrinsic information govern cell fate choice of multipotent caudal hindbrain neural crest cells.

4.1 INTRODUCTION

A challenge in understanding cell fate choice is to identify how individual embryonic stem cells make lineage decisions in order to differentiate into diverse adult cell types. A remarkable example of such a stem cell population is the neural crest, which forms multiple derivatives ranging from peripheral neurons and glia to pigment cells, cartilage, and muscle cells[1]. A long-standing question is whether individual neural crest cells are multipotent stem cells or fate-restricted progenitors, each "predetermined" to from a particular cell type. While this question has been elegantly tackled for trunk neural crest cells in the mouse using *Confetti* technology[2], lineage analysis at other levels of the neuraxis has been more challenging due to their vast array of derivatives coupled with long distances traveled. The question of multipotency is particularly pertinent to neural crest cells arising from the caudal hindbrain, which undergo some of the longest migrations of any embryonic cell type and populate derivatives as diverse as muscle of the heart[3,4], and neurons and glia of the sympathetic and enteric nervous system (ENS)[5].

The caudal hindbrain neural crest arises adjacent to the middle of the otic vesicle to the level of somite 7 and is termed "vagal" neural crest. Transplantation and cell labeling techniques have shown that the vagal region can be subdivided into two populations. Cells

arising from adjacent to the mid-otic vesicle to somite 3, corresponding to rhombomeres (r) 5 and 6, are called the "cardiac" neural crest since many of these cells populate the heart, contributing to the aorticopulmonary septum, cardiac ganglia, pharyngeal arch arteries, cardiomyocytes as well as parts of the thymus, thyroid and parathyroid[3,4,6]. In contrast, the "posterior vagal" neural crest arising adjacent to somites 4-7 develops into ganglia of the sympathetic and enteric nervous systems[5].

Grafting experiments at the population level have suggested differences in developmental potential of vagal neural crest cells depending upon their rostrocaudal level of origin. For example, when small grafts of quail neural folds were transplanted into chick hosts from which the vagal neural crest was removed, cells from adjacent to somite 3 could form enteric neurons whereas those from adjacent to somite 1 failed to do so[7]. Similarly, GFP labeling via somite level-specific electroporation or transplantation in chicken embryos has shown that while cardiac neural crest cells migrate to the heart and the gut, posterior vagal neural crest cells contribute only to the ENS[8,9]. However, disagreement remains on the nature of the migratory pathways and cell types emerging from the cardiac neural crest region. Whereas Kuo and Erickson suggest that cardiac neural crest cells take different pathways to the heart than to the gut[8], Espinosa and colleagues highlighted the role of vagus nerve in guiding Schwann cell precursors migration toward the ENS[9]. These population studies clearly show that cells delaminating from the cardiac level can contribute to both cardiovascular system and the ENS, albeit the source of the cells, whether of neural crest and/or Schwann cell precursor origin, remains a matter of debate[8,9].

These studies raise the intriguing question of whether individual neural crest cells are multipotent, with the potential to form both cardiac and enteric derivatives, or if there are distinct precursors fated to populate each of these distant destinations that migrate differentially. Addressing this question requires examining the developmental potential of individual cardiac neural crest precursor cells. This has been done *in vitro* by isolating cardiac neural crest cells at migratory[10] and post-migratory[11] stages. In these clonal cultures, some individual neural crest-derived cells were capable of generating multiple cell fates, including pigment cells, smooth muscle cells, connective tissue cells, chondrocytes and sensory neurons. Further studies showed that the scope of developmental potential is partially restricted in TRKC mutant mice[12], suggesting that environmental factors may play a role in maintaining stem cell properties of the cardiac neural crest. While these experiments have tested the potential of cardiac neural crest cells removed from the embryonic milieu and grown at clonal density, it is technically difficult to extend these analyses *in vivo*.

To meet this challenge, here we perform clonal analysis of the cardiac neural crest in vivo at high resolution. We first use replication-incompetent avian (RIA) retroviruses[13–19] that express distinct fluorophores to identify clonally related progeny of premigratory cardiac and posterior vagal neural crest cells. Moreover, we establish an assay for anterograde lineage tracing of migratory cells. Through sparse viral infection and photo-conversion using a one-photon laser, we can precisely photo-label single migrating cells within the complex context of an embryo. Finally, by coupling molecular perturbations with our recently established dynamic imaging approach[20], we show that early cardiac neural crest

cells migrate stochastically; once within the pharyngeal junction, they migrate toward both the heart and gut, as a result of target-specific responses to CXCR4 and RET signaling. While posterior vagal neural crest cells are also multipotent, they contrast with cardiac crest cells by only contributing to ENS and sympathetic ganglia. Taken together, our study reveals interesting similarities and differences between individual neural crest precursors emerging from distinct levels of the caudal hindbrain. While both cardiac and posterior vagal neural crest cells are multipotent, they undergo differential migration. Cardiac neural crest cells can populate both the heart and gut under the influence of differential guidance cues, whereas posterior vagal neural crest cells migrate to the gut in a manner apparently independent of these guidance cues.

4.2 RESULTS

4.2.1 MULTIPLEX CLONAL ANALYSIS SHOWS THAT PREMIGRATORY NEURAL CREST CELLS AT THE "CARDIAC" LEVEL ARE MULTIPOTENT

At Hamburger Hamilton (HH) stage 9, cardiac neural crest precursors are positioned within the dorsal neural tube and about to delaminate. A mixture of RIA retroviruses encoding distinct fluorescent proteins (Fig4-1a) was injected into the neural tube from mid-otic to somite 3 level and embryos were harvested 48 hours post infection (Supplementary Fig4-1a, b show examples of embryos immediately after and 48 hours post-injection). A slice was cut directly posterior to the otic placode (Fig4-1b) to obtain a transverse view of all cardiac neural crest-related structures (Fig4-1c, grey), including the dorsal neural tube (dNT), cranial nerve nine (CN-IX), pharyngeal arch arteries (PAA), and outflow tract

(OFT). The tissue slice was imaged live in order to preserve native fluorescence signal without compromising normal biological processes.

To determine the probability of multiple infection and thus assess clonality, we performed a calculation similar to that used for trunk neural crest precursors[16,21] but revised to account for the increased numbers of Pax7+ cells in the caudal hindbrain compared with the trunk. After estimating the numbers of Pax7+ versus total number of cells of the hindbrain, we calculated the probability of multiple infections P{n} using the following equation:

$$P\{n\} = \frac{m^n e^{-m}}{n!} \quad (1)$$

where n is the number of viral particles simultaneously infecting a premigratory neural crest cell (Pax7+); m is average number of viral particles per Pax7+ cell (Supplementary Fig4-1c, d). To determine m, we measured the titer of the virus which was ~1 x 10^7 pfu/ml, in the volume injected into the embryo, which was typically ~0.5µl, corresponding to ~5,000 particles injected. Of these viral particles, the proportion infecting Pax7+ cells equals to the ratio between the number of Pax7+ cells and total cells in the hindbrain neural tube (~0.258). Thus, the number of viral particles infecting Pax7+ cells is around 1292. The number of Pax7+ cells (~5863 cells) in the caudal hindbrain was estimated based on average number of cells on each section and thickness of the caudal hindbrain segment; m is therefore around 0.22. Collectively, this led to the conclusion that probability of a single cell being simultaneously infected by two or more viruses are low (0.019 for double infection and 0.0014 for triple infection)[16,21]. Thus, in both double and triple infections, the unique fluorescence signatures from multiple infection events can be utilized as clonal

readouts. To further improve the stringency of our clonal analysis, we defined a clone by three criteria: a rare complex color combination produced by two or more infections of an individual precursor (multiple infection); similar intensity of fluorescent signal (due to site of integration within the genome); subcellular localizations of fluorescent proteins (Fig4-1a, e.g. nuclear, mitochondrial, membrane or actin cortex).

Upon visual inspection of living tissue, fluorescence was detected in all cardiac neural crest derived regions (Fig4-1d). Zooming in on neural crest derivatives, clones with identical color/subcellular signatures were identified in multiple structures. For example, a clone simultaneously expressing H2B-RFP, H2B-YFP and Mito-CFP shared progeny in the dNT (Fig4-1e), CN-IX (Fig4-1f), PAA (Fig4-1g) and OFT (Fig4-1h). In general, neural crest-derived clones displayed variable sizes, with an average of 9 cells per clone, indicating diverse proliferative properties. 18/86 (21%) of these clones developed into two or more neural crest derivatives in addition to the dNT and 4/86 (4.6%) of the clones exhibited an even higher degree of multipotency with daughter cells residing in all three neural crest derivatives (Fig4-1i, Supplementary Data 4-1a). In contrast, 24/86 (28%) clones gave rise to progeny within a single location.

Immunofluorescence analysis showed that clonally related cells can adopt multiple cell fates even within a single derivative. For example, descendants of a rare clone expressing H2B-RFP, Mem-YFP and Mito-CFP were only seen within CN-IX. However, staining with the neuronal marker HuC/D at embryonic day 7 (E7), a time after neuronal differentiation, revealed one cell at the center of CN-IX that expressed the neuronal marker

HuC/D (Fig4-1j), but another HuC/D negative cell of the same clone at the periphery of the ganglion, a location where presumptive glial cells often reside, consistent with a presumptive non-neuronal cell fate (Fig4-1k). These results suggest that individual premigratory cardiac neural crest cells can produce diverse cell types even when in close proximity, indicating that location alone may underestimate the developmental potential within a clone.

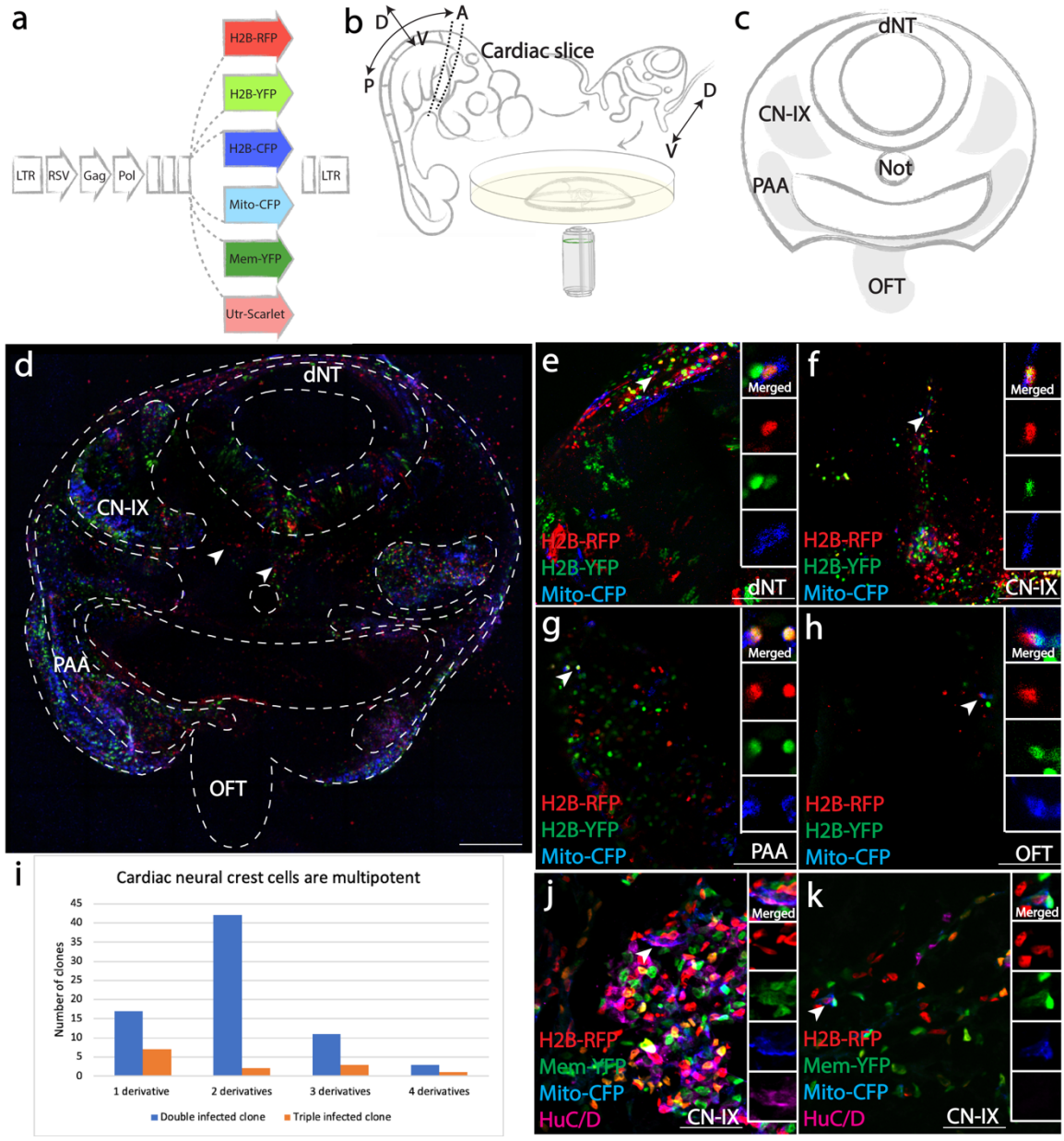

Figure 4-1. Multiplexed clonal analysis reveals multipotency of premigratory cardiac neural crest cells. (a) Sequences encoding H2B-RFP, H2B-YFP, H2B-CFP, Mito-CFP, Mem-YFP and Utrophin-Scarlet were cloned downstream of RSV promoter of the RIA vector for combinatorial infection. (b) Schematic of in vivo slice culture. At HH21, a ~500μm thick slice was obtained posterior to the otic placode. The slice was then embedded in 1% agarose and imaged using inverted confocal microscopy. A, anterior; P, posterior; D, dorsal; V, ventral. (c) Schematic diagram of cardiac neural crest-derived tissues (grey). Dorsal neural tube (dNT),

cranial nerve nine (CN-IX), pharyngeal arch arteries (PAA) and outflow tract (OFT) were imaged and scored for cells with identical clonal signatures. (d) A tiled multiplex image of the cardiac slice, representative of 23/23 embryos. CN-IX, PAA, OFT and Schwann cells (arrowhead) were infected by a mixture of RIAs. Red signal along the pharyngeal endoderm does not represent virally labelled cells. Instead, it is a result of autofluorescence from tissue debris common in chick explant cultures. (e-h) Clonally related cells (ID: Supplementary Data 4-1a-84) infected by three viruses (H2B-RFP, H2B-YFP, Mito-CFP, arrowhead) were identified in all four cardiac neural crest derivatives: dNT (e), CN-IX (f), PAA (g), OFT (h). In (h), RFP and YFP signals did not align in the OFT as a result of heart beating during image acquisition. (i) Bar graph showing distribution of double (blue) and triple (orange) infected clones. (j-k) In clones that appeared to be restricted in one location, cells could acquire distinct fates. At E7, one cell in a rare clone near CN-IX expressing H2B-RFP, Mem-YFP and Mito-CFP differentiated into HuC/D expressing neuron (j), while another cell of the same clone remained HuC/D negative (k). Scale bars: d 500μm; e-h 100μm; j, k 60μm.

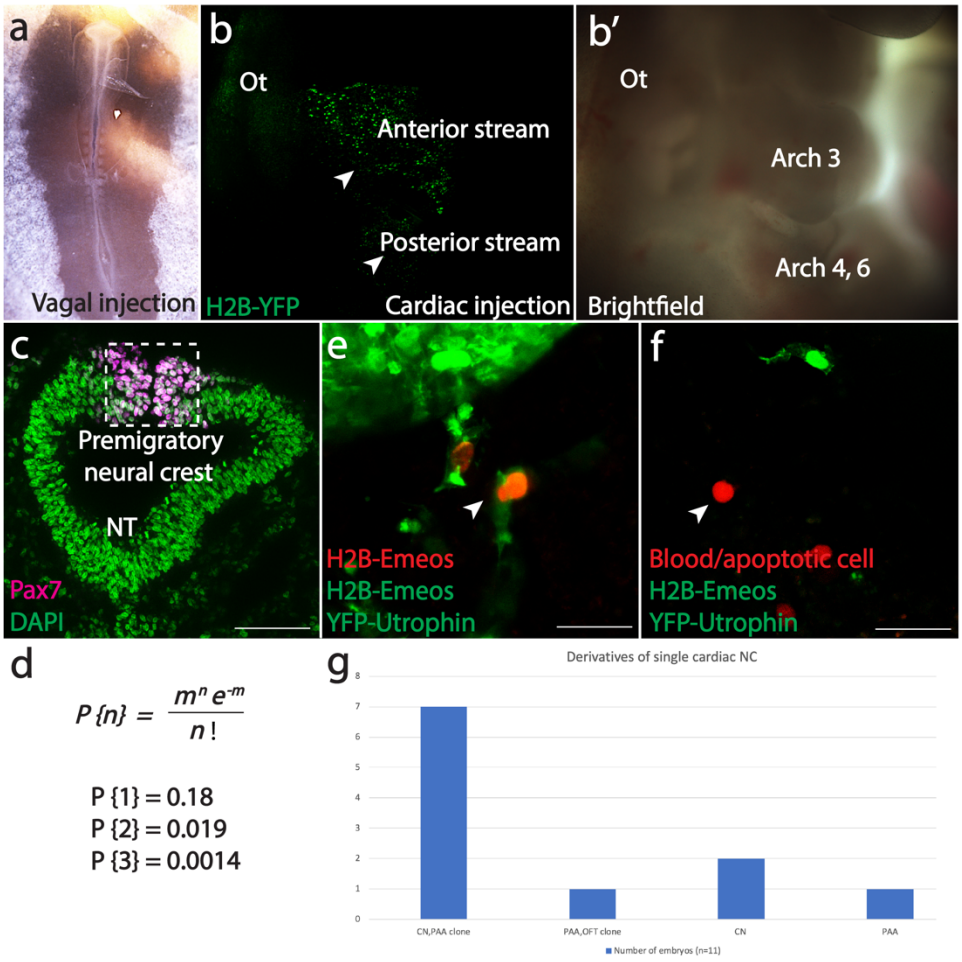

Supplementary Figure 4-1: Supplementary information for clonal analysis and cardiac neural crest single-cell photoconversion. (a) A chick embryo immediately after injection. The entire region of the neural tube adjacent to mid-otic to somite 7 is labelled with viral mixture (blue). Note that the first two somites are disappearing. (b, b') An embryo was specifically injected at the cardiac level between mid-otic to somite 3. 48 hours post injection, virally labelled cells (green) migrated exclusively into pharyngeal arches 3, 4, 6, suggesting axial specificity (23/23). (c) To estimate probability of double and triple infections, number of neural crest precursor cells (Pax7+, magenta) and total cells in the hindbrain (DAPI, green) were quantified (12/12). Amongst all viral particles injected, particles infecting Pax7+ cells can be derived by the ratio between Pax7+ cells and total cells in the hindbrain (~0.258). (d) At the vagal level, approximately 1292 viral particles infected ~5863 Pax7+ cells with equal probability. Following a Poisson distribution of multiple

infection21, probability of double infection and triple infection is 0.019 and 0.0014 for vagal neural crest cells, respectively, (n, number of viral particle(s) infecting a cell; m, ratio of viral particle number and Pax7+ cell number). (e) 12 hours post-conversion, the converted cell divided into two daughter cells, with red H2B-Emeos in the nucleus and YFP-Utrophin delineating cellular structures. (f) Although blood cells or apoptotic cells can also possess red nuclear-like signal, YFP-Utrophin will not be present in those cells. Thus, the cell in f (arrowhead) was not counted as a derivative of the converted cell. (g) Number of bi-location and uni-location cardiac clones observed in single-cell photoconversion assay. Abbreviations: CN, cranial nerve; PAA, pharyngeal arch arteries; OFT, outflow tract. Numbers in parenthesis shows the number of images with the phenotype presented in the figure out of all images taken. Scale bars: c 160μm; e, f 20μm.

4.2.2 SINGLE-CELL PHOTOCONVERSION SHOWS THAT MIGRATORY "CARDIAC" NEURAL CRESTS ARE MULTIPOTENT

Next, we asked whether cardiac neural crest cells retain multipotency during dorsoventral migration. As these cells move toward the heart, it becomes difficult to utilize multiplex viral labeling owing to increasing tissue depth and the large number of virally infected cells. We therefore developed a technique, comprised of sparse viral infection followed by one-photon laser photoconversion, to label a single migrating cell with exquisite spatiotemporal control.

To this end, we constructed a recombinant RIA virus encoding H2B-Emeos that exhibits high levels of photoconversion efficiency and fluorescence intensity. Previously, two methods for single-cell photoconversion have relied on confined axial excitation of cells expressing photoactivatable or photoconvertible proteins. While the femtosecond pulsed two-photon laser serves as the gold standard for this purpose because of its low scattering

near-infrared light confines the excitation[22], several studies have reported that negligible photoconversion was achieved even using high-power illumination and long-term exposure. Primed conversion, in which simultaneous illumination of the specimen with both 488 nm and 730 nm lasers, can also achieve single-cell photoconversion[23]. However, the requirement of additional hardware (a filter cube to transmit both lasers) and the use of high-power infrared laser (730 nm) preclude its wide application. Therefore, we addressed these issues by manipulating viral titer to sparsely tag neural crest cells, which can be efficiently converted through the non-confined 405 nm one-photon laser, thus simplifying the tools for clonal analysis. While used here for clonal analysis of the neural crest, this could easily be adapted to diverse embryonic tissues, model organisms and adult stem cells.

Using low viral titers, we achieved sparse labeling of cardiac neural crest cells. A single labeled cell was identified in the optical path, and converted from green to red using 405 nm laser illumination. This approach provides an efficient way to spatially single out an individual progenitor cell for lineage tracing. To distinguish the converted red neural crest cells from blood cells that emit red autofluorescence (Supplementary Fig4-1e, f), we used a 2A bicistronic system to incorporate YFP-Utrophin (targeting the cortex beneath the plasma membrane) in the same virus (Fig4-2a1). We injected recombinant virus into the neural tube and focused on a region with a single migratory cell along the imaging axis (Fig4-2a2, 2'). We then photoconverted the nucleus from green to red while the cell membrane remained green in color (YFP-Utrophin) (Fig4-2a3, 3', b, b' in explant culture). This specific fluorescence signature permits accurate tracking of the labeled progeny cells

during normal development. Despite dilution after cell division, the signal was detectable by confocal imaging at 24 hours after tissue fixation and immunohistochemistry with anti-HNK1, a molecular marker for migrating neural crest cells (Fig4-2a4, c, c' in cryosections).

Whereas some sister cells remained in close proximity after cell division (3/11), in the majority of cases (8/11), clonally related cells were dispersed in multiple cardiac neural crest derivatives (Supplementary Fig4-1g). For instance, we observed bipotent clones with sister cells in cranial nerve nine (CN, Fig4-2d1) and pharyngeal arch arteries (PAA, Fig4-2d2) as well as clones with cells in both pharyngeal arch arteries (PAA, Fig4-2e1) and the outflow tract (OFT, Fig4-2e2). Thus, this approach confirms multipotency of individual cardiac neural crest cells in a manner independent of multiple infection and highlights the fact that neural crest multipotency is retained at the migratory stage.

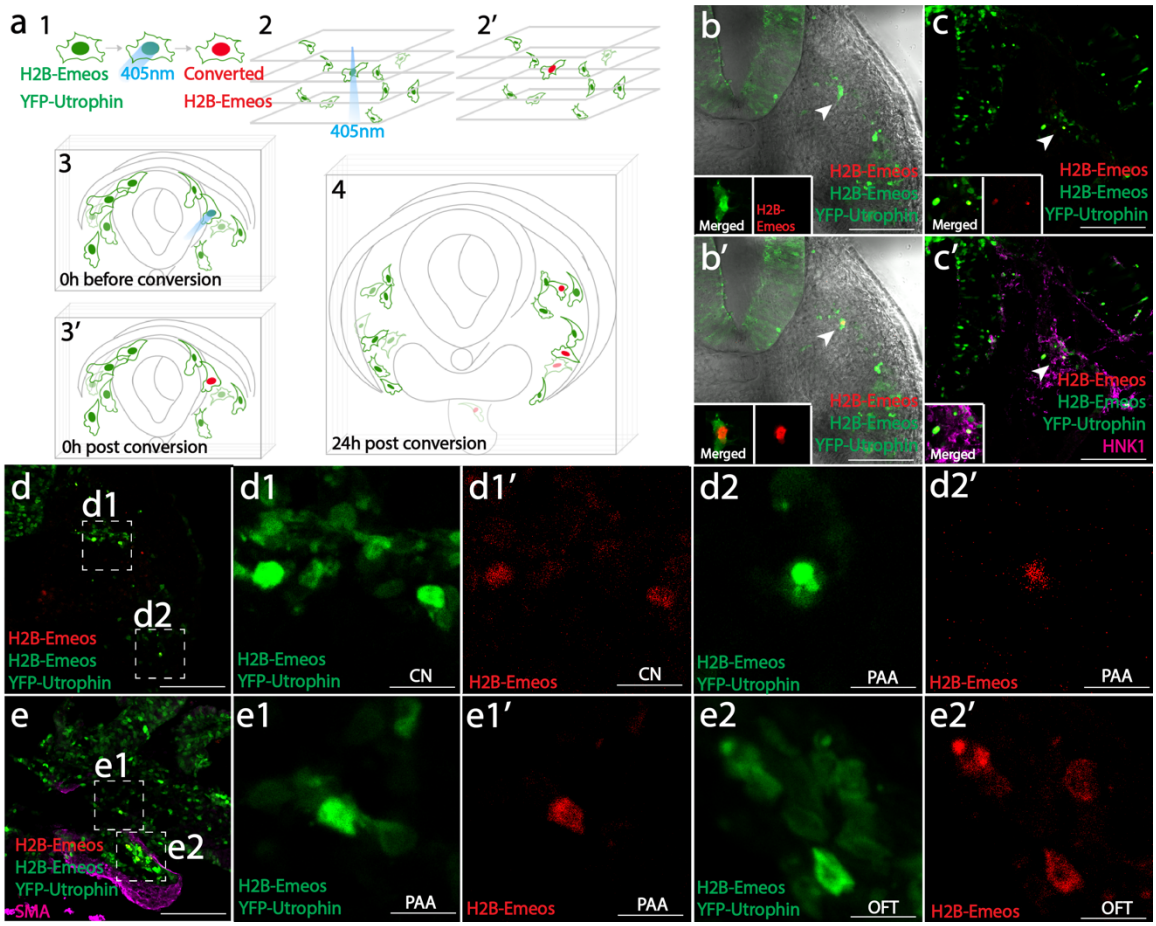

Figure 4-2. Single-cell photoconversion reveals multipotency of migratory cardiac neural crest cells. (a) Implementing single-cell photoconversion technique in embryo slice. In (1), cells were labelled with virus expressing both YFP-Utrophin and H2B-Emeos. A single migratory neural crest cell was converted (2, 2', 3, 3'), and the tissue slice was cultured for 24 hours until its progenies migrated to their destinations (4). Clones are assessed based on red fluorescence in the nucleus and green fluorescence underneath the plasma membrane. (b, c) A representative experiment of single-cell photoconversion and lineage tracing. One migratory cell was photoconverted (b, b'); after 24 hours, two daughter cells were observed in the migration stream (c), where cranial nerve is expected to form. Both cells were positive for neural crest marker HNK1 (c', magenta). (d) An example of a clone with one cell in the cranial nerve (inset d1, CN), and the other cell in prospective pharyngeal arch arteries (Inset d2, PAA). (e) An example of a clone with one cell located in pharyngeal arch arteries (Inset e1, PAA), and three cells migrating further into the outflow tract (Inset e2,

OFT). Also see Supplementary Fig4-1e, f for signal detection method and summary of the results (Supplementary Fig4-1g). Scale bars: b-e 200μm; Insets d1, d2, e1, e2 12.5μm.

4.2.3 PREMIGRATORY AND MIGRATORY NEURAL CREST CELLS AT THE "POSTERIOR VAGAL" LEVEL ARE MULTIPOTENT

Having demonstrated the utility of multiplex clonal analysis and single-cell photoconversion at the cardiac level, we applied both approaches to explore clonal relationships within the posterior vagal neural crest region. The same mixture of RIA retroviruses (Fig4-1a) was injected to fill the entire vagal neural tube, adjacent to somites 1-7, prior to cell delamination. 48 hours post-infection, a tissue slice was cut between the levels of somite 4 and 7 (Fig4-3a). Rare color combinations could be identified in four locations including dNT, dorsal root ganglia (DRG), sympathetic chain (SYM), and enteric nervous system (ENS) (Fig4-3b, grey). For instance, a clone expressing Utrophin-Scarlet, H2B-YFP and Mito-CFP was observed in all four locations (Fig4-3d-g). In contrast to the cardiac crest, ~40% of posterior vagal clones (38/95) were confined in a single derivative. We noted that 9/38 (24%) of these "single derivative clones" were located only in the ENS, the most ventral derivative along the migration route (Supplementary Data 4-1b), without sister cells in the neural tube or the sympathetic chain adjacent to somites 4-7. However, a large number of clones (36/95, 38%) gave rise to progeny in three or four derivatives (Fig4-3c, Supplementary Data 4-1b). As further validation of the multipotency of some posterior vagal neural crest cells at migratory stages, we optically highlighted a single migratory posterior vagal crest cell (Fig4-3h), and confirmed that it was able to give rise to both sympathetic ganglion cells (Fig4-3i) and part of the enteric nervous system (Fig4-3j).

The fact that so many clones contributed only to the ENS raised two possibilities. First, ENS precursors from the posterior vagal stream may be ‘set aside’ prior to emigration. Alternatively, due to an overlapping contribution of the cardiac neural crest and posterior vagal neural crest populations to the gut[8,9], instead of being posterior vagal crest-derived, these apparently “single-derivative clones” in the ENS might share clonal origin with the more anterior cardiac neural crest.

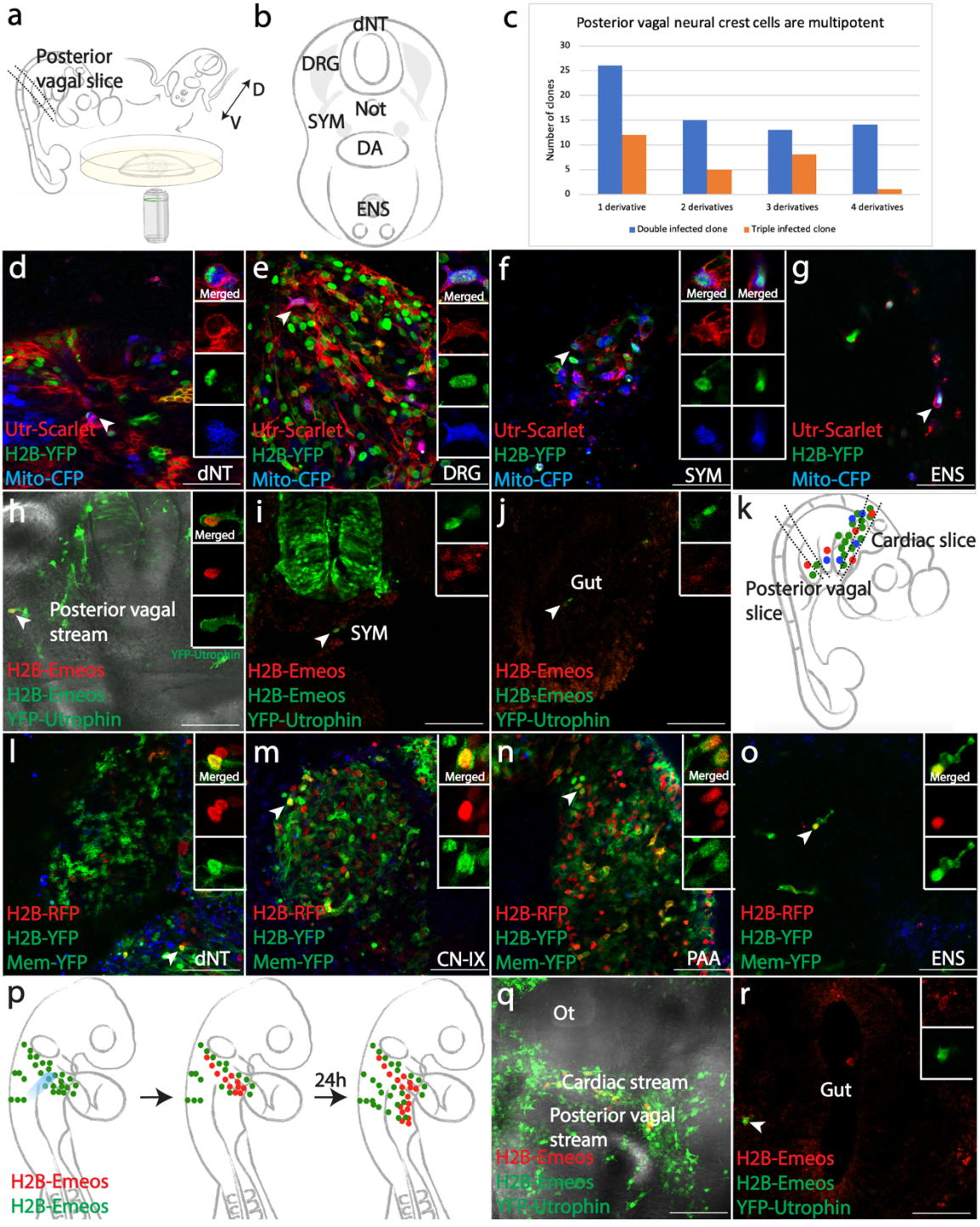

Figure 4-3. Posterior vagal neural crest cells are multipotent and converge with cardiac neural crest cells to form enteric neurons. (a) Schematic of in vivo slice culture in multiplex clonal analysis at the posterior vagal

level. At HH21, a ~500μm slice was obtained at somites 4-7, embedded in 1% agarose and imaged. D, dorsal; V, ventral. (b) Schematic of posterior vagal neural crest-derived tissue (grey), including dorsal neural tube (dNT), dorsal root ganglia (DRG), sympathetic chain (SYM) and enteric nervous system (ENS). (c) Distribution of double (blue) and triple (orange) infected clones among multiple derivatives. (d-g) Utrophin-Scarlet, H2B-YFP, Mito-CFP-coexpressing cells (ID: Supplementary Data 1b-81) were identified in all four locations. (h-j) Multipotency of migratory posterior vagal crest cells was confirmed by photoconverting a cell after delamination (h). 24 hours post conversion, derivatives of the photoconverted cell were observed in future sympathetic chain (i) and around the gut (j). (k) In HH21 embryos, two slices were obtained for a transverse view of cardiac and posterior vagal crest derivatives. (l-o) Triply infected cells in the ENS shared clonal signature with other cells in the cardiac slice. A H2B-RFP, H2B-YFP, Mem-YFP-positive clone (ID: Supplementary Data 4-1c-61) was observed in dNT (l), CN-IX (m), PAA (n), and ENS (o). (p) The principle of stream-specific photoconversion assay. UV light was used to specifically convert post-otic cardiac crest cells. If cardiac neural crest cells contribute to the ENS, descendants with red fluorescence should be observed around the gut. (q) In an embryo immediately after conversion, cardiac crest cells were specifically labelled in red. (r) 24 hours post-conversion, a converted cell was found near the gut, indicating a cardiac origin of ENS. See Supplementary Fig4-2l for absence of converted cell in dorsal posterior vagal crests, ruling out the possibility of unspecific conversion. Scale bars: d-g, l-o 100μm; h-j, q, r 160μm.

4.2.4 CARDIAC NEURAL CREST ORIGIN OF SOME ENTERIC NEURONS

To distinguish between these two possibilities, we injected the RIA viral mixture into the lumen of the neural tube specifically at the cardiac neural crest (mid-otic to somite 3) axial level and analyzed slices at both the cardiac and posterior vagal crest regions (Fig4-3k). For clonal analysis, four sites including the dorsal neural tube (dNT), cardiac neural crest derivatives (CN-IX, PAA, OFT, Fig4-1c) and the ENS (Fig4-3b) were imaged to enable assessment in both dorsal-ventral and anterior-posterior extent of the clones. We first

screened for specificity of the initial viral infection by examining the posterior vagal neural tube, where we found no fluorescently labeled cells (Fig4-3k).

Importantly, we noted that a considerable number of ENS cells shared clonal signatures with sister cells in cardiac crest derivatives. For instance, we identified a triple labelled clone expressing H2B-RFP, H2B-YFP and Mem-YFP with cells in the dNT at the cardiac crest level (Fig4-3l), CN-IX (Fig4-3m), PAA (Fig4-3n) and ENS (Fig4-3o). In addition, cells in the ENS were clonally related to other cardiac crest derivatives in 24/25 (96%) of cases. 25/72 (35%) of all clones in the cardiac crest shared common progenitor with the gut (Supplementary Data 4-1c). These results show that a significant proportion of cardiac crest clones also contribute to the ENS.

To validate the types of derivatives formed by clonally related cells, we used several markers that reflect mature cell type markers. Antibodies against HuC/D and TuJ1 were used to detect mature neurons, tyrosine hydroxylase (TH) for sympathetic neurons, P0 for Schwann cells and smooth muscle actin (SMA) as a mesenchymal cell fate marker in mature pharyngeal arch arteries. Analysis of immunofluorescence showed that at E7, clonally related cells that localized in different derivatives expressed distinct cell fate markers. For example, in the same embryo, H2B-RFP, H2B-YFP and Mito-CFP infected cells represent a rare clone. Around the CN-IX, cells of this clone gave rise to neuronal (Supplementary Fig4-2a,c), glial (Supplementary Fig4-2b), and Schwann (Supplementary Fig4-2d) cells, as well as in rare cases, sympathetic (Supplementary Fig4-2k) lineages. In the gut, a portion of the cells differentiated into enteric neurons (Supplementary Fig4-2e,

g) and Schwann cells (Supplementary Fig4-2h). While clonally related cells differentiated into smooth muscle of the pharyngeal arch arteries, the HuC/D-negative cells in the gut did not form smooth muscle (Supplementary Fig4-2f). Ventrally into the pharyngeal arches and the heart, some cells contributed to smooth muscle of the arteries (Supplementary Fig4-2i) and neurons in the outflow tract (Supplementary Fig4-2j).

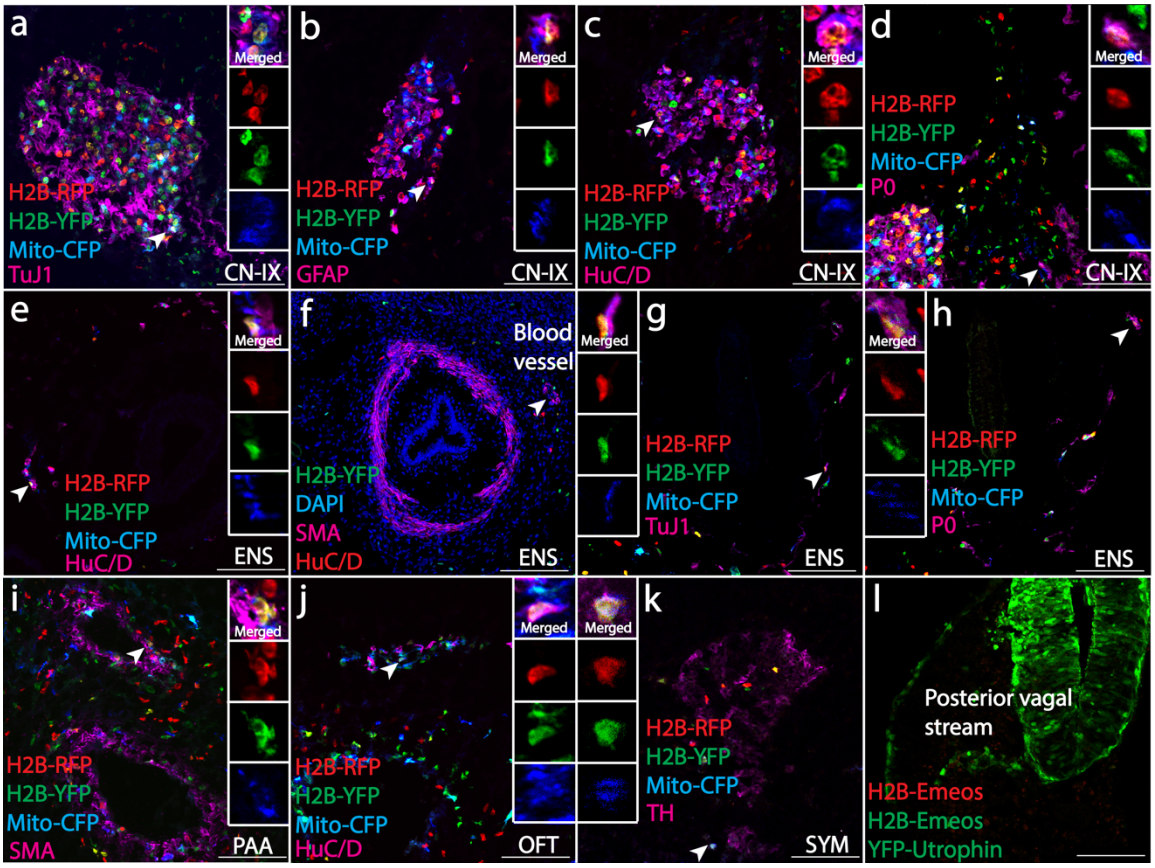

Supplementary Figure 4-2: Cell fate analysis of clonally labelled vagal neural crest cells and stream-specific photoconversion. At E7, in H2B-RFP, H2B-YFP, Mito-CFP triple infected clone, cells acquired diverse cell fates, including neurons (a, c), glia (b) and Schwann cells (d) in cranial nerve nine (CN-IX) and surrounding tissue. In the enteric nervous system (ENS), they gave rise to neuronal (e, g) and Schwann cells (h). However, neural crest cells did not generate smooth muscle layer of the gut, despite in blood vessels (arrowhead) (f).

Cells of the clone also contributed to smooth muscle surrounding pharyngeal arch arteries (i), neuronal cells in the outflow tract (j), and in rare cases posterior sympathetic neurons (SYM) (k). (l) In stream-specific photoconversion, a transverse section at posterior vagal region was obtained. The ventral portion is presented in Fig4-3r. In the dorsal portion, no photoconverted cell was visible, indicating that photoconversion was specific for cardiac neural crest cells. Scale bars: a-k 100μm; l 160μm.

As an alternative means of assessing whether cells derived from the cardiac level migrate from the pharyngeal junction posteriorly into the gut, we photoconverted a stream of migrating cardiac crest cells within the arches (Fig4-3p, q). 24 hours later, photoconverted progenies were observed in the gut region posterior to the original cardiac crest (Fig4-3r) but absent from dorsal regions of the same embryo where the posterior vagal stream is located in (Supplementary Fig4-2l). This result independently confirms the cardiac crest origin of these photo-labelled enteric cells.

4.2.5 CELLS INDIVIDUALLY MIGRATING FROM CARDIAC AND POSTERIOR VAGAL NEURAL CREST STREAMS INTERMIX

To gain insight into the cellular mechanisms underlying multipotency, we optimized experimental conditions of tissue slice cultures[19,20], and performed *in vivo* time-lapse imaging to capture cellular behaviors. We first focused our analysis on migrating neural crest cells expressing membrane-YFP at both the cardiac (Fig4-4a, Supplementary Fig4-3a, Supplementary Movie 4-1) and posterior vagal levels (Fig4-4g, Supplementary Fig4-3b, Supplementary Movie 4-2). Visual inspection suggested that cells migrated randomly as individuals, though as a population they moved directionally from dorsal to ventral. The heterogeneous movement of the population necessitated quantitative analysis. As such, we

conducted squared displacement (SD) analysis, a widely used method to estimate the nature of object motion, which revealed that cells exhibited a mixture of directed movement, constrained movement, and free diffusion (Fig4-4b, h). As a consequence, little correlation was observed between the original positions of the cells and their total displacement (Fig4-4c-e, i-k). Sister cells were typically far apart after separation (Fig4-4f, l, m). Based on these findings, we propose that early individual cell migration is stochastic in nature, leading to a random clonal distribution along the dorsoventral axis. However, clonally related cells at both the cardiac and the posterior vagal levels experience disparate environments, which may promote differentiation into distinct cell types at later developmental stages.

If cell migration occurs randomly along the anterior-posterior axis, the cardiac and posterior vagal streams, rather than migrating as separate populations[8,9], are likely to intermix. To test this possibility, we examined cell behaviors at the pharyngeal junction where cardiac neural crest cells start to migrate into heart and enteric structures. When Utrophin-Scarlet or H2B-YFP expressing cardiac neural crest population was imaged in the lateral view, we noticed that as the stream reached pharyngeal arch 6, some cells began to migrate posteriorly along the developing gut (Fig4-4n, Supplementary Movie 4-3; n', Supplementary Movie 4-4). Taken together, these studies strongly suggest that stochastic cell migration is an important factor and may contribute to the generation of the diverse cell types from cardiac and posterior vagal neural crest cells (Fig4-4o).

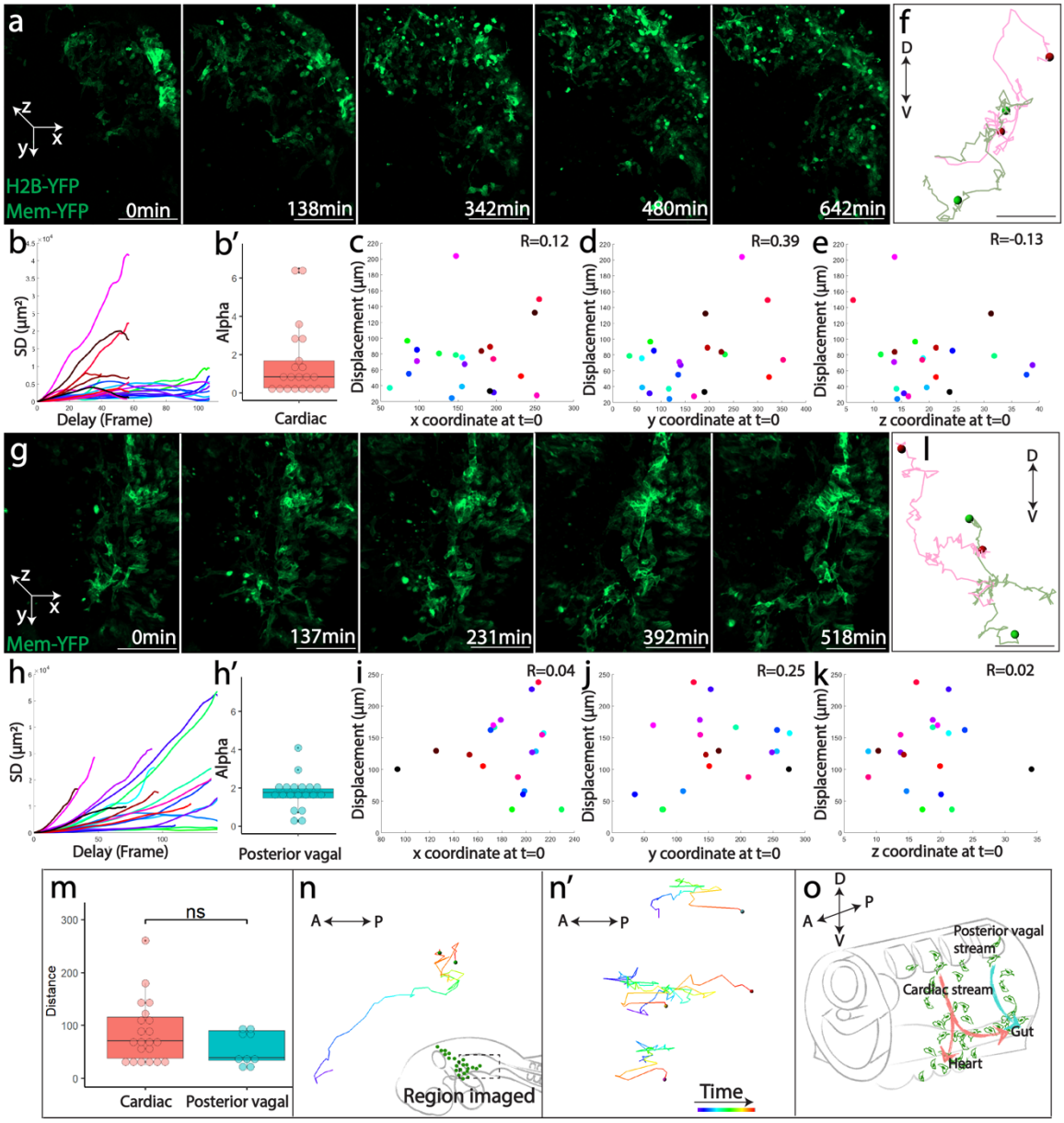

Figure 4-4. Vagal neural crest cells display individual and stochastic early cell migration. (a, g) Selective snapshots of the migratory cardiac (a) and posterior vagal (g) neural crest cells expressing membrane-YFP. In the coordinate system defined to facilitate quantitative analysis, dorsal-most position in the neural tube was set as the origin. The y axis was defined parallel to dorsoventral (DV) direction. The mediolateral (ML) axis aligns parallel to the x axis. The z axis runs in the anteroposterior direction (AP). See Supplementary Fig3a, b for snapshots with brightfield channel displaying tissue morphology. (b, h) Squared displacement

(SD) analysis of cell trajectories shows that both cardiac (b, n= 21 cells examined over 2 time-lapse imaging experiments) and posterior vagal (h, n= 18 cells examined over 1 time-lapse imaging experiment) neural crest cells exhibit three types of migration, including free diffusion ($\alpha \approx 1$), directed motion ($\alpha > 1$) and constrained motion ($\alpha < 1$). α values are shown in b' and h' for cardiac and posterior vagal populations, respectively. (c-e, i-k) The correlation between cell positions in x (c, i), y (d, j), z (e, k) axis at time 0 and their total displacement was plotted for both cardiac (c-e) and posterior vagal (i-k) neural crest cells. The close-to-0 values of correlation coefficients (R) suggest no notable correlation between initial positions and distances travelled. (f, l) Examples of sister cell trajectories at the cardiac (f) and posterior vagal (l) levels. The dots represent the final positions of sister cells. D, dorsal; V, ventral. (m) The distance between sister cells by the end of imaging were measured. There was no statistically significant difference between the cardiac (n= 21 cell divisions examined over 2 time-lapse imaging experiments) and posterior vagal (n = 9 cells examined over 1 time-lapse imaging experiment) population (two-sided rank-sum test). (n, n') Cell trajectories of cardiac crest migration from pharyngeal arch to the gut (n, replicate n') along the anteroposterior axis. The region imaged is shown in the dashed box of (n). Color coded timescale (from purple to red) is presented in (n'). A, anterior; P, posterior. (o) Summary of vagal neural crest migration with a convergence of cardiac neural crest and the posterior vagal crest to populate the ENS. In box-and-dot plots (b', h', m), the box bottom, median line, and box top represent the 25th (Q1), 50th (Q2) and 75th percentile (Q3), respectively. Whisker ends represent Q1 – 1.5*IQR and Q3 + 1.5*IQR, respectively. IQR is interquartile range (Q3-Q1). Scale bars: a, g 100μm, f, l 30μm.

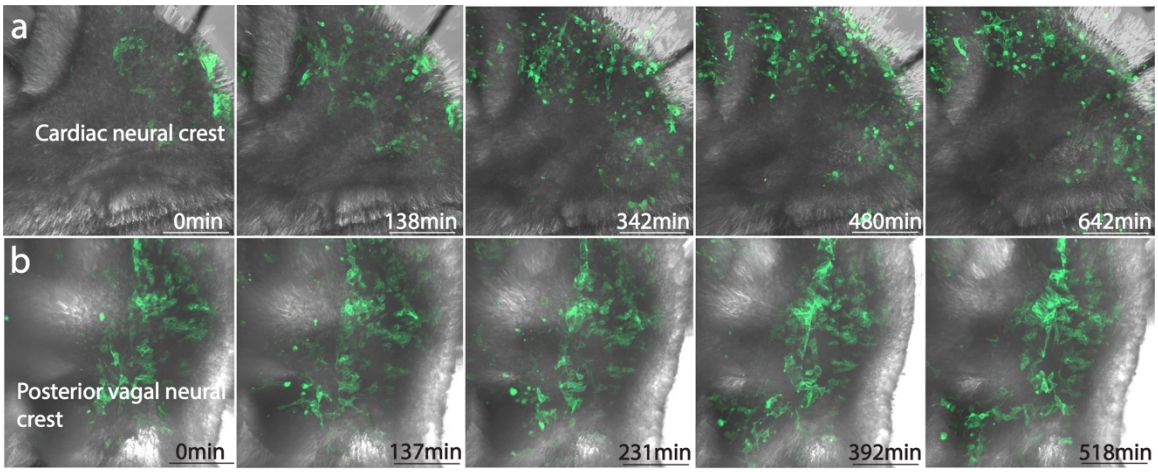

Supplementary Figure 4-3: Individual cell migration of vagal neural crest cells. Time-lapse imaging with the brightfield (grey) view on the cardiac (a) and posterior vagal (b) neural crest cells expressing membrane-YFP. Scale bars: a, b 100µm.

4.2.6 PERTURBATION OF FGF, CXCR4 AND RET SIGNALING REVEALS ENVIRONMENTAL INFLUENCES ON THE DIRECTIONAL MIGRATION OF CARDIAC NEURAL CREST CELLS

Finally, using retrovirally mediated molecular perturbations, we explored how cardiac and posterior vagal neural crest cells may differentially respond to environmental cues during early migration and particularly at the pharyngeal junction before entering the heart or the gut. Several signaling pathways have been suggested to play a role in aspects of vagal neural crest migration including FGF, ENDOTHELIN, NT3, EGF, SDF and GDNF signaling[9,24,25]. To test whether these may differentially affect cardiac versus posterior vagal neural crest populations, we generated recombinant virus overexpressing dominant-negative (DN) mutants of receptors involved in these signaling pathways: FGFR1, CXCR4, RET, EDNRB, TRKC, ERBB2 and tested their roles *in vivo*. This approach has

the advantage of placing identifiable mutant neural crest cells in an otherwise normal environment. Of the DN mutants tested, positive results were obtained for Fgfr1 [26,27], Cxcr4 [28–30] and Ret [31,32](Fig4-5a), corresponding to signaling mediated by Ffg8, Sdf1 and Gdnf ligands. The results show that vagal neural crest cells respond to these signaling pathways in temporally and axial level-specific manners.

First, we tested the effects of perturbing FGF signaling. Blocking Fgfr1 resulted in little or no migration of mutant cardiac neural crest cells, causing an absence of mesenchymal cells in pharyngeal region at E3 (Fig4-5b, c) and paused development afterwards. Thus, Fgfr1 is required for cardiac neural crest cells during early migration.

In contrast to blocking FGF signaling, cells with dominant negative mutant forms of Cxcr4 and Ret underwent normal initial migration into the pharyngeal arches (Fig4-5d, e for DN-Cxcr4; Fig4-5 f, g for DN-Ret). In the long term, however, abrogation of CXCR4 signaling blocked the migration of cardiac neural crest cells into the heart (Fig4-5 j-k), but had no effect on migration to or formation of proximal ganglia and pharyngeal arches (Fig4-5h, i) or invasion of the gut (Fig4-5l). As there is variation in virus titer, the numbers of DN-mutant virus infected cells cannot be directly compared with cells infected by control virus. Therefore, the ratio of cells in the gut was normalized to those in the cranial ganglia. At E7, these ratios are similar for CXCR4-perturbed cells (13.3%) and control cells (13.9%), suggesting that the effect of CXCR4 loss-of-function is likely to be specific to cardiovascular migration (Supplementary Data 4-2). On the other hand, cardiac neural crest

cells overexpressing DN-Ret were able to form proximal ganglia and contribute to the cardiovascular system (Fig4-5 m-p), but failed to populate the foregut (Fig4-5q).

In order to compare the distance that RET mutant cells and normal cells migrated along the gut, we co-injected DN-Ret virus together with H2B-RFP control virus. We first checked infection specificity by examining labeling in the neural tube of the targeted axial levels. Both cardiac specific injection (at somite level 1-3) and vagal injection (at somite level 1-7) showed that control and RET mutant cells reached the anterior foregut proximal to the pharyngeal junction (Fig4-5r, t, An. foregut). However, the majority of cells that invaded the more posterior foregut were control cells (Fig4-5s, u, Foregut). Quantitative analysis shows that DN-Ret infection resulted in an approximately 86% reduction of cells in the foregut, compared with H2B-RFP control (Supplementary Data 4-2). Interestingly, although both arrived at the pharyngeal arches, cells expressing DN-Ret predominantly formed smooth muscle cells lining the arteries rather than migrating posterior-ventrally into the gut, contrasting with their H2B-RFP expressing counterparts. Furthermore, RET dependency is likely to be specific to the cardiac neural crest, because in embryos where the entire vagal neural crest population was infected, the midgut was populated by DN-Ret expressing cells (Fig4-5v), which are derived from posterior vagal neural crest cells[33].

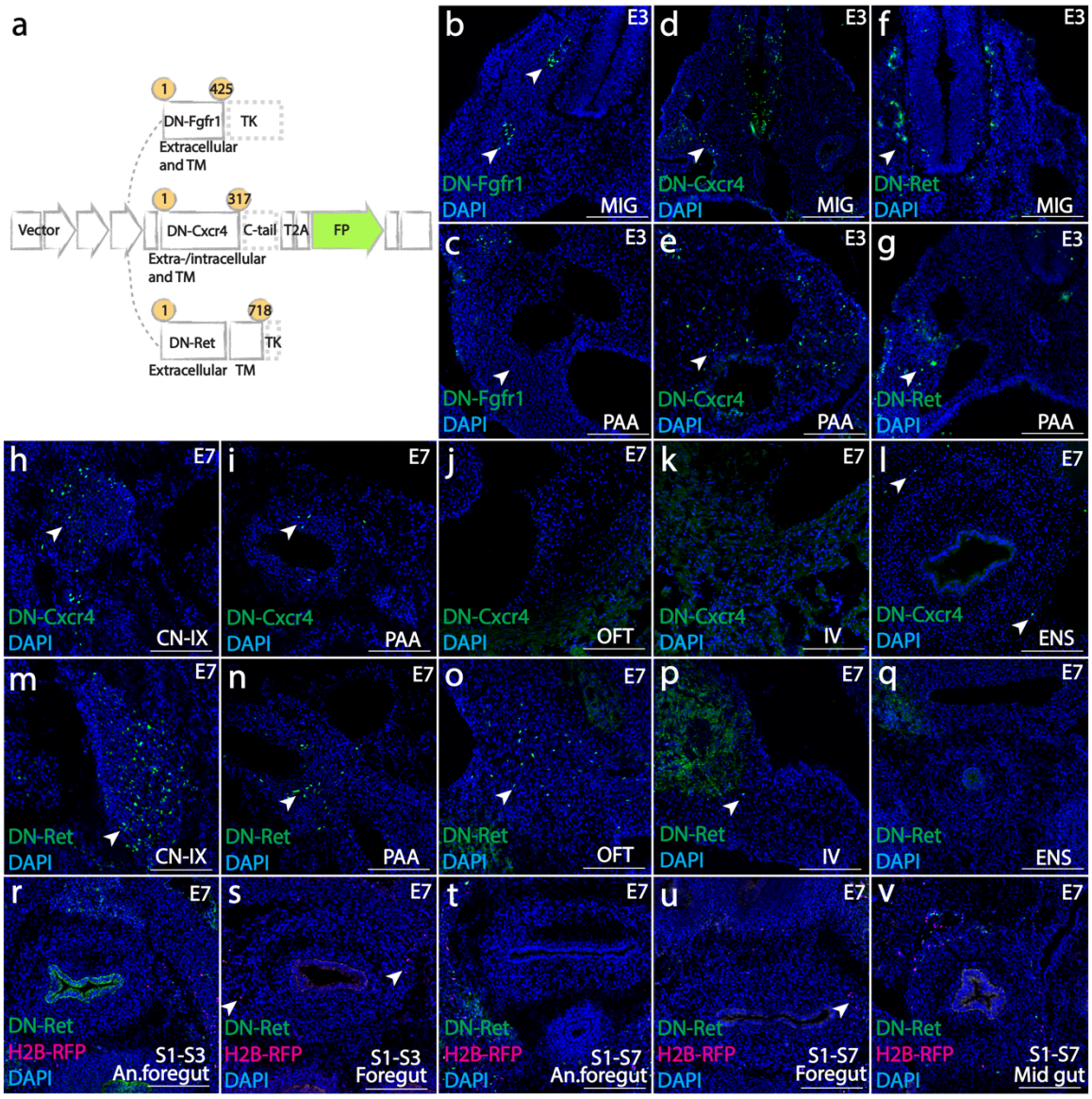

Figure 4-5. Molecular cues required for vagal neural crest cells to adopt cardiac and enteric fates. (a) Viral constructs over-expressing dominant-negative mutants of Fgfr1 (containing amino acids (aa) 1-425 of the full-length receptor) and Ret (aa 1-718) by truncating the tyrosine kinase domain, and Cxcr4 (aa 1-317) with c-tail eliminated. The ranges of amino acids are presented in yellow circles. All mutant constructs are labelled with fluorescent protein (FP, green). (b, c) Blocking FGFR1 signaling restricted cardiac neural crest cells within the ganglia (b, 3/3) and prevented pharyngeal mesenchyme formation (c, 6/7) at E3. (d-g) DN-Cxcr4 and DN-Ret had no apparent effect on initial migration into the ganglia or pharyngeal arches (d (2/2), e (5/5)

for Cxcr4; f (3/3), g (8/9) for Ret). (h-l) At E7, DN-Cxcr4 expressing cells formed cranial ganglia (h, CN-IX, 2/2), cells around pharyngeal arch arteries (i, PAA, 7/7), and enteric nervous system (l, ENS, 6/7). However, no DN-Cxcr4 expressing cells gave rise to the outflow septum (j, OFT, 5/5) or interventricular septum (k, IV, 2/2). (m-q) DN-RET expressing cells formed cranial ganglia (m, CN-IX, 4/4), cells around pharyngeal arch arteries (n, PAA, 6/6), cardiac outflow tract (o, OFT, 9/9) and interventricular septum (p, IV, 2/2); however, cells failed to enter the foregut (q, ENS, 7/9). (r-v) The influence of RET signaling on vagal neural crest cells is restricted in the cardiac population. Co-injection of DN-Ret and H2B-RFP (magenta) control virus into somite 1-3 showed that despite both mutant and control virus-infected cells were present in anterior foregut (r, An. Foregut, 8/8) near the pharyngeal junction, DN-Ret expressing cells failed to enter the foregut (s, 13/15). When the entire vagal population (S1-S7) was infected, both control and Ret mutant cells reached the anterior foregut (t, An. Foregut, 10/12). However, only control cells invaded the foregut (u, 8/9). DN-Ret expressing cells arising from posterior vagal crest cells was able to populate the midgut (v) (10/10). Numbers in parenthesis shows the number of images with the phenotype presented in the figure out of all images taken. Scale bars: b-v 160μm.

4.3 DISCUSSION AND CONCLUSION

Our study shows that many caudal hindbrain neural crest cells are multipotent and further reveals that individual cardiac neural crest precursors can give rise to both mesenchymal cardiovascular derivatives and neuronal ENS derivatives. Even at early migratory stages, single-cell photoconversion confirms multipotency and shows that daughter cells often take distinct migration routes post-division. This serves as a mechanism to randomly distribute multipotent neural crest cells prior to differentiation. Moreover, dynamic imaging accompanied by stream-specific photoconversion demonstrates that neural crest cells from different migratory streams intermix. Specific signaling cues guide multipotent cardiac neural crest-derived cells toward specific organs.

At odds with arguments for lineage restriction[34,35], our findings in both the cardiac and posterior vagal axial levels are in good agreement with the idea that neural crest cells are largely multipotent, as well documented for neural crest cells at the trunk level[2,36,37]. While there is apparent heterogeneity within delaminating vagal neural crest population, recent single cell RNA-seq analysis of the vagal neural crest gene regulatory network has revealed a SOX10high/FOXD3+ subpopulation that appears to contribute to neural, neuronal and mesenchymal fates[38]. This early SOX10/FOXD3 cluster is likely to represent the multipotent population captured by our clonal analysis. According to our findings, ~20% of individual cardiac crest clones contribute to two or more different neural crest sites as well as the dorsal neural tube, demonstrating broad developmental potential. Although most neural crest cells migrate from dorsal to ventral, there is also movement along the anterior-posterior axis particularly within the pharyngeal arches. As a consequence, our analysis likely reflects an underestimate, as some progeny may not be included in transverse slices used in our analysis. In addition, temporal differences in delamination may account for variation in clone size since cells delaminate from the neural tube for an approximately 24-hour period. Cells emerging earliest can migrate the furthest to populate the most distal structures and may undergo more cell divisions than those emerging later. This is consistent with findings using *WNT1-CRE* and *P0-CRE* to conduct population level lineage tracing of cardiac neural crest in mice[39], which showed that the cardiac neural crest is comprised of a mixture of differentiated and undifferentiated cells. Here we extend this finding by dissecting the clonal relationship within the mixture of cells. *Confetti* technology has been used to look at later clonal relationships within enteric ganglia and suggest that there is localized clonal expansion and interaction with neuroectodermal cells, with some

clones contributing to diverse types of neurons and glia[40]. Our study complements this previous work by taking the study to a single cell level at early developmental stages.

Posterior vagal crest clones appear to be tightly related, with 38% of clones found in multiple neural crest sites, compared with 21% of the cardiac crest clones. This may reflect intrinsic differences in cell behavior between these two populations. Posterior vagally-derived tissues are enclosed within a smaller physical compartment, whereas cardiac crest cells are more loosely arranged mesenchymal cells that can easily migrate into adjoining branchial arches. In contrast to the cardiac neural crest, the posterior vagal neural crest does not contribute to cardiovascular derivatives, but exclusively gives rise to sympathetic chain ganglia and ENS cells.

Our clonal analysis shows that progeny of an individual cardiac crest cell not only migrate into the cardiovascular system, but also intermix with the posterior vagal crest and migrate posteriorly to adopt enteric ganglion fate. Amongst all candidate genes that we screened, FGFR1, CXCR4 and RET all influenced the migration of caudal hindbrain neural crest cells, with the latter two apparently required for the decision to migrate toward the heart versus the gut, respectively. Previous studies have shown that FGF signaling is essential for the cardiac neural crest fate decision[24], which is mediated by a low level of Fgf8 secreted at midbrain-to-hindbrain boundary[41–43], as well as during early migration[24], which is affected by high FGF8 expression in the pharyngeal arches[44]. Our results agree with and extend this by showing that blocking Fgfr1 results in abrogation of cardiac neural crest-derived pharyngeal mesenchymal cells. Once the cardiac neural crest cells have entered

the pharyngeal arches, further migration into the heart and the gut requires a different subset of signaling molecules. Our results suggest that CXCR4 signaling selectively promotes migration to the heart, consistent with the coordinate expression of CXCR4 by cardiac neural crest cells and its ligand SDF1 in the ectoderm[45]. Indeed, loss of CXCR4/SDF1 signaling has been shown to cause conotruncal defects in mice[46] and chick[29]. Moreover, we find that it does not affect migration into the gut, suggesting a cardiac-specific chemoattraction. At early stages, the CXCR4 and RET mutant phenotype is less penetrant, likely due to delayed generation of mutant protein after viral integration which takes more than 24 hours[29]. In contrast to CXCR4, RET is required for cardiac neural crest cells to invade the gut, under the guidance of its ligand GDNF expressed in the gut mesenchyme[47], but has no influence on cells migrating to the cardiac outflow tract. RET deficiency results in reduced number of enteric neurons[48,49]. Since the dominant negative receptors are only synthesized at a high level after 1 day, the infected cells are undergoing active migration to the branchial arches prior to onset of the inhibitory effect. Moreover, a similar ratio of dominant negative and control virus infected cells are present in cranial nerve nine and the pharyngeal junction, to where cell migration is not affected. Therefore, the effects of CXCR4 and RET are more likely to be on their direction of migration rather than survival.

We posit that slight differences in the reception of CXCR4/SDF versus RET/GDNF signaling amongst cardiac crest-derived sister cells within the pharyngeal junction may bias their migration toward either the heart or the gut, thus reflecting the mechanism contributing to their multipotency and diverse derivatives. Initially stochastic cell

migration accounts for the disparate distribution of clonally related cells along the dorsoventral axis, resulting in a random assortment of cells with broad developmental potential within the pharyngeal junction. In response to directional signals, a subset of cells migrates to the heart or the gut and differentiates according to environmental cues therein. Altogether, these results suggest that caudal hindbrain neural crest cells truly represent a multipotent stem cell population with signals from the local environment dictating their final cell fate choice (Fig 4-6).

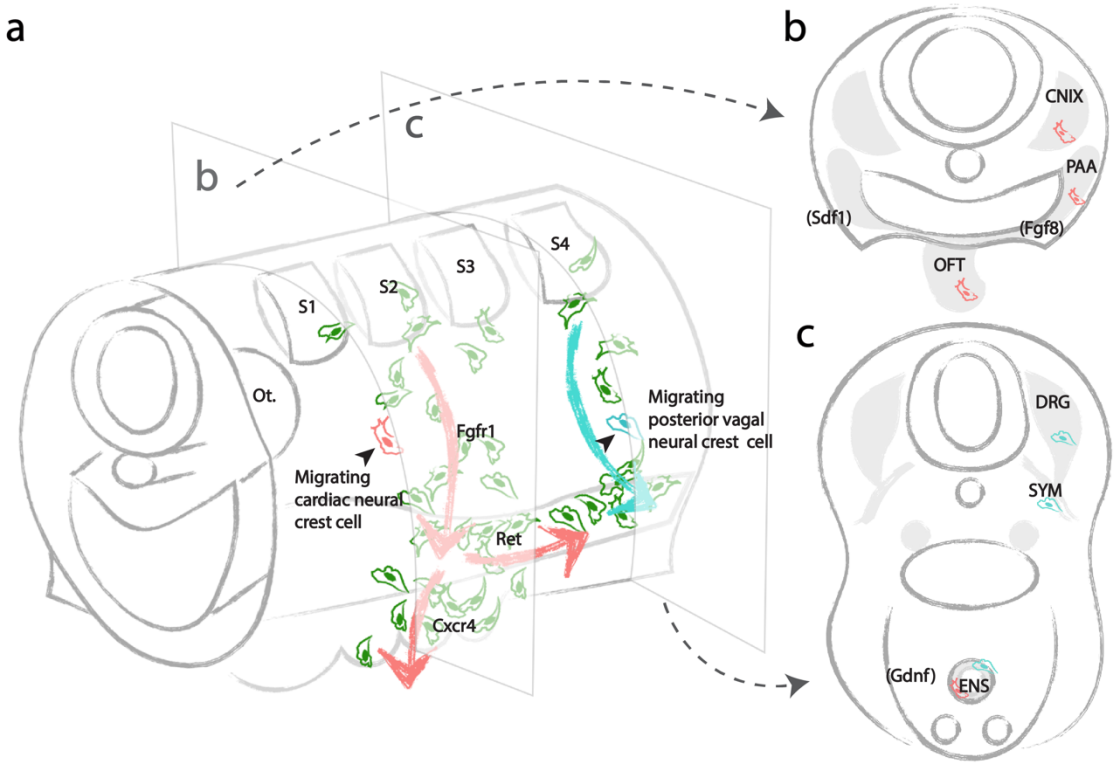

Figure 4-6. Developmental potential of individual vagal neural crest stem cells and bi-directional cardiac neural crest migration driven by molecular cues. (a) Early cardiac neural crest cells (red) from the mid-otic to somite 3 exhibit stochastic migration. A subset of randomly selected progenies migrates into the pharyngeal junction in an FGF-dependent manner, and subsequently into the heart or the gut in response to

CXCR4 or RET, direction according to distribution of environmental signals (FGF8 expressed in pharyngeal arches, SDF1 expressed by ectoderm in coordination with migrating neural crest, and GDNF expressed in gut mesenchyme). In contrast, posterior vagal neural crest cells emigrated from somite 4-7 (blue) are less sensitive to RET signaling. (b) As a result, individual premigratory and migratory cardiac neural crest cells are multipotent, capable of giving rise to all cardiac crest-derivatives. (c) Individual premigratory and migratory posterior vagal neural crest cells are multipotent, contributing to diverse components of the sympathetic nervous system. The ENS is composed of neural crest cells of both cardiac and posterior vagal clonal origins.

4.4 MATERIALS AND METHODS

Molecular cloning and virus preparation

AscI, SpeI, NotI were inserted upstream of ClaI site to create a modified RIA vector. H2B-YFP (#96893), H2B-RFP (#92398), Mito-CFP (#36208), Membrane-YFP (#56558), Utrophin-Scarlet (#26739)16, H2B-CFP (#25998), Emeos (#73792) encoding plasmids were obtained from Addgene. For retroviral lineage analysis, H2B-YFP, H2B-RFP, Mito-CFP, Membrane-YFP, Utrophin-Scarlet, H2B-CFP were inserted between Not1 and Cla1 sites. To create photoconvertible construct, Emeos protein linked with H2B was inserted in between AscI and SpeI; YFP-Utrophin was inserted between Not1 and Cla1. For molecular perturbations, DN-FGFR1 (#80431), CXCR4 (#98967) and RET (#23906) plasmids were obtained from Addgene. Truncated FGFR1 and CXCR4 receptors were cloned from these templates and subsequently inserted between Not1 and Cla1 sites in RIA. Truncated RET was inserted between Asc1 and Spe1 sites in RIA. Primer sequences are displayed in Supplementary Table 1. To produce recombinant RIA virus, plasmids for RIA

and ENV-A (a gift from Dr. Connie Cepko) were transfected into chick DF1 cells (ATCC, Manassas, VA; #CRL-12203, Lot number 62712171, Certificate of Analysis with negative mycoplasma testing available at ATCC website) in 15cm culture dishes. 24 hours post-transfection, 12ml of supernatant containing the virus was collected every 12 hours for 4 days, kept at -80°C until concentration. For each viral concentration, 48ml of supernatant was centrifuged at 75500 g for 1.5 hr. After centrifugation, 20-30 µl of DMEM was left in the tube to dissolve the pellet containing RIA. The resulting viral stock has a titer of 1 x 107 pfu/ml. Viral stocks were stored in -80°C until injection.

Multiplex retroviral lineage analysis

To make the working solution, equal volumes of RIA viral stocks encoding H2B-YFP, H2B-RFP, Mito-CFP, H2B-CFP, Membrane-YFP and Utrophin-Scarlet were mixed. 0.3µl of 2% food dye (Spectral Colors, Food Blue 002, C.A.S# 3844-45-9) was added into the viral mixture as an indicator. ~0.5µl of working solution was injected into the lumen of the neural tube adjacent to mid-otic until somite 3 to label cardiac crest, or from mid-otic to somite 7 to label the vagal population. For in vivo clonal analysis (n = 35), chick embryos were sealed after injection, incubated at 37°C for 2 days, harvested at Hamburger Hamilton (HH) Stage 21, screened for specific labeling in the neural crest. A ~500 µm thick transverse slice at cardiac (n = 14), posterior vagal (n = 12) or both (n = 9) regions were cut. Locations with virally labelled cells were imaged using 20x lens on confocal microscope (Zeiss LSM 800). In cardiac clonal analysis, dorsal neural tube, cranial nerve nine, pharyngeal arches, and outflow tract were imaged; in posterior vagal clonal analysis,

dorsal neural tube, dorsal root ganglia, sympathetic ganglia, and the gut were imaged. For cardiac clonal analysis of both cardiac and enteric derivatives, cranial nerve nine, pharyngeal arches, and outflow tract from the cardiac slice, as well as the gut from posterior vagal slice were imaged. In those posterior vagal slices, the dorsal regions were not analyzed because the signal was absent (injection specificity screened based on this criterion). For immunohistochemistry (n = 12), embryos were fixed at E7 in 4% PFA in PB for 30 mins at 4°C, embedded in O.C.T compound (Sakura #4583) and cryo-sectioned (Microm HM550 cryostat).

Single-cell and stream-specific photoconversion

Photoconvertible construct encoding H2B-Emeos and YFP-Utrophin was injected into the lumen of the neural tube adjacent to where the targeting neural crest emerges. At HH13, a transverse slice spanning 2 somites was obtained, immobilized in glass imaging dish. 405 nm laser was used to selectively convert H2B-Emeos from green to red in one migrating cardiac neural crest cell per slice for single-cell photoconversion (n = 11), one migrating posterior vagal neural crest cell for single-cell photoconversion (n = 5), or all post-otic migrating cardiac crest cells for stream-specific photoconversion (n = 2). Immediately after conversion, an image with z-stack spanning the tissue depth above and below the converted cell was obtained as a proof of specificity. Slice was then placed back to the incubator at 38 degree Celsius. 24 hours post incubation, slices were fixed in 4% PFA in PBS for 15 mins at 4°C, embedded in O.C.T compound (Sakura #4583) and sectioned (Microm HM550 cryostat) for cell fate analysis. Photoconverted progenies were identified based on

a simultaneous presence of red nuclear and YFP-Utrophin signals. Although blood cells can also produce red nuclear-like autofluorescence, these cells were excluded from the analysis due to lack of YFP-Utrophin signal at the cortical region (Supplementary Fig4-1e,f).

In vivo time-lapse imaging

In HH9 embryos, cardiac neural crest from the mid-otic placode to somite 3, or vagal neural crest from mid-otic placode to somite 7 were labelled with ~0.5µl of viruses described above. Embryos were harvested 22 hours post injection (HH13), sliced, and cultured in neurobasal media (GIBCO #12349-015). Transverse view was imaged for cell division tracking for migrating cardiac (n = 2) and posterior vagal (n = 1) neural crest cells; lateral view was imaged for cell migration along the gut (n = 2).

Retrovirally-mediated molecular perturbations

RIA-H2BEmeos-DNFgfr1 (n = 11), H2BEmeos-DNCxcr4 (n = 4) or DNRet-H2BEmeos (n = 10, 8/10 injected with H2B-RFP control) were supplemented with 0.3µl of 2% food dye (Spectral Colors, Food Blue 002, C.A.S# 3844-45-9) to make the working solution. ~0.5µl of working solution with a titer of ~106 particles per mL was injected into the lumen of the neural tube posterior to mid-otic to somite 3 (S1-S3 in brief) to infect cardiac neural crest, or from mid-otic to somite 7 (S1-S7 in brief) to infect vagal neural crest. Embryos were sealed with surgical tape, continues to incubate at 37°C until E3 or E7 for analysis.

H2BEmeos was used as a cell marker instead of a photoconvertible protein in these experiments.

Immunohistochemistry

O.C.T. compound was removed by incubating the frozen section for 3mins in 1xPBS at room temperature. Tissue sections were then permeabilized with 0.3% vol/vol Triton-X100in 1xPBS. Blocking buffer was prepared with 1xPBS, 5% vol/vol normal donkey serum, 0.3% vol/vol Triton-X100. Sections were incubated with primary antibody at 4°C overnight (primary antibodies used: 1:500 Mouse anti-smooth muscle actin IgG2a, Sigma-Cat#A2547, clone 1A4 monoclonal; 1:500 Mouse anti-HuC/D IgG2b, Invitrogen-Cat#A21271, clone 16A11 monoclonal; 1:500 Mouse anti-TuJ1 IgG2a, Biolegend-Cat# 801201, clone TUJ1 monoclonal; 1:500 Rabbit anti-Tyrosine Hydroxylase (TH), Millipore-Cat# AB152, polyclonal; 1:10 8-IE7 (monoclonal mouse anti-GFAP IgG1), DSHB, 1:10 3H5 (monoclonal mouse anti-HNK1 IgM), DSHB, 1:10 PAX7 (monoclonal mouse anti-Pax7 IgG1), DSHB, 1:10 IE8 (monoclonal mouse anti-P0 IgG1), DSHB. After primary antibody incubation, sections were washed for 3 times (each 15 mins) in 1xPBS, and incubated with secondary antibody for 45mins at room temperature (secondary antibodies used: 1:1000 goat anti-mouse IgG2a 633, #A21136 (polyclonal), 1:1000 goat anti-mouse IgG1 647, #A21240 (polyclonal), 1:1000 goat anti-mouse IgG2b 647, #A21146 (polyclonal), 1:1000 goat anti-mouse IgM 647, #A21238 (polyclonal), 1:1000 donkey anti-rabbit 647, #A31573 (polyclonal), Invitrogen Molecular Probes). Immunostained tissue

was imaged using a Zeiss AxioImager.M2 with Apotome.2 or Zeiss LSM 800 confocal microscope.

Statistics and reproducibility

For multiplexed retroviral clonal analysis, slice cultures were generated in biological replicates of 14, 12, or 9, respectively, at cardiac, posterior vagal, or both regions. Because correct targeting is a prerequisite for slice culture, all 23 cardiac slices were processed as indicated in Fig1d (23/23 slices) and migration pattern analyzed as in Supplementary Fig4-1b. Fig4-1e-h, Fig4-3d-g, Fig4-3l-o are examples of a triply labelled clone with derivatives found in multiple locations at the cardiac, posterior vagal, and both levels. Because viral infection of progenitor cells is random, each clone represents an independent event. Therefore, we provide individual data points for each clone observed (Supplementary Data 4-1) as well as distribution of clone types among replicates (Fig4-1i, Fig4-3c). Because the probably of triple infection are rare, antibody dilutions were first tested on uninfected embryos. Immunohistochemistry was performed in individual embryos (n = 12 replicates) where a triple labelled clone (H2B-YFP, H2B-RFP, Mito-CFP) was observed in cranial nerve nine (CN-IX), the enteric nervous system (ENS), pharyngeal arch arteries (PAA), outflow tract (OFT), and sympathetic chain (SYM) (Fig4-1j-k, Supplementary Fig4-2a-k). Note that Fig4-1j-k, Supplementary Fig4-2a-k are not the same clone. A triple labelled clone with broad distribution as shown in Fig4-1e-h, Fig4-3d-g, Fig4-3l-o, Supplementary Fig4-2a-k is relatively rare (Fig4-1i, Fig4-3c). For clonal analysis via photoconversion, we performed single-cell photoconversion with n = 11 replicates on cardiac neural crest, n = 5

replicates on posterior vagal neural crest cell and n = 2 replicates on all post-otic migrating cardiac crest cells for stream-specific photoconversion. In all 11 cardiac single cell photoconversion experiments, the converted cells were similar to the one in Fig4-2b (represents 11/11). All slices were subsequently processed for antibody staining to obtain Fig4-2c, d, e. Because behavior of each photoconverted progenitor cell is independent from other cells, we recorded locations of each clone as a distribution shown in Supplementary Fig4-1g. Note that 8/11 clones are located in more than one derivative. Fig4-2d represents 7/11 clones, while Fig4-2e represents a rare case (1/11) because the outflow tract tends to have lower numbers of neural crest-derived cells. Supplementary Fig4-1e, f shows converted signal and autofluorescence from blood cells, representative of all 18 experiments. For single posterior vagal neural crest photoconversion, similar results were observed in 5/5 experiments as shown in Fig4-3h; Fig4-3i-j (one of the sister cell after cell division migrated into the gut) occurred in 2/5 experiments. Results for stream-specific photoconversion shown in Fig4-3q-r, Supplementary Fig4-2l were observed in 2/2 experiments. Immunohistochemistry for premigratory Pax7+ cells was performed in n=3 embryos, with all displaying similar patterns as shown in Supplementary Fig4-1c. Fig4-4a, 4g (same as Supplementary Fig4-3a, 3b) include representative images from 5 evenly distributed timepoints over Supplementary Movie 4-1, 4-2 as an overview of cell migration. Molecular perturbation was performed with n = 11 replicates for DN-Fgfr1, n = 4 replicates for DN-Cxcr4 and n = 10 replicates for DN-Ret (8/10 injected with H2B-RFP control). The numbers for representative images in Fig4-5b-v are presented in the figure legend.

Imaging data analysis

Pax7+ and DAPI+ cells were quantified using Manual Cell Counting in FIJI v1.0 software. Cell numbers after CXCR4 and RET disruption were quantified using Manual Cell Counting with FIJI v1.0 software. For each embryo, two to three randomly selected transverse sections were quantified. To analyze the role of DN-Cxcr4 in cell migration to the enteric nervous system, numbers of labeled cells were counted in images of the foregut and cranial nerve nine. The average cell number in the foregut was normalized to cell number in the cranial nerve, to account for titer variation between experiments. The resulting ratio was compared between DN-Cxcr4 and control virus injected group. For the role of RET signaling during cardiac neural crest migration into the foregut, the numbers of DN-Ret-expressing and control virus-expressing cells in the foregut were normalized to their counterparts in the pharyngeal junction (anterior to the foregut). Dynamic imaging data was exported from ZEN (blue edition) software and processed using IMARIS 9.1.0 software. In each timeframe, the center of a cell was identified according to the position of its nucleus. Position information was connected to reconstitute cell trajectory, with the x, y, z coordinates in each frame extracted for further analysis. The squared displacement (SD) analysis was conducted using mean square displacement analysis of particles trajectories package in MATLAB R2017a. The SD curves were fitted to a power function $f(x)=b*x^{\alpha} + c$. $\alpha \approx 1$ implies free diffusion, $\alpha < 1$ implies constrained movement, while $\alpha > 1$ implies directed movement. Plots of initial coordinates against displacement distances were generated using MATLAB R2017a. Box-and-dot plots were generated using ggplot2

package in R. Two-sided Wilcoxon rank-sum test was used for statistical comparison between two groups.

ACKNOWLEDGEMENT

This work was supported by NIHRO1HL14058 to M.E.B. We thank Dr. Carlos Lois and the Biological Imaging Facility of the Beckman Institute for sharing equipment.

4.5 REFERENCE

1. Bronner, M. E. & LeDouarin, N. M. Development and evolution of the neural crest: An overview. *Dev. Biol*. 366, 2–9 (2012).

2. Baggiolini, A. et al. Premigratory and migratory neural crest cells are multipotent in vivo. *Cell Stem Cell* 16, 314–322 (2015).

3. Kirby, M. L., Gale, T. F. & Stewart, D. E. Neural crest cells contribute to normal aorticopulmonary septation. *Science* 220, 1059–61 (1983).

4. Jiang, X., Rowitch, D. H., Soriano, P., McMahon, A. P. & Sucov, H. M. Fate of the mammalian cardiac neural crest. *Development* 127, 1607–16 (2000).

5. Le Douarin, N. M. & Teillet, M. A. The migration of neural crest cells to the wall of the digestive tract in avian embryo. *J. Embryol. Exp. Morphol*. 30, 31–48 (1973).

6. Tang, W., Martik, M. L., Li, Y. & Bronner, M. E. Cardiac neural crest contributes to cardiomyocytes in amniotes and heart regeneration in zebrafish. *Elife 8*, (2019).

7. Barlow, A. J., Wallace, A. S., Thapar, N. & Burns, A. J. Critical numbers of neural crest cells are required in the pathways from the neural tube to the foregut to ensure complete enteric nervous system formation. *Development* 135, 1681–1691 (2008).

8. Kuo, B. R. & Erickson, C. A. Vagal neural crest cell migratory behavior: A transition between the cranial and trunk crest. *Dev. Dyn*. 240, 2084–2100 (2011).

9. Espinosa-Medina, I. et al. Dual origin of enteric neurons in vagal Schwann cell precursors and the sympathetic neural crest. *Proc. Natl. Acad. Sci. U. S. A*. 114, 11980–11985 (2017).

10. Ito, K. & Sieber-Blum, M. In vitro clonal analysis of quail cardiac neural crest development. *Dev. Biol*. 148, 95–106 (1991).

11. Ito, K. & Sieber-Blum, M. Pluripotent and developmentally restricted neural-crest-derived cells in posterior visceral arches. *Dev. Biol.* 156, 191–200 (1993).

12. Youn, Y. H., Feng, J., Tessarollo, L., Ito, K. & Sieber-Blum, M. Neural crest stem cell and cardiac endothelium defects in the TrkC null mouse. *Mol. Cell. Neurosci*. 24, 160–170 (2003).

13. Li, Y., Li, A., Junge, J. & Bronner, M. Planar cell polarity signaling coordinates oriented cell division and cell rearrangement in clonally expanding growth plate cartilage. *Elife 6*, (2017).

14. Li, Y. et al. Discs large 1 controls daughter-cell polarity after cytokinesis in vertebrate morphogenesis. *Proc. Natl. Acad. Sci. U. S. A.* 115, E10859–E10868 (2018).

15. Li, Y. et al. In Vivo Quantitative imaging provides insights into trunk neural crest migration. *Cell Rep*. 26, 1489-1500.e3 (2019).

16. Tang, W., Li, Y., Gandhi, S. & Bronner, M. E. Multiplex clonal analysis in the chick embryo using retrovirally-mediated combinatorial labeling. *Dev. Biol*. 450, (2019).

17. Li, Y. et al. Dynamic imaging of the growth plate cartilage reveals multiple contributors to skeletal morphogenesis. *Nat. Commun*. 6, 1–10 (2015).

18. Li, Y. & Dudley, A. T. Noncanonical frizzled signaling regulates cell polarity of growth plate chondrocytes. *Development* 136, 1083–1092 (2009).

19. Tang, W.& Bronner, M.E. Neural crest lineage analysis: From past to future trajectory. *Development* 147(20):dev193193 (2020).

20. Li, Y. et al. Macropinocytosis-mediated membrane recycling drives neural crest migration by delivering F-actin to the lamellipodium. *Proc. Natl. Acad. Sci. U. S. A.* (2020).

21. Figliozzi, R. W., Chen, F., Chi, A. & Hsia, S.-C. V. Using the inverse Poisson distribution to calculate multiplicity of infection and viral replication by a high-throughput fluorescent imaging system. *Virol. Sin*. 31, 180–3 (2016).

22. Gurskaya, N. G. et al. Engineering of a monomeric green-to-red photoactivatable fluorescent protein induced by blue light. *Nat. Biotechnol*. 24, 461–465 (2006).

23. Dempsey, W. P. et al. In vivo single-cell labeling by confined primed conversion. *Nat. Methods* 12, 645–648 (2015).

24. Kirby, M. L. & Hutson, M. R. Factors controlling cardiac neural crest cell migration. *Cell Adh. Migr.* 4, 609–621 (2010).

25. Anderson, R. B., Newgreen, D. F. & Young, H. *Neural Crest and the Development of the Enteric Nervous System.* (2013).

26. Martínez-Morales, P. L. et al. FGF and retinoic acid activity gradients control the timing of neural crest cell emigration in the trunk. *J. Cell Biol*. 194, 489–503 (2011).

27. Amaya, E., Musci, T. J. & Kirschner, M. W. Expression of a dominant negative mutant of the FGF receptor disrupts mesoderm formation in xenopus embryos. *Cell* 66, 257–270 (1991).

28. Heredia, J. D. et al. Mapping interaction sites on human chemokine receptors by deep mutational scanning. *J. Immunol.* 200, 3825–3839 (2018).

29. Escot, S., Blavet, C., Härtle, S., Duband, J. L. & Fournier-Thibault, C. Misregulation of SDF1-CXCR4 signaling impairs early cardiac neural crest cell migration leading to conotruncal defects. *Circ. Res.* 113, 505–516 (2013).

30. Cronshaw, D. G., Nie, Y., Waite, J. & Zou, Y.R. An essential role of the cytoplasmic tail of CXCR4 in G-protein signaling and organogenesis. *PLoS One* 5, e15397 (2010).

31. Johannessen, C. M. et al. COT drives resistance to RAF inhibition through MAP kinase pathway reactivation. *Nature* 468, 968–972 (2010).

32. Drosten, M. et al. Role of MEN2A-derived RET in maintenace and proliferation of medullary thyroid carcinoma. *J. Natl. Cancer Inst*. 96, 1231–1239 (2004).

33. Hutchins, E. J. et al. Migration and diversification of the vagal neural crest. *Dev. Biol*. 444, S98–S109 (2018).

34. Raible, D. W. & Eisen, J. S. Restriction of neural crest cell fate in the trunk of the embryonic zebrafish. *Development* 120, 495–503 (1994).

35. Henion, P. D. & Weston, J. A. Timing and pattern of cell fate restrictions in the neural crest lineage. *Development* 124, 4351–9 (1997).

36. Bronner-Fraser, M. & Fraser, S. E. Cell lineage analysis reveals multipotency of some avian neural crest cells. *Nature* 335, 161–164 (1988).

37. Bronner-Fraser, M. & Fraser, S. Developmental potential of avian trunk neural crest cells in situ. *Neuron* 3, 755–66 (1989).

38. Ling, I. T. C. & Sauka-Spengler, T. Early chromatin shaping predetermines multipotent vagal neural crest into neural, neuronal and mesenchymal lineages. *Nat. Cell Biol*. 21, 1504–1517 (2019).

39. Nakamura, T., Colbert, M. C. & Robbins, J. Neural crest cells retain multipotential characteristics in the developing valves and label the cardiac conduction system. *Circ. Res.* 98, 1547–1554 (2006).

40. Lasrado, R. et al. Lineage-dependent spatial and functional organization of the mammalian enteric nervous system. *Science* 356(6339): 722–726 (2017).

41. Trainor, P. A., Ariza-McNaughton, L. & Krumlauf, R. Role of the isthmus and FGFs in resolving the paradox of neural crest plasticity and prepatterning. *Science* 295 (5558): 1288–1291 (2002).

42. Lumsden, A., Sprawson, N. & Graham, A. Segmental origin and migration of neural crest cells in the hindbrain region of the chick embryo. *Development* 113(4):1281-91 (1991).

43. Kirby, M. L. Plasticity and predetermination of mesencephalic and trunk neural crest transplanted into the region of the cardiac neural crest. *Dev. Biol*. 134, 402–412 (1989).

44. Sato, A. et al. FGF8 signaling is chemotactic for cardiac neural crest cells. *Dev. Biol*. 354, 18–30 (2011).

45. Escot, S. et al. Disruption of CXCR4 signaling in pharyngeal neural crest cells causes DiGeorge syndrome-like malformations. *Development* 143(4): 582–8 (2016).

46. Sierro, F. et al. Disrupted cardiac development but normal hematopoiesis in mice deficient in the second CXCL12/SDF-1 receptor, CXCR7. *Proc. Natl. Acad. Sci.* U. S. A. 104, 14759–14764 (2007).

47. Natarajan， Dipa, Marcos-Gutierrez， Camelia, Pachnis, V. & Graaff， Esther, D. Requirement of signalling by receptor tyrosine kinase RET for the directed migration of enteric nervous system progenitor cells during mammalian embryogenesis. *Development* 129(22): 5151–60 (2002).

48. Yan, H. et al. Neural cells in the esophagus respond to glial cell line-derived neurotrophic factor and neurturin, and are RET-dependent. *Dev. Biol.* 272, 118–133 (2004).

49. Durbec, P. L., Larsson-Blomberg, L. B., Schuchardt, A., Costantini, F. & Pachnis, V. Common origin and developmental dependence on c-ret of subsets of enteric and sympathetic neuroblasts. *Development* 122(1):349-58 (1996).

Chapter V

CONCLUSIONS

In developmental biology, fate mapping has played an essential role to understand how a fertilized egg divides and differentiates to give rise to diverse yet highly coordinated cell types in an organism. Population and clonal level lineage analysis has contributed to many discoveries about the neural crest in vertebrate embryos.

In this work, we introduced a new tool utilizing Replication Incompetent Avian retroviruses (RIAs) to perform population and clonal level lineage analysis. We first validated the method by examining subcellular localization of the fluorescent proteins and rate of co-infection *in vitro*. Next, we applied the RIAs into chick trunk neural crest to demonstrate cell multipotency. At a population level, we performed lineage tracing using a single RIA and showed that cardiac neural crest cells contribute to the myocardium in chick and mouse. Applying multicolor RIAs at a clonal level, we identified individual vagal neural crest cells can give rise to cell types in both the heart and the gut, suggesting that premigratory vagal neural crest cells are multipotent. We further utilized the RIAs to conduct single-cell photoconversion assay which allows for anterograde tracing and confirmed that migrating neural crest cells retain multipotency, with stochastic post-mitotic migration behavior driving sister cells into distinct directions. Finally, we performed RIA-mediated molecular perturbation to show that CXCR4 and RET are essential guidance cues for neural crest cells in the pharyngeal junction to enter the cardiac and enteric region, respectively. Together, our results expanded the lineage tracing toolset in avian embryos utilizing the RIA viruses,

enriched our current understanding regarding neural crest developmental potential, cell fates, and behavior of individual migratory cells, and can be further adapted to explore the transcriptome and chromatin landscape on population and clonal levels.